

8-18-2003

Seismicity in the vicinity of Yucca Mountain, Nevada, for the period October 1, 2001 to September 30, 2002

David H. von Seggern

University of Nevada, Reno, vonseg@seismo.unr.edu

Kenneth Smith

University of Nevada, Reno, ken@seismo.unr.edu

James N. Brune

University of Nevada, Reno, brune@seismo.unr.edu

Richard Quittmeyer

Amy J. Smiecinski

University of Nevada, Las Vegas, smiecins@unlv.nevada.edu

Follow this and additional works at: https://digitalscholarship.unlv.edu/yucca_mtn_pubs

 Part of the [Geophysics and Seismology Commons](#)

Repository Citation

von Seggern, D. H., Smith, K., Brune, J. N., Quittmeyer, R., Smiecinski, A. J. (2003). Seismicity in the vicinity of Yucca Mountain, Nevada, for the period October 1, 2001 to September 30, 2002.

Available at: https://digitalscholarship.unlv.edu/yucca_mtn_pubs/90

This Technical Report is protected by copyright and/or related rights. It has been brought to you by Digital Scholarship@UNLV with permission from the rights-holder(s). You are free to use this Technical Report in any way that is permitted by the copyright and related rights legislation that applies to your use. For other uses you need to obtain permission from the rights-holder(s) directly, unless additional rights are indicated by a Creative Commons license in the record and/or on the work itself.

This Technical Report has been accepted for inclusion in Publications (YM) by an authorized administrator of Digital Scholarship@UNLV. For more information, please contact digitalscholarship@unlv.edu.


Seismicity in the Vicinity of Yucca Mountain, Nevada, for the Period October 1, 2001, to September 30, 2002

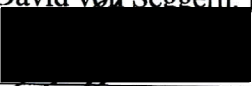
Final
08/18/2003

Prepared by the Nevada Seismological Laboratory
for the U.S. DOE/UCCSN Cooperative Agreement
Number DE-FC28-98NV12081
Task 12: Southern Great Basin Seismic Network Operations

Document ID: TR-03-002, Rev. 0

Originators:



David von Seggern, Nevada Seismological Laboratory


Ken Smith, Nevada Seismological Laboratory

Approvals:




 _____ James Brune, Principal Investigator	<u>8/19/03</u> Date
 _____ Richard Quittmeyer, Technical Reviewer	<u>8/22/2003</u> Date
 _____ Amy Smiecinski, QA Manager, UCCSN	<u>9-5-03</u> Date

TABLE OF CONTENTS

Abstract	4
1. Introduction	6
2. Data Collection and Processing	7
2.1 Station Description	7
2.2 Data Collection Method	9
2.3 Downtime and Problems	11
2.4 Daily Processing	12
2.5 Finalizing the Earthquake Catalog	13
3. Seismicity Characteristics	18
3.1 Spatial Pattern of Earthquakes	18
3.2 Moment Rate	20
3.3 Depth Distribution	22
3.4 Magnitude Distribution and Threshold	23
4. Little Skull Mountain Earthquake of 06/14/2002	26
4.1 Introduction	26
4.2 Distribution of 2002 Earthquake Activity	27
4.3 Faulting Within the Aftershock Zone	30
4.4 Constraints on a Complex Faulting Model	31
4.5 Strong-Motion Records and Ground-Motion Observations	31
4.6 Comparisons with 1992 Strong-Motion Recordings at Lathrop Wells	37
5. Death Valley Seismicity	38

6. Earthquakes Near Yucca Mountain	40
7. Focal Mechanisms	41
8. Observed Explosions	44
9. Summary	46

References

Tables

Figures

Appendices

1. Status of the Data
2. Station Data and Description for the SGBDSN
3. Catalog of FY02 Earthquakes
4. Events Identified as Blasts in FY02

Abstract

Starting on October 1, 1995, the monitoring of seismicity within the southern Great Basin near Yucca Mountain was performed with a new digital network. This network features three-component recording with 24-bit A/D conversion in the field. Continuous data are collected at 20 sps, and event triggered windows are collected at 100 sps. A seismic bulletin of events is made by automatically associating triggers among stations, classifying the local earthquake events, and locating the earthquakes and computing their magnitudes with conventional methods. This report covers the operational and seismic results of the seventh year (FY02) of the digital network monitoring.

The FY02 earthquake bulletin includes over 5000 events within about 65 km of Yucca Mountain. This is roughly twice the average number of events in the previous six years and is due to the occurrence of a significant $M = 4.4$ earthquake on 06/14/2002 within the aftershock zone of the 1992 $M = 5.6$ Little Skull Mountain earthquake. This event was followed by nearly 3000 aftershocks through September 30, 2002. Hypocentral depths of the recent aftershocks are largely concentrated in the range of 8-12 km, consistent with previous years. Earthquakes outside the LSM aftershock zone are largely in the 4-12 km range. The observed minimum detection thresholds for earthquakes within the network range in M_L from -0.5 to 0.5 or greater, with the lower threshold achieved for earthquakes in the LSM and Yucca Mountain areas where the network is most dense.

The $M 4.4$ earthquake at Little Skull Mountain on 06/14/2002 was the major event in the network during FY02. During FY02 only the $M 4.4$ Little Skull Mountain earthquake provided usable strong-motion recordings. The maximum acceleration of 0.084 g was observed at the station LSC

nearly directly above the hypocenter, and maximum accelerations in a range of .004 to .032 g were observed near Yucca Mountain, with top end of the range observed at station WHBS on the pad of the proposed Waste Handling Building. Recorded accelerations were roughly in agreement with those predicted in the PSHA (Probabilistic Seismic Hazard Analysis) study for Yucca Mountain.

From the FY02 earthquakes, 46 new short-period, first-motion focal mechanisms were reliably determined. These, and the roughly 300 from the previous six years, show a consistent picture of the overall stress field in the region of the digital network. The mean tensional axis is oriented at roughly 60° west of north, at shallow dip, and the pressure axis at roughly 30° east of north, with greater variability in the dip direction accounting for a range of both strike-slip and dip-slip faulting within the general NW-SE extension.

In FY02 five additional small earthquakes occurred within 10 km of the ESF, all with magnitudes < 0.0. In addition, a small earthquake was located in the southern part of the Yucca Mountain block, more than 10 km from the ESF, and another in Crater Flat.

In the Death Valley region, two earthquakes measured $M > 3$ within the park boundaries. Little of the observed seismicity in the Death Valley region can be related to the two large faults there: Furnace Creek and Death Valley.

1. Introduction

This report covers the seismicity observed within the Yucca Mountain region during the seventh year of operation of the Southern Great Basin Digital Seismic Network (SGBDSN). Originally brought into operation on October 1, 1995, the digital network has now grown to 30 three-component stations within roughly 50 km of Yucca Mountain. In addition, 19 sites at relatively close distances from Yucca Mountain are equipped with strong-motion sensors. This network (weak and strong motion) addresses the seismic hazard of the Yucca Mountain area by providing important magnitude data for earthquake recurrence estimates, spatial hypocentral data for inference of active faults and verification of tectonic models, actual ground motion data for comparison with predictions, and source data for characterizing faulting and determining stress patterns.

This report is organized to first present the basic information on the network performance. This comprises a brief description of the data recording, an explanation of recording problems, a discussion of the processing procedures, and explanation of how the final catalog is produced. The report then presents the recorded and located seismicity as measured by the SGBDSN in FY02 (10/01/2001 through 09/30/2002). A more detailed treatment of special events or topics is given; among these are the 06/14/2002 $M = 4.4$ earthquake at Little Skull Mountain, earthquakes for which focal mechanisms could be determined, and earthquakes close to Yucca Mountain. The seismicity of Death Valley is treated, making use of stations remaining from an earlier analog network. This is possible due to the integration of all Nevada seismic stations under the Antelope seismic processing software, as described later.

2. Data Collection and Processing

2.1 Station Description

As of September 2002 the Southern Great Basin Digital Seismic Network (SGBDSN) included 30 digital seismograph stations. Figure 2-1 shows these locations; they are Q data from DTN # UN0006SPA012DV.001 and are listed in Appendix 2. Two additional stations (ECO and YFT) were installed by Sandia National Laboratories (SNL) but are considered effectively part of the SGBDSN, with all normal QA procedures applied to them. These two stations are tied into the SGBDSN telemetry system, and data are transmitted and processed in the same way as for all other SGBDSN sites. Some stations of the former analog monitoring network (Southern Great Basin Seismic Network – SGBSN) have been maintained outside the SGBDSN to aid in the characterization of Death Valley area seismicity and in regions not monitored effectively outside of the SGBDSN. A map of a larger area showing the analog (SGBSN) stations along with the digital (SGBDSN) stations is shown in Figure 2-2. (These SGBSN locations are also Q data and taken from DID #023DV.001.) Data from analog stations were used to determine focal mechanisms and to aid in the location of events, both topics covered later in this report. Note that the stations SHP and NEN in Figure 2-2, providing some coverage of the Las Vegas area southeast of Yucca Mountain, are digital stations installed in southern Nevada by NSL (Nevada Seismological Laboratory) and are not part of the SGBDSN. The SGBDSN stations transmit to one of the five telemetry nodes shown in Figure 2-3. The exact installation dates of the SGBDSN stations, along with the location information for each, are listed in Appendix 2. All digital stations use Geotech S-13 seismometers currently. The last four CMG-40 seismometers were phased out at AMD, SPC, TYM, and TIM in

FY02. Stations ECO and YFT are configured with Geotech GS-13 seismometers. The AL5 station within Alcove 5 of the Exploratory Studies Facility (ESF) uses a Mark Products three-component L4 seismometer. Neither the GS-13 nor Mark Products seismometers are used in magnitude computations. Also, no analog station data are used to calculate earthquake magnitudes. Ten digital sites are equipped with strong-motion instrumentation (see Appendix 2). Supplemental 16-bit A/D cards were added to onsite recorders in order to handle the output from RefTek Model 133-05 accelerometers. Data from these strong-motion sites are available in near-real-time and recorded and archived along with all SGBDSN data. The strong-motion data will be discussed in a later section of this report.

The response in digital counts to ground displacement versus frequency of the SGBDSN instruments is shown in Figure 2-4. These responses are nominal for all instruments in the two main groups, S-13 or CMG-40. Actual calibration data show that there is only a maximum of $\pm 10\%$ deviation for any particular instrument from the nominal curves. Calibration pulses were analyzed monthly to ensure that none of the instruments drifted outside of this range. The free period of the S-13 (and GS-13) instruments was nominally set to 1.0 s and that of the CMG-40 instruments to 30 s. The damping coefficient was nominally set to 0.7 (critical damping) in all cases. Sensors of the remaining stations of the analog network have a similar free period and damping coefficient. The SGBDSN S-13 response peaks at about 40 Hz at high frequency, as compared to 20 Hz for the instruments of the analog network. The 40 Hz cutoff is due to anti-aliasing filters in the DAS (Digital Acquisition System) units. It is important to point out that the much higher noise floor of the analog recordings results in a much narrower usable frequency band than achieved in the SGBDSN. This was demonstrated in von Seggern et al. (2001) for a collocated pair of digital and analog stations. The CMG-40 instruments are recorded at a lower gain than the S-13 instruments in

order to provide broadband, on-scale recordings in the event of a larger earthquake. The S-13's, as configured with the RefTek recorders, can clip at short distances (< 10 km) for $M_L = 3$ earthquakes.

Station locations were determined with a Trimble GPS unit in a differential mode for early site installations and then by Garmin GPS units after May 2000 when selective data availability was discontinued and accuracy of ordinary GPS units became 10 meters or less. Locations in Appendix 2 are for the seismometers themselves, not the antenna position.

2.2 Data Collection Method

The field data acquisition systems are described in von Seggern and Smith (1997). During the time period covered by this report, two data streams were in effect at all stations except ECO and YFT: 1) a 20-sps, 3-component, continuous data stream and 2) a 100-sps, 3-component, triggered data stream. Stations ECO and YFT only had the triggered stream. The former was enabled with a “continuous” trigger specification, which creates contiguous trigger windows of 30 minutes duration each. The latter was controlled by an “event” trigger specification with the following parameters:

short-term average (STA) length	0.4 seconds
long-term average (LTA) length	10.0 seconds
STA/LTA trigger threshold	3.5
pre-trigger record length	30 seconds
total record length	150 seconds
channels included in trigger	Z, N, E
threshold exceeded by at least n channels	1

A third data stream has been added for the 10 stations equipped with accelerometers. This stream is “cross-triggered” from the 100-sps seismometer stream described above, and the data are also

recorded at 100 sps. The manner of data collection at the NSL was previously described in von Seggern and Smith (1997). Raw data are archived in large 24-hour files (one per station) that contain all original data packets sent from the field acquisition units. Such files are termed “refraw” files, and the actual file names end with this term. We call the set of these files the “upstream” recording, and it is archived on DVD media. These DVDs are submitted to the YMP Records Processing Center, as in all prior years, as a raw data record.

On January 1, 2000, a major transition to the Antelope seismic processing system was made (von Seggern et al., 2000). This transition for the entire NSL network incorporated recording and processing of seismic data from the SGBDSN. The SGBDSN data, directed to files as described above, are also transmitted in near-real-time to the Antelope system where it is then available for review and analysis with the seismic data processing tools of the Antelope system. In automating some seismic network operations through Antelope, additional data processing measures are incorporated in the data flow. These introduce potential failure points in the data collection process if we rely exclusively on the Antelope system for a final data archive. We implemented new archival procedures on January 1, 2000, to put the data on 4-mm DAT tapes in Antelope format as a “downstream” dataset. Depending on the use of the data, retrieval from one or the other (upstream or downstream) of the archived datasets is possible. The upstream archival dataset, although more complete, can often be more difficult to use than the downstream dataset. In addition to storing waveform data, Antelope also stores various parametric data in tables, collectively called Datascope (Quinlan, 1998).

2.3 Downtime and Problems

The reliable collection of data is subject to the following problems:

- * seismometer malfunction or failure
- * DAS malfunction or failure
- * radio transmission interference
- * telemetry interference or failure
- * hardware failure at the central recording site
- * software failure at the central recording site

Except for seismometer malfunction and some types of DAS malfunction, the nature of these problems is that no data are recorded rather than data are corrupted. The case of corrupt data is covered by writing appropriate Non-Conformance Reports. Seismometer performance is controlled by procedures in IPR-001 (“Operation of the Yucca Mountain Seismic Network”). In this fiscal year of operation, various examples of all of the above types of problems occurred. A more accurate, station-specific, method of tracking downtime from the upstream recording was devised for this fiscal-year report. It is based on querying the Datascope table called “reno.wfdisc” for recorded time intervals for each station. (These Datascope tables are in the daily Antelope directories /ymp16/yyyy/jjj on the YMP computing system at the NSL, where yyyy = year and jjj = julian day. Data in these tables are non-QA.) Downtime for any given station is simply the total span of time minus the total of these time intervals for that station. Figure 2-5 is a summary of the downtime for each station within the SGBDSN. (The SNL stations ECO and YFT are run in triggered mode only and so are not represented here.) This figure shows that the downtime was under 5% for all stations. The least downtime, at station HEL, is approximately 0.3%; five other stations have roughly 0.4% downtime. HEL was installed on 06/24/2002 and therefore was not operating during all of FY02. Ignoring it, the 0.4% of the five stations is then interpreted as the upper bound of the network-wide downtime, that is, when not all stations were recorded. This network-wide downtime is significantly better than the same as reported in previous years (von Seggern and Smith, 2002). The largest

downtime is associated with station AL5. This station, placed in Alcove 5 of the ESF, has a unique telemetry connection and a unique power supply mode, both of which have been troublesome during this fiscal year. The FY02 downtime of AL5 is, however, a large improvement over FY01 (von Seggern and Smith, 2002).

The downtime inferred from gaps in recording does not exactly represent when data are unrecoverable. The upstream recording to reflow files, as discussed above, is actually more complete due to the fact that Antelope software failures would further add to the outage as seen in the Antelope archive of data. Data from the reflow files are fully recoverable and, in fact, can be replayed through the Antelope system in a non-real-time mode. We have had occasion to do this, with satisfactory results. The decision to replay the reflow data is made on the length of the “hole” in the Antelope archive and the appearance of any significant earthquakes in that time period. If problems, such as telemetry failure, affect both the upstream and downstream archives, then recovery is generally not possible. An exception is when the outage has short duration (~ 15 to 30 minutes) because the data are saved in a FIFO (first-in, first-out) memory in the DAS units until transmission can be restored. We are not aware of any events with $M > 2$ falling in the 0.4% of overall downtime for FY02. Most of the downtime in Figure 2-5 relates to times where only one station or only a part of the network was down. Single-station downtimes only marginally impact the ability to locate events within the network. Multiple-station downtimes have greater impact on this ability; but, even with a few stations operative, events of $M > 1$ within the SGBDSN can usually be located accurately.

2.4 Daily Processing

The daily processing routine is outlined in Figure 2-6. It was fully described in von Seggern and Smith (2001) for FY00 and has not changed since. The preliminary processing is done with the Antelope system of BRTT, Inc., and the preliminary event locations and magnitudes are kept in the Datascope database (Quinlan, 1998). Waveforms are excerpted for these events and kept online with the database.

The last step in preliminary analysis is for the events to be checked and initialed on record sheets called the "Yucca Mountain Seismic Event Sheet." These sheets are made by subsetting the Antelope database for events within 65 km of Yucca Mountain (specifically, the station RPY). Events are reviewed according to IPR-002 ("Determining the Location of Earthquakes Recorded by the Yucca Mountain Seismic Network") and initialed by professional staff on the record sheets. In this process events may be relocated and magnitudes recomputed; the revised information is captured in the database. This is still not the "final" qualified information. Also at this time, a review is made on classification of events other than local earthquakes (for instance, blasts).

2.5 Finalizing the Earthquake Catalog

The final locations and magnitudes for the FY02 earthquakes were obtained according to UCCSN procedures IPR-002 and IPR-003 ("Determining the Magnitude of Earthquakes Recorded by the Yucca Mountain Seismic Network"). The location program specified in IPR-002 is HYPOINVERSE, V1.0 (STN 10080-1.0) (Klein, 1989). The magnitude program specified in IPR-003 is MLCALC, V1.0 (STN 10081-2.0), which was internally developed and implements the local magnitude calculation of Richter (1935); this magnitude is widely termed " M_L ". Again, we note that

non-SGBDSN arrivals may be used in the locations, depending on seismological judgment. This enables us to improve the locations of events around the fringe of the SGBDSN. With regard to final magnitudes, we emphasize that only SGBDSN waveforms are used, specifically only those from S-13 stations within the SGBDSN, as required by IPR-003.

The preliminary earthquake catalog for FY02, as residing in the Datascope database, contained a total of 5249 earthquakes. The procedure for computing final locations prescribes that the arrival times and preliminary locations be extracted from the Datascope tables and reformatted for input to the program HYPOINVERSE (Klein, 1989); this was done with the program DB2PHS (STN # 10637-1.0). The procedure requires that a single velocity model be used for the entire suite of earthquakes; this model, called the "moonhof" model (Hoffman and Mooney, 1984), has the following structure:

Depth (km)	P velocity (km/s)
0.0	3.00
1.0	6.00
25.0	6.35
30.0	6.60
35.0	7.80

S-wave velocities are computed from P-wave velocities using a Poisson ratio of 0.25. Note that the velocity of the second layer in IPR-002 is given as 5.85 km/s, not 6.00 km/s. This alteration crept into the velocity model and has affected all SGBDSN locations since the start of operations in October 1995. A Non-Conformance Report (NCR # UNR-03-0011) was filed and has been closed. This NCR contains an impact analysis which basically states that the result of this error on locations is insignificant.

HYPOINVERSE was run in batch mode with the altered velocity model. A few hypocenters were

eliminated because they had four or less arrivals. At this point, events with large azimuthal gaps ($>300^\circ$) and with large horizontal error (> 5 km for one sigma) were culled out for review. Events just west of the Little Skull Mountain area were also reviewed because several of them were considered unreliable. This unreliability was due to the fact that, for many of these events, the only observing stations were LSC, FMW, STH, and CAF (3 or 4 of them), which are nearly in a linear configuration (see Figure 2-1). This review criterion eliminated several events. The procedure then calls for removing arrivals having residuals greater than 0.3 seconds. The program was rerun with these removed, and many additional events could not be located because the number of acceptable arrivals fell below five. Through all these criteria, 77 events were subtracted from the original 5249, less than 2%. None of these had a magnitude larger than 2.0. A total of 5172 events remained in the final catalog which is listed in Appendix 3. The final magnitudes (M_L) were then computed according to IPR-003.

Note that the catalog of events in Appendix 3 includes error bars (+/- one standard deviation) for the horizontal (erh) and vertical (erz) precision of the hypocenters. These errors, indicative of the location quality, are considerable in some cases (on the order of several km) and are generally greater for erz values than for erh ones. The density of these errors, in 1-km bins, is shown in Figure 2-7 (Q data, derived from DID # 012DV.014). In the case of horizontal errors, 96% of the events have standard errors < 2 km. For a 95% confidence ellipse and assuming a normal density of errors, it should be doubled to 4 km. Assuming a circular 95% confidence region, one computes the area as $\pi 4^2 \approx 50 \text{ km}^2$.

The results here must be weighed in relation to the assumptions (mostly programmatic) used in

producing the final locations. One of these assumptions was that the earth can be represented by a homogeneous, plane-layered model. This implies the use of a single 1-D velocity model for the entire network region. This “1-D earth” assumption has been inherent in all reporting since the start of seismic monitoring in 1978. We regard this assumption as satisfactory for the intended primary uses of the data. Further refinement of hypocenters through a 3-D model and through advanced relative location algorithms is beyond the scope of this report but may be important for future work in understanding details of faulting and tectonics in the Yucca Mountain vicinity.

Station corrections are often used with a 1-D model to improve locations; but we chose to not utilize them. This too has been true for all the earthquake catalogs produced since the start of seismic monitoring in the Yucca Mountain region. Again, ignoring such first-order terms is satisfactory for the intended primary uses of the data. We now have a large enough dataset to compute these terms but expect that they will be highly azimuthal and distance dependent: a sign of significant 3-D velocity heterogeneity. When 3-D location programs are applied to the hypocenters produced here, the station effects will be automatically and accurately accounted for.

Aside from the location precision indicated by the *erh* and *erz* values, there is the question of accuracy. Especially for events near the fringe of the SGBDSN network on the west side, the addition of analog readings, if available, should have improved both location precision and accuracy in nearly every case. However, it is important to note that, even with excellent station coverage in both distance and azimuth, locations can be significantly off. The non-proliferation explosion (NPE) of September 22, 1993, was recorded by the entire analog network and had excellently timed arrivals; but its computed location, with depth constrained to the known 0.4 km, was off by approximately 2 km horizontally (von Seggern and dePolo, 1994). The 95% confidence ellipse

around the computed epicenter had a semi-major axis of only 0.5 km and thus failed to cover the true location. This inaccuracy is due to the significant 3-D velocity variations in the southern Great Basin that are not accounted for in routine location with a 1-D plane-layered velocity model.

3. Seismicity Characteristics

3.1 Spatial Pattern of Earthquakes

Earthquake activity in the vicinity of Yucca Mountain has been described in numerous annual reports prior to this. For reference, the historical seismicity of 1868 to 1978 (Meremonte and Rogers, 1987; DTN # GS900983117411.004) is shown in Figure 3-1; and the seismicity for the years 1978-1995, when the area was monitored with the analog network, is shown in Figure 3-2. Also for reference, the seismicity for the years FY1995-FY2001, when the SGBDSN was operative, is shown in Figure 3-3. (The historical catalog data in Figure 3-1 is non-Q data; Figure 3-2 is a combination of Q and non-Q data for which the DTN #'s are listed in Appendix 1; and Figure 3.3 presents Q data for which the DTN #'s are also listed in Appendix 1.)

The historical catalog includes large uncertainties in locations and magnitudes, and spatial representation of actual seismicity may not be very accurate. Many earthquakes in the historical catalog have no assigned magnitude and are presumed to be $M < 5$ prior to 1932; $M < 4$ between 1932 and 1968, when the California networks started locating events in Nevada; and $M < 3$ after 1968 when instrumentation relating to the underground nuclear testing program was installed. The 1978-1995 data (SGBSN era) have much lower uncertainties in magnitudes and locations, and regional spatial patterns can be established. However, we speculate that much of the SGBSN-era activity (Figure 3-2) in the northwest NTS region consists of induced seismic events associated with underground nuclear tests conducted during the years 1978 through 1992. It is possible that they may even be aftershocks induced by high-yield, underground nuclear explosions (UNE) in the late

1960's and early 1970's (Hamilton et al., 1972). Many of these UNE events had magnitudes near or over 6.0; for a comparable M 5.6 earthquake at Little Skull Mountain in 1992, aftershocks are still be located at the rate of about 2 per day.

Since October 1, 1995, the seismicity within the Yucca Mountain region has been located with the SGBDSN, and a map of the activity in the period starting then and continuing until September 30, 2001 is shown in Figure 3-3. For this era the figure shows the continued dominance of aftershocks of the June 29, 1992, M 5.6 Little Skull Mountain (LSM) earthquake; they constitute roughly one-half of the SGBDSN catalog. This figure also illustrates the diffuse zone of activity associated with the M 4.7, 27 January 1999 Frenchman Flat earthquake and the continuing aftershock sequence east of LSM. A diffuse, approximately N-S trending, line of earthquakes between 116.8 W and 116.6 W, as also seen in the SGBSN plot of Figure 3-2, is reflected in the SGBDSN plot of Figure 3-3. The zone of activity near 37.2 N, 116.6 W seen in Figure 3-3 (called the Thirsty Canyon swarm) was preceded by earlier activity in Figure 3-2. In view of the fact that this swarm occurred near the end of a lineation in Figure 3-2 extending from northwest NTS, we speculate that this swarm activity may be related to earlier large underground nuclear tests in the northwest part of the NTS. Activity near the northeast corner of the NTS has been notably higher since the inception of SGBDSN monitoring when Figures 3-2 and 3-3 are compared and the differing time periods (18 years and 6 years, respectively) are taken into account. This was the area of the M 4.1 Groom Lake earthquake of 04/26/1999.

For the period of this report (FY02), Figure 3-4 shows the epicenters of the 5172 earthquakes located with the SGBDSN. (This figure presents Q data, with DID # 012DV.014.) The same epicenters, but without scaling by magnitude, are shown on a map of shaded elevation in Figure 3-5. The notable

features of the FY02 seismicity pattern are: 1) the large number of aftershocks near Little Skull Mountain (roughly 20 km southeast of the ESF), most of which are related to the M 4.4 earthquake there on 06/14/2002; 2) the cluster of events to the northeast of the LSM aftershocks in the Cane Springs Wash area, and 3) the cluster of mostly $M > 1$ events at the edge of the network (37.1N, 117.0W). The second cluster described here is in an area of only slight activity prior to FY02. The third cluster occurs in an area of diffuse activity prior to FY02. This may reflect the fact that the location of events in this area is probably improved significantly since the installation of station HEL (Figure 2-1) and since the conversion of station TYM from CMG-40 to S-13 sensors. Lastly, some activity near 37.2 N, 116.6 W, which is the site of the Thirsty Canyon swarm in 1996-1997, is still apparent in FY02.

The largest event in the FY02 catalog was the M 4.4 earthquake on 14 June 2002 in the Little Skull Mountain aftershock zone. We have named this event the "Little Skull Mountain II" earthquake. This event's symbol on Figure 3-4 is mostly obscured by the numerous aftershocks that followed it. Section 4 of this report will discuss that sequence in detail. The only other events with $M > 3$ in the FY02 catalog were a M 3.09 earthquake in the LSM aftershock zone on 5 May 2002 and an M 3.13 earthquake on 18 June 2002. (Note that another apparent $M > 3$ event at 36.5N, 116.6W is actually $M = 2.94$ but the plotting program puts it in the $M \geq 3$ class.) A total of 26 events had $2 < M_L < 3$ in FY02; almost all of which were aftershocks associated with the M 4.4 event.

3.2 Moment Rate

In the previous annual report (von Seggern and Smith, 2002), we discussed the fact that the moment

rate had significantly decreased in the past few years in the vicinity of Yucca Mountain and postulated that this may be the start of a longer-term trend. The M 4.4 event on 14 June 2002 was therefore somewhat unexpected. We extend our previous plot through the end of FY02 as shown in Figure 3-6. (This data is derived from the seismicity catalogs listed in Appendix 1 and is non-Q because it includes the non-Q 1978-1992 portion.) This plot only uses events with $M > 3$ and within 65 km of Yucca Mountain (station RPY, to be precise). The effect on the cumulative moment of neglecting all $M_L < 3$ earthquakes is less than 10%. Seismic moment is computed from magnitude by the Hanks and Kanamori (1979) formula:

$$\log_{10}M_0 = 1.5(M_L + 10.7)$$

The total moment is dominated by the LSM earthquake of 29 June 1992. Note that the seismic moment rate is extremely low prior to the LSM earthquake. No events with $M_L > 3.4$ occurred within the 65-km radius circle in the 13 years prior to the LSM earthquake. The period between the LSM and FF earthquakes has a notably greater rate than prior to the LSM earthquake. From the time of the Frenchman Flat (FF) earthquake (01/27/1999) until the Little Skull Mountain II earthquake, the moment release rate has been low compared to the few years prior to the FF earthquake, but not especially low compared to the years prior to the LSM earthquake.

The data in Figure 3-6, as was pointed out in von Seggern and Smith (2002) using data through FY01, do not strongly support the idea that an unusually long period of quiescence is underway; and the occurrence of the M 4.4 event on 14 June 2002 has further lessened support for any inference that a long-term quiescent period is underway. The longevity of the trend, if it might exist, will only be established with continued monitoring.

3.3 Depth Distribution

For the FY02 catalog, the distribution of hypocenter depths is shown in Figure 3-7 (Q data, based on DID # 012DV.014). Due to the dominance of LSM seismicity, the catalog was subsetted into LSM and non-LSM groups and separate depth distributions were formed. The LSM aftershock zone was defined as the rectangle (36.68, -116.35) to (36.78, -116.20). This graph is very similar to that for the previous year (von Seggern and Smith, 2002), except that the number of LSM events is much larger. Overall, non-LSM events occur in a broad source zone of 4-12 km. The number of events at 0-4 km depth for this group is probably biased by a significant number of events whose depth was not well determined; however, many earthquakes in the Rock Valley area, south of Little Skull Mountain, are known to have shallow depth. Specifically, the significant number of events overall with depth < 2 km, approximately 230 or 4% of the catalog, is probably a result of poor location quality and not indicative of actual shallow depth of faulting. Depths for the LSM events are more narrowly distributed, mostly in the 8-12 km range. Due to the dense station coverage in the LSM area, depths are more accurately computed than for the SGBDSN area as a whole, with very few having depths < 4 km.

The depth distributions shown on Figure 3-7 are not significantly different than those shown in previous SGBDSN seismicity reports. Moreover, the distribution of very shallow and relatively deep events (not shown) is also very similar to the distribution of the previous year (von Seggern and Smith, 2002). These events tend to lie in less dense areas of station coverage. The plot of hypocentral error versus event depth in von Seggern and Smith (2002) shows that the large majority

of the events have fairly well-determined depths but that many of the hypocenters computed to be shallow actually have large vertical error bars, indicating that the hypocentral depth is not well determined. It is likely that their true depths would fall in the range of > 4 km. It is important to note that the events with relatively deep hypocenters, say > 12 km, have fairly typical vertical errors (von Seggern and Smith, 2002); thus, we conclude that their computed depths are close to actual.

3.4 Magnitude Distribution and Threshold

As discussed in Section 2, the SGBDSN catalog magnitudes were computed using the original Richter (1935) M_L formula and attenuation relation, except for the fact that SGBDSN velocity seismograms were converted to pseudo-Wood-Anderson seismograms. Analysis of SGBDSN magnitudes in von Seggern and Smith (1997) showed that the Richter M_L formula applies sufficiently well to the SGBDSN region of coverage and should not introduce any bias. A good check on SGBDSN magnitudes can be made by comparing magnitudes of larger earthquakes with published magnitudes from the NEIC (National Earthquake Information Center, Golden CO) catalog. A summary of comparison data was made in von Seggern and Smith (2001); the conclusion was that there was no more than +0.1 unit bias for the SGBDSN magnitudes relative to the NEIC ones. Due to the recent low seismicity rate and consequent lack of adequately sized earthquakes, the only additional comparison for FY02 was the 14 June 2002 earthquake at Little Skull Mountain. The SGBDSN magnitude (M_L) of 4.42 is somewhat higher than the NEIS m_b of 4.3 but is below the Berkeley (BRK) M_L of 4.6. We have recognized that California network estimates of magnitudes in southern Nevada tend to be larger than Nevada network ones, and we are investigating this bias on a continuing basis.

For the 5172 earthquakes in the SGBDSN FY02 catalog, Figure 3-8 (Q data based on DID # 012DV.014) shows the cumulative recurrence curve. The threshold of complete detection appears to be approximately $M_L - 0.3$. This is somewhat below, by 0.2 or 0.3, that stated in previous SGBDSN seismicity reports. The explanation is surely due to the large preponderance of FY02 events in the LSM area where the current station density is quite high. As shown in von Seggern and Smith (1997), the threshold for events near the perimeter of the network is significantly greater, more on the order of $M_L = 1$.

The b value in the equation

$$\log_{10}(N) = a - b M_L$$

was determined by the method given in Aki (1965) for the data in Figure 3-8. The estimated slope of 0.94 appears to fit the data well until the tail at higher magnitudes. The slope of 0.94 agrees well with the slopes of 0.91 and 0.95 computed for the FY01 and FY00 data, respectively (von Seggern and Smith, 2001; von Seggern and Smith, 2002). The fit to the FY98-99 data by von Seggern et al. (2001) gave $b = 0.86$, and the fit to the FY96-97 data by von Seggern and dePolo (1998) gave $b = 0.77$. Thus the current data suggest a higher b -value than the earlier SGBDSN results. We note again that the number of relatively large earthquakes in FY00, FY01, and FY02 is significantly less than in previous years of SGBDSN monitoring, and this lack of larger events tends to give a higher b -value.

4. Analysis of the June 14, 2002, M 4.4 Little Skull Mountain, Nevada, Earthquake

4.1 Introduction

The June 14, 2002, M 4.4 earthquake that occurred within the aftershock zone of the M 5.6 June 29, 1992, Little Skull Mountain (LSM) earthquake can be interpreted to be the largest aftershock of the LSM sequence. This event took place approximately 20 km southeast of Yucca Mountain (Figure 4-1). The data of Figure 4-1 come from two sources: 1) the non-Q background is the relocation dataset of Smith et al., 2001, and 2) the FY2002 Q data is from DID # 012DV.014. As a result of an order of magnitude increase in the sensitivity and detection capability of the digital seismic network that was installed around Yucca Mountain in the mid-1990's, around 2900 aftershocks of the event were determined through September 30, 2002. In contrast, an equivalent number of events were located for the entire 1992 Little Skull Mountain sequence (mainshock M 5.6) based on data from the older analog network. We summarize the geometry of the aftershock distribution, present interpretations of the aftershock locations within the context of the seismotectonics of the LSM sequence and southern NTS region, and make interpretations from the regional strong-motion records regarding local site effects at Yucca Mountain relative to the LSM source region. Smith et al. (2001) and Meremonte et al. (1995) have written on the 1992 LSM sequence, and the 2002 earthquake can be interpreted as an aftershock to that earthquake. One interpretation from the present analysis is that the June 14 event is a complex source, most likely composed of two sub-events. This conclusion is based on a comparison of waveforms from several earthquakes recorded at the Lathrop Wells strong-motion station that show variable complexity in the time-series records. The peak acceleration for

the earthquake was recorded at the Little Skull Mountain station directly above the earthquake and its aftershocks (84 cm/s^2).

4.2 Distribution of 2002 Earthquake Activity

Early aftershock locations are of good quality due to the dense distribution of seismic stations surrounding the LSM area. In particular, a recently installed station on Paleozoic rocks at Stripped Hills south of LSM shows especially good signal-to-noise and closes the location gap to the south for the sequence. Minimal location gap (the largest solid angle in the epicenter stations distribution geometry) is a key parameter for confidence in earthquake locations. Figure 4-2a shows the distribution of early post June 14 earthquake activity plotted on relocations of the 1992 LSM aftershock sequence from Smith et al. (2001) and on the remainder of locations (from DID # 012DV.014) through 09/30/2002. Although the 2002 data plotted here is Q (DID # 012DV.014), the 1992 relocated data is not. This period of aftershock activity clearly shows the relationship to the more extensive 1992 aftershock zone. It also illustrates that 2002 activity primarily extended the entire LSM aftershock zone southward toward the Stripped Hills and the Rock Valley fault zone. Although this region of the LSM aftershock zone was active during 1992, it did not represent the primary zone of faulting during the June 1992 M 5.6 LSM mainshock. Figure 4-2b shows the entire set of 2002 aftershocks that were located with HYPOINVERSE, about 2900 events (from DID # 012DV.014). Again, these are Q data from DID # 012DV.014. The orientation for the perspective view (Figure 4-3) is also shown on Figure 4-2a. The recent activity is confined to the western edge of the 1992 LSM aftershock zone. From this relationship, the June 2002 sequence can be interpreted as additional LSM aftershocks. Note that the June 14 M 4+ event itself occurred near the hypocenter of the 1992 M 5.6 LSM mainshock and at nearly the same depth (LSM mainshock 11.7 km depth

from Smith et al., 2001). The NE-striking, SE-dipping 1992 LSM mainshock fault plane is defined by the NE alignment of aftershock activity extending NE from the 1992 LSM mainshock epicenter (Figure 4-2a) and 2002 activity; this seismicity forms the primary fault plane of the 1992 mainshock (striking NE and dipping steeply to the SE).

A perspective view (Figure 4-3) of June 2002 activity implies that the recent sequence has involved two faults within the LSM aftershock zone. This figure shows the best 349 events from a double-difference algorithm (Waldhouser, 2001) applied to the 2900 located earthquakes of the 2002 sequence. (This non-Q dataset is contained in the file /ymp5/ympev/operations/FY2002/catalog/selected.reloc.) One structure strikes NE and may represent the western extent of 1992 mainshock faulting, and another strikes approximately NS while dipping at a high angle (60-70 degrees) to the east. This subsidiary structure to the mainshock fault plane was suggested by Smith et al. (2001) from the distribution of LSM aftershocks and the NS-striking, normal-faulting focal mechanism of the 13 September 1992, M 4.5 aftershock. The 13 September 1992, event appears to have taken place on this structure and the 14 June 2002 event may have involved slip on this same structure as well. The sources used to construct the composite source below are also shown on Figure 4-2a (Evt #1; May 25, 2002, and Evt #2: June 18, 2002). The epicenter of the 14 June 2002 mainshock is between Evts #1 and #2. Therefore it appears that Evt #1 was on the 1992 mainshock fault plane and Evt #2 occurred on the subsidiary NS-striking structure to the south. This interpretation is consistent with the 14 June 2002 mainshock being a composite of faulting on two structures, as will be described in more detail below.

We now discuss the waveform data for these events. The weak-motion and strong-motion data from these events was gathered under IPR-001 and IPR-004. Programs involved in the data reduction to

obtain data for the figures in this section and for the remaining figures of this chapter are: TERRA2SAC (STN # 10642-2.0), REF2ORB (STN # 10640-1.6), and SAC (STN # 10085-00.46). Figure 4-4 shows the near-source stations that were used to calculate the local magnitude. The program MLCALC (STN # 10081-2.0) was used in this calculation. (The data for the magnitude calculations came from MOL # 20020912.0548 for the permanent seismic network, including the telemetered strong-motion stations.) Most near-source velocity instruments clipped on the record, and local telemetered strong-motion stations were mainly used to determine the event magnitude. Figure 4-5 summarizes a number of fault-plane solutions for the mainshock and two other principal events of the most recent activity, as listed in Table 4.1. Figure 4-5a shows the U.C. Berkeley regional moment-tensor solution developed from broadband recordings. The complex faulting process suggested above based on the geometry of the aftershock distribution may result in the large CLVD component of the UC Berkeley moment-tensor solution (Figure 4-5a), where the regional waveform mechanism reflects faulting on two fault planes. Figure 4-5b shows a first-motion, short-period focal mechanism for the June 14 event. This plot and the ones for the subsequent figures 4.5c and 4.5d were made with the program FPFIT (STN # 10083-1.0). The strike of north-trending fault plane is rotated 15 degrees westward relative to the LSM mainshock mechanism of Meremonte et al. (1995) and Smith et al. (2001). This is consistent with the general N-S alignment of the 2002 aftershock activity. Figure 4-5c is the short period mechanism for the May 25 event and Figure 4-5d is that of the June 18 aftershock. From these well-constrained, near-source mechanisms, it is clear that the May 25 earthquake is on a separate structure than the June 14 mainshock and June 18 aftershock.

4.3 Faulting Within the Aftershock Zone

From the aftershock and focal mechanism data, the 1992 LSM mainshock and the June 14 event may have both initiated at the intersection of the two structures identified in both the 1992 and the 2002 aftershock distributions. Also, the LSM mainshock may have been a complex faulting event involving down-dip motion on the primary NE-striking, SE-dipping fault plane with a small component of down-to-the-east dip-slip motion on this subsidiary structure (Smith et al., 2001). The left-slip component in the LSM mainshock focal mechanism (Smith et al., 2001) and the June 14 mechanism (Figure 4-5b) may both be reflecting this faulting process. In this interpretation, both the 1992 M 5.6 and 2002 M 4.4 initiated at the intersection of a NE-striking, SE-dipping fault and N-striking, E-dipping structure. These events are less than 1 km epicentral distance apart and are at nearly the same depth (locations suggest a difference of 200 meters in depth). Whereas the 1992 event involved primary moment release on the NE-striking fault, the 2002 event was primarily confined to the N-striking fault. It is likely that the events included faulting on both of these structures. Displacements on these structures are inconsistent with the geometry and sense of motion for local mapped Quaternary faults on LSM and may therefore represent a modern style of deformation. This is consistent with the low slip rate tectonics of the southern NTS region. This faulting mechanism would result in difficulties in modeling the near source spectra based on the assumption of a ω^{-2} Brune (1971) source model as well as in determining the regional moment tensor; the source mechanism may involve two distinct events, possibly on different structures, in a complex faulting process.

4.4 Constraints on a Complex Faulting Model

In comparing the waveforms from the strong-motion station at Lathrop Wells, Nevada (Figure 4-1), the 14 June 2002 mainshock record (Figure 4-6) can be reproduced as a composite of the May 25 and June 18, 2002, M 2.8 events, also recorded at Lathrop Wells. (The data for this figure comes from MOL # 20020920.0275.) Both of these M 2.8 earthquakes show simple waveforms whereas the 14 June 2002 mainshock is clearly a complex record (Figures 4-6, 4-7). Time shifting Evt #2 relative to Evt #1 by 0.8 seconds with respect to the P-wave arrival time and scaling the amplitudes appropriately for each and simply adding the time-series records, we can nearly reproduce the mainshock records even at high frequencies (Figure 4-6). Figure 4-7 shows the fit at long periods. In previous studies in the Yucca Mountain area, we have measured the slope of the spectra at high frequencies from local earthquakes to estimate the parameter 'kappa', a measure of near surface attenuation and therefore a critical parameter for estimates of potential ground shaking from larger earthquakes. Significant events, such as the June 14 earthquake, are therefore important for establishing 'kappa' estimates for less frequent $M > 4$ local earthquakes. However, because it is demonstrated that the June 14 earthquake involves a complex source, kappa estimates, whose typical calculation is based on assumptions of a simple source model and simple spectral shape, have not been determined for the June 14 strong motion records.

4.5 Strong-Motion Records and Ground-Motion Observations

The June 14 earthquake was recorded on all 9 stations of the Yucca Mountain strong-motion network that consists of 16-bit standalone (non-telemetered) triggered accelerometers as well as 9 of the 10 SGBDSN telemetered stations recently configured with accelerometers (YCW was down). SGBDSN stations record triggered 16-bit acceleration time-series. Table 4-2 is a summary of the

peak accelerations and the station distances from the Yucca Mountain area for the June 14 earthquake. Figure 4-8 is a compilation of the peak ground accelerations (PGA) recorded at Yucca Mountain area strong-motion stations in cm/s^2 . Largest peak accelerations were recorded at the Little Skull Mountain cliff station (84 cm/s^2) and at Lathrop Wells (45 cm/s^2). Figure 4-9 shows the attenuation of PGA with distance for the June 14 data along with a predicted attenuation curve from Yucca Mountain PSHA activities (Wong and Stepp, 1998) with respect to an M 4.4 event. It is emphasized that there is no one single prediction of PGA from that study because those predictions were developed by several “experts”. In Figure 6-1 of that report, the Somerville prediction line is somewhat of a median prediction among the six experts, with perhaps $\pm 30\%$ range in all the predictions. Therefore, for purposes of simple comparison with the actual PGA’s, we used the Somerville regression coefficients a_i listed in Appendix I of that report as “Horiz PGA”. The prediction equation is taken from eq. 6-1a of the PSHA study; this equation is applicable to small earthquakes for which $M < 6.25$:

$$\mu = a_1 + a_2 (M - 6.25) + a_6 (8.5 - M)^2 + [a_3 + a_5(M - 6.25)] \ln[(R^2 + a_8^2)^{1/2}] + a_7 F$$

where

$\mu = \ln(\text{PGA})$ in g

M = event magnitude

R = “rupture” distance (km)

F = 1 (a switch to give a_7 weight for normal faults)

In this case, the magnitude of the 14 June 2002 LSM earthquake is 4.42. Although eq. 6-1a contains

two terms for weighting the hanging-wall versus the foot-wall side of a normal fault, they are actually zero due to the relatively small magnitude of this event (see eq. 6-2 of the PSHA study) and so not used here. Due to the small area of the rupture plane for this earthquake ($< 1 \text{ km}^2$), the “rupture” distance is well approximated by the hypocentral distance, using the location depth of 11.9 km. Using the Somerville coefficients and converting hypocentral distance to epicentral distance r , we get simply:

$$\mu = 1.234 - 1.800 \ln[(r^2 + 196.4)^{1/2}]$$

Conversion to acceleration a in linear units of cm/s^2 gives:

$$a = 980 \exp\{1.234 - 1.800 \ln[(r^2 + 196.4)^{1/2}]\}$$

This expression was computed at coarse intervals of 10 km for Figure 4-9. The fit to the actual data must be viewed in light of the fact that the PSHA study predicted the ground motion at repository level, with the overburden stripped off, presenting a medium with a free surface at repository level. Thus the free-surface effect is in both the actual and predicted points, but the attenuation effect of the repository overburden is not. The attenuation effect of this roughly 300-m overburden is not yet well determined. The PSHA curve agrees somewhat well with the PGA’s for the 14 June 2002 event, but one cannot attach much importance to this conclusion due to the fact that the PSHA did not predict true surface accelerations. Variability in actual PGA’s reflects differences in site conditions at local strong-motion stations; such real effects make it even more difficult to compare this data with PSHA results.

Figure 4-10 shows the acceleration time history from the YMP Strong Motion Network station at Lathrop Wells and two components of the strong-motion records at SGBDSN station LSC on the crest of Little Skull Mountain (the north component was not operating). Station LSC is nearly directly above the hypocenter of the June 14 earthquake. It is located on Pliocene basalts forming the north-trending, gently dipping slope of Little Skull Mountain; these basalts overlay the Miocene tuff sequence. Station LWLS is located on a thick section of sediments (probably on the order of 300-600m) that compose the northern extent of Amargosa Valley at Lathrop Wells. The base of the sedimentary section is most likely Paleozoic based on the local Paleozoic outcrops to the east of Lathrop Wells. These two distinct geologic conditions are most likely reflected in the waveforms at the respective stations. Typical of LSC records for LSM earthquakes, the June 14 waveforms are complex and the S-wave train shows multiple pulses that could represent multi-pathing in the shallow tuff sheets and/or an underlying Paleozoic geomorphic surface that was buried by the Miocene tuffs. The LSC record is also likely conditioned by the topographic effect imposed by the steep, south-facing LSM escarpment. In contrast, due to the thick sedimentary section at Lathrop Wells, records at this station often show clean and simple S-wave pulses for many events. This may also result from the lack of Miocene tuffs along the ray path to Lathrop Wells. On the other hand, significant high-frequency attenuation is expected from the thick sedimentary section that will be complicated by amplification, at relatively longer periods, in the low-velocity sedimentary section. Lathrop Wells is about 11 km epicentral distance from the sources. Contrary to many recordings on tuffs in the Yucca Mountain area, simple pulses from LSM earthquakes are often observed at Lathrop Wells.

Figure 4-11 shows the corresponding acceleration spectra with the Lathrop Wells and LSC time-series records. Spectra for all events in this report are determined from 5-second time windows that

are demeaned and tapered prior to performing the FFT. Spectra were determined in the SAC processing system (STN 10085-00.46). The relative differences in the high-frequency component of the spectra at LSC and LWLS are apparent in the comparison of the spectral amplitudes.

Figure 4-12 shows the velocity time-series from station AL5 (in the ESF at Alcove 5) at a depth of about 300 meters from the surface and surface station RPY in the repository. The relative amplitudes between RPY and AL5 are due to the free-surface effect that increases the RPY surface amplitudes relative to those on underground records at AL5. The amplification of RPY relative to AL5 is due to the low surface velocities balanced by the seismic attenuation and scattering in the upper 300 meters. Differences in the AL5 and RPY waveforms result from the complexities in the structure of the tuff sequence and local surface conditions at RPY. Station AL5 is richer in high-frequency energy, and the slope in the decay at high frequencies is relatively less than at station RPY (Figure 4-13). Also, the spectral amplitude in the 2-10 Hz band at RPY is larger, reflecting the free surface and near-surface amplification effects. Figure 4-14 shows the RPY/AL5 spectral amplitude ratio.

Figures 4-15 and 4-16 compare the records at strong-motion station MDVS (Midway Valley) and WHBS (Waste Handling Building). MDVS is located about 300 meters east of the ESF pad on Midway Valley sediments, and WHBS was installed on the 50x150 foot concrete slab of the sheet metal shop facility near the proposed Waste Handling Building. WHBS shows a clear resonance near the 10 Hz band (Figure 4-16) that dominates the waveforms. These amplitudes are largest on the north component, which is the longer aspect ratio of the structure and may be reflecting the concrete slab itself. This resonance may also be the result of engineered fill on the ESF pad. The amplitudes at WHBS are higher by about a factor of 2 relative to MDVS. In spite of this resonance,

WHBS implies stronger attenuation in high frequencies (steeper roll-off in the 10-50 Hz band – Figure 4-16 WHBS), again possibly due to the pad or the engineered fill material. This resonance at 10 Hz is not seen on any other strong-motion records and is obviously some type of local shallow site effect unique to WHBS. Recently installed strong-motion instruments on the ESF pad will better resolve the local site effects.

Figures 4-17 and 4-18 compare closely located stations TYMS and SYMS. TYMS is located on the crest of Yucca Mountain and SYMS is about halfway down the steep, west-facing wall of upper Solitario Canyon. These stations are within about 1 km of one another. The time-series at upper Solitario has higher amplitude than that for the station at the crest of Yucca Mountain and is distinctly richer in high frequencies. This station may be incorporating resonances in the drainage sediments in Solitario Canyon, or this difference may reflect the location of the station on a steep slope. In other words, these stations incorporate different local topographic effects: TYMS on the crest of the mountain and SYMS on a steep slope. Whatever the case, this comparison illustrates the complexities in generalizing ground motion effects over large areas when very local effects, including source azimuths relative to local structures, ultimately control the frequency content and peak ground motions at a site.

4.6 Comparisons with 1992 Strong-Motion Recordings at Lathrop Wells

Figures 4-19 and 4-20 compare time-series and acceleration spectra from the 14 June 2002 and 13 September 1992 Little Skull Mountain M 4.4 and M 4.5 earthquakes, respectively. The 1992 event was recorded on the Blume strong-motion network station that is co-located with the modern station at Lathrop Wells. (Although the 2002 data is Q data, the status of the 1992 Blume data is non-Q.)

These events show similar focal mechanisms, hypocentral depths, and magnitudes (Smith et al., 2001, discuss the 13 September 1992 event). The relative complexities in the sources are apparent in the time series (Figure 4-19). The simple S-wave pulse in the 13 September 1992 record implies a simple source; whereas, in comparison, the 14 June 2002 event clearly indicates a complex event. Therefore, it is apparent that simple events in the Little Skull Mountain source region can be identified at Lathrop Wells and that we can therefore use this station to make first-cut assessments of the complexities of LSM sources. Comparisons of the acceleration spectra for these events at Lathrop Wells also indicate the relative differences in the frequency content of the sources. Therefore, generalizing about source mechanism parameters in the Little Skull Mountain area may underestimate the necessity for evaluating source complexities in isolating ray-path and site-attenuation parameters with respect to the resulting ground-motion estimates at Yucca Mountain for earthquakes in this source region.

5. Death Valley Seismicity

Earthquakes in the Death Valley region had been reported by the USGS (Harmsen 1994, and references therein) from 1978 through September 1992. In October 1992 NSL obtained the seismic monitoring task for the Yucca Mountain Project. The record of seismicity in Death Valley has been somewhat non-uniform since 1992 because of the transition from the analog network to the site-specific digital network in late 1995. The analog stations in Death Valley National Park were retained after this transition though. We only began to again treat Death Valley seismicity in the FY00 and FY01 seismicity reports (von Seggern and Smith, 2001; von Seggern and Smith, 2002); this report discusses the seismicity for FY02.

In January 2000 NSL combined its digital and analog stations into a single system, called Antelope, for data collection and analysis, as discussed earlier in this report. Event location was notably improved in the Death Valley region due to the availability of the Yucca Mountain digital stations in routine analysis. In addition, it was now possible to compute Richter local magnitudes for most events in this region. Especially in the past year, the addition of digital stations HEL and LEC within the eastern portion of the park has improved location capability for the Death Valley region. We have created an Antelope-derived catalog for FY02 for the southern Great Basin, including the Death Valley region. (This catalog was derived from the Antelope “reno” tables in the directory /ymp16/catalog of machine “electrum”.) Local magnitude M_L was used if available; in those few cases where only duration magnitude was available, we converted it to local magnitude using the relationship given in von Seggern and Smith (1997):

$$M_L = -1.24 + 1.31M_D$$

The Death Valley earthquake locations and magnitudes used here are not Q data; this data is in DID # 012DV.018. The epicenter plot of this dataset is shown in Figure 5-1 on a shaded digital elevation map so that the relation of seismic activity to tectonic features can be more easily seen. Except for $M > 3$, all earthquakes are plotted with the same symbol size. Within the current boundary of the park as shown, the largest event in FY02 was the 02/25/2002 M 3.4 earthquake in the southern part of the park. In addition, another $M > 3$ earthquake occurred just within the park at the north end. A cluster of events occurred just outside the southwestern part of the park and near the northern tip of the Slate Range. The largest event in this cluster was an M 4.3 event on 09/28/2002, and it was preceded by an M 4.0 event on the same day.

The prominent cluster of events near (37° 20' N, 117° 10' W) is the continuing aftershock sequence of the 08/01/1999 M 5.7 Scotty's Junction earthquake (von Seggern et al., 2001). There are two other small clusters southwest of the aftershock sequence; and these align with the Scotty's Junction sequence along an azimuth of roughly N30E, which is nearly in agreement with the azimuth (~N20E) of the preferred fault plane of the Scotty's Junction earthquake. This orientation would be consistent with a conjugate plane for the Furnace Creek Fault that nearly parallels the park's eastern border (California-Nevada line); however, there is no particular support for this interpretation from the topography in Figure 5-1. Neither is there any apparent expression in the seismic activity of the well known Furnace Creek and Death Valley Faults. Overall, except for the clusters mentioned here, the seismic activity in Death Valley National Park and its immediate surroundings is diffuse. Moreover, it does not readily relate to physiographic appearances.

6. Earthquakes Near Yucca Mountain

From May 1995 through September 2001, 21 earthquakes have been documented within 10 km of station RPY which is located directly above the ESF (von Seggern and Smith, 2002). Figure 6-1 shows a plot of the seismicity in FY02 within roughly 15 km of station RPY. (This figure presents Q data from DID # 012DV.014.) For FY02 we located five more earthquakes within the radius of 10 km from station RPY; these were all east of the ESF tunnel. All had magnitudes < 0.0 . One additional earthquake was located within the southern Yucca Mountain block and one in Crater Flat; both had $M < 0.0$. The five inside the 10-km radius and the 2 additional events in the south Yucca Mountain block and in Crater Flat are listed in Table 6-1. Depths of these events fall in the range of roughly 4-8 km, except for one (03/11/2002) at 12 km. The event with the anomalous 12 km depth was carefully reviewed, and its depth was judged to be correct. Station coverage (Figure 2-1) is excellent for all of these earthquakes, with one or more stations within one focal depth; therefore hypocenters are well constrained. Due to the small size of the FY02 events in Table 6.1, focal mechanisms could not be determined for any of them.

The recurrence rate established by earthquakes within 10 km of Yucca Mountain (centered at station RPY) was examined in von Seggern et al. (2001) and shown to be significantly less than for the entire area enclosed by the SGBDSN or for the southern Great Basin as a whole. The three additional events of FY01 and the five additional ones in FY02 do not significantly add to the total event list, are roughly what is expected, and thus do not change this conclusion. After seven years of monitoring, the average rate in the 10-km circle is roughly three events per year, with most magnitudes being less than zero.

7. Focal Mechanisms

The determination of focal mechanisms for earthquakes in the SGBDSN FY02 catalog was done in a manner closely following that reported in von Seggern and Smith (1997) using observed P-wave polarities. The actual program used for determining focal mechanisms is FPFIT, V1.0 (STN 10083-1.0) (Reasenberg and Oppenheimer, 1985).

We have combined data from the SGBSN analog network with that from the SGBDSN digital network to obtain improved datasets for determination of focal mechanisms. Since 01/01/2000 when we began processing all data through Antelope, combining data from the two networks is simply automatic because both networks are processed together. Note, however, that the number of analog stations that were available in the southern Great Basin became small by FY02 (Figure 2-2).

Due to the concentration of events in the LSM area after the 14 June 2002 event, it was decided to not develop focal mechanisms for events in this area, except for the three already covered in Section 4. A very large number of focal mechanisms already exist for this area (von Seggern et al., 2001), and any further information developed from the FY02 data would be mostly redundant. Excluding the LSM area then, a preliminary list of 108 events was made by searching the final FY02 catalog for events larger than $M = 1$ with greater than 15 stations associated to them. The input data for FPFIT, including the first motions, were taken from the HYPOINVERSE “arc” output. Before running FPFIT though, a thorough review of all first motions was done because the initial first motions are computer-generated. In this review roughly a quarter of the first motions were changed. Also, some first motions at additional stations, not initially picked, were found to be satisfactory.

Changes and additions were hand-entered into the “arc” file. A few events (19) were found to have insufficient data or to not have a large enough azimuthal range of data to provide reliable focal mechanisms, and these events were removed.

Program FPFIT was run on the data of the 89 events. Details describing the methodology of this program are given in von Seggern and Smith (1997). After an initial run of FPFIT, not all mechanisms were well defined. Most of the events showing multiple solutions were rejected. However, in a few cases it was reasonable to prefer one solution over the other(s). For instance, where only one of the multiple solutions was tectonically viable (for instance, no near-horizontal fault plane), this solution was accepted. Another situation in which one solution might be objectively preferred over the others is when one or more critical stations with clear first motions agrees with only one of the solutions. A few discrepant first motions were reviewed and changed if thought to be wrong, and a final run of FPFIT was made.

Table 7-1 lists the 46 events for which acceptable focal mechanisms were determined, including the three LSM ones previously mentioned. This table uses the “fps” format in which FPFIT outputs its results. Figure 7-1 shows all the focal mechanisms listed in the table. (Both the table and the figure are Q data from DID #012DV.015. Note that magnitudes on the figure are incorrectly listed as “0.0” whereas Table 7.1 lists them correctly.)

We plot the azimuth and dip of the tension and pressure axes in Figure 7-2 on the lower focal hemisphere. (These data are derived from the data of DID # 012DV.015 by a simple 3-D trigonometric transformation and are thus Q.) These new mechanisms generally agree with the overall trend established by a review of over 400 mechanisms in von Seggern et al. (2001); this trend

is approximately WNW-ESE for the tension axes. However, there are several mechanisms with their tension axis rotated towards the north from the mean reported in von Seggern et al. (2001). These mechanisms happen to all be associated with the seismic activity in the north-central part of the Nevada Test Site on Figure 3-4 at approximately 37.15° , -116.25° . One event (05/28/2002) on Figure 7-2 has a very anomalous tension axis at roughly 10° east of north. Because it is well constrained by the first motions (Figure 7-1), this result is acceptable. The particular event associated with this mechanism plots on Pahute Mesa near roughly 37.3° , -116.4° in the northwest part of the Nevada Test Site on Figure 3-4.

8. Observed Explosions

In previous years, explosions were routinely observed within the southern Great Basin on the seismic recordings of the SGBDSN stations. These explosions were recognized simply by their signal character in almost all cases and were generally ignored in post-processing. A few special cases, such as known tests on the Nevada Test Site, were located and analyzed to varying degrees. Signal features characteristic of explosions include: 1) all compressional first arrivals, 2) emergent arrivals due to ripple-firing in quarry blasting, 3) “ringing” appearance due to the same ripple firing, 4) prominent surface waves due to very shallow or surficial sources, 5) lack of clear S waves, 6) similarity among the envelopes of the traces on all three components and 7) a depleted high-frequency component relative to earthquakes. The three-component recording of SGBDSN stations has made it simpler to positively identify blasts as compared to the predominantly single-component SGBSN analog network.

During FY02 the following approach was used in treating possible explosions seen on SGBDSN records. Using the automatic list of Antelope events, analysts identified events with the above characteristics as blasts and attempted to locate them in all cases, constraining the depth to zero. Only a few were unable to be located. When all of FY02 was processed by the analysts, a search of the Antelope catalog was made for events that were identified as blasts by the analysts and that fell within 65 km of station RPY at Yucca Mountain. Appendix 4 lists the 36 events found, and Figure 8-1 shows a plot of their epicenters. (These data, taken from the preliminary event lists, are non-Q; they are contained in DID # 012DV.017). The presumed blasts in FY02 are mostly east of Mercury, Nevada, on the NAFB range and are assumed to be ordnance explosions. Only two blasts measured

$M > 1$, with one being on NTS. The presumed blasts on NTS are assumed to be related to miscellaneous construction activity. The threshold of detection for blasts within the SGBDSN has been established from a few confirmed blasts to be roughly 100 lbs of explosive. This threshold will vary considerably throughout the SGBDSN.

9. Summary

In FY02 the SGBDSN comprised 30 digital sites and performed at a highly reliable level, with over 99.6% uptime in data collection at the central recording site. For FY02 nearly 5300 earthquakes were located within the coverage of the SGBDSN network (defined as 65-km radius around station RPY); of these, 5172 earthquakes were well enough located to be included in the FY02 seismicity catalog. Aside from the earthquakes detected with the network, 36 presumed manmade events were identified and located in FY02.

Only one earthquake in FY02, the M 4.4 earthquake on 14 June 2002 near Little Skull Mountain, was large enough to generate usable data on the strong-motion network. This event caused accelerations of 0.015 to 0.032 g near the north portal of the ESF, at an epicentral distance of roughly 18 km, and nearly 0.1 g at station LSC above the hypocenter. The accelerations at the ESF are roughly in agreement with what is predicted in the PSHA study for Yucca Mountain. This earthquake occurred within the aftershock zone of the 1992 Little Skull Mountain earthquake; if taken to be an aftershock, it is the largest since an M 4.5 event on 13 September 1992. The faulting mechanism of the current event is complex, being somewhat well modeled by the waveforms of two smaller events with distinctly differing mechanisms. The current event occurred near the apparent junction of two faults, one being that which was originally ruptured in the 1992 earthquake and which trends NE and the other being that which is associated with some of the aftershocks since 1992 and which trends northerly and dips steeply.

For FY02 a total of 46 events in the SGBDSN catalog were large enough to have focal mechanisms

reliably determined. Generally, the tension axes of the mechanisms cluster closely at low dip angles and at azimuths around 45° west of north, or its opposite at 45° east of south. The pressure axes are more scattered, showing a broader range of dips, but aligning generally along 45° east of north. This result generally agrees with focal mechanisms previously reported for the SGBDSN monitoring area, but includes several events in the north part of the NTS with more north-trending tension axes than expected.

In FY02 five more earthquakes were located within 10 km of the proposed repository (specifically, station RPY). None of this group had an $M_L > 0.0$. This low seismicity rate is about normal compared to the rate established in prior years of SGBDSN monitoring. In addition, one more event was located within the southern part of the Yucca Mountain block, although at greater than 10 km from RPY, and another event was located in Crater Flat where activity is generally very low.

Seismicity during FY02 in the Death Valley area included an M 4.3 event just to the southwest of the park boundary. Two events with $M > 3$ occurred within the park boundaries. No clear correlations of seismicity with the prominent faults of this area, Death Valley and Furnace Creek, are apparent. We judge that hypocenter locations and detection thresholds have improved within the park area due to the installations of stations HEL and LEC within the park boundaries in the spring of 2002.

References

- Aki, K., 1965. Maximum-likelihood estimate of b in the formula $\log \tilde{A} = a - bM$ and its confidence limits, *Bull. Earthquake Res. Inst., Tokyo Univ.*, 43, 237-239.
- Hamilton, R M, B. E. Smith, F. G. Fischer, and P. J. Papanek, 1972. Earthquakes caused by underground nuclear explosions on Pahute Mesa, Nevada Test Site, *Bull. Seism. Soc. Am.*, 62, 1319-1341.
- Hanks, T. C., and H. Kanamori, 1979. A moment magnitude scale, *J. Geophys. Res.*, 84, 2348-2350.
- Harmsen, S. C., 1994. Preliminary seismicity and focal mechanisms for the southern Great Basin of Nevada and California: January 1992 through September 1992, U. S. Geological Survey Open-File Report 93-369.
- Hoffman, L. R., and Mooney, W. D., 1984. A seismic study of Yucca Mountain and vicinity, southern Nevada — Data report and preliminary results, U. S. Geological Survey, Open-File Report 83-588.
- Klein, F. W., 1989. Users guide to HYPOINVERSE, a program for VAX computers to solve for earthquake locations and magnitudes, U. S. Geological Survey Open-File Report, 89-314, TIC # 243752.
- Meremonte, M. E., Gomberg, J. and Cranswick, E., (1995). Constraints on the 29 June 1992 Little Skull Mountain sequence provided by robust hypocentral estimates: *Bull. Seism. Soc. Am.*, 85, 1039-1049.
- Meremonte, M. E., and Rogers, A. M., 1987. Historical catalog of southern Great Basin earthquakes 1868-1978, U. S. Geological Survey, Open-File Report 87-80.
- Quinlan, D., 1998. A tutorial for Datascope: the ASIS relational database system, Boulder Real Time Technologies, Inc., Boulder, Colorado, TIC # 244129.
- Reasenber, P. A., and Oppenheimer, D., 1985. FPFIT, FPLOT, and FPPAGE: Fortran computer programs for calculating and displaying earthquake fault-plane solutions, U. S. Geological Survey, Open-File Report 85-739, TIC # 230395.
- Richter, C. F., 1935. An instrumental earthquake magnitude scale, *Bull. Seism. Soc. Am.*, 25, 1-32.
- Smith, K.D., Brune, J.N., Savage, M., dePolo, D.M., and Sheehan, A. (2001). The 1992 Little Skull Mountain earthquake sequence, *Bull. Seism. Soc. Am.*, 91, 1595-1606.

Von Seggern, D., and D. DePolo, 1994. Seismicity for the southern Great Basin of Nevada and California in 1993, report to the Yucca Mountain Project, DOE–YMSCO, Las Vegas NV (MOL #19980310.0113)

Von Seggern, D. H., and K. D. Smith, 1997. Seismicity in the vicinity of Yucca Mountain, Nevada, for the period October 1, 1995, to September 30, 1996. Report to the Yucca Mountain Project, DOE–YMSCO, Las Vegas NV (MOL #19981124.0334).

Von Seggern, D. H., and D. M. dePolo, 1998. Seismicity in the vicinity of Yucca Mountain, Nevada, for the period October 1, 1996, to September 30, 1997. Report to the Yucca Mountain Project, DOE–YMSCO, Las Vegas NV (DTN #MO980683117412.000).

Von Seggern, D. H., G. P. Biasi, and K. D. Smith, 2000. Network operations transitions to Antelope at the Nevada Seismological Laboratory, *Seism. Res. Lett.*, 71, 444-448.

Von Seggern, D. H., K. D. Smith, and G. P. Biasi, 2001. Seismicity in the vicinity of Yucca Mountain, Nevada, for the period October 1, 1997, to September 30, 1999. Report to the Yucca Mountain Project, DOE–YMSCO, Las Vegas NV (MOL #20010725.0221).

Von Seggern, D. H., and K. D. Smith, 2001. Seismicity in the vicinity of Yucca Mountain, Nevada, for the period October 1, 1999, to September 30, 2000. Report to the Yucca Mountain Project, DOE–YMSCO, Las Vegas NV (MOL #20010725.0220).

Von Seggern, D. H., and K. D. Smith, 2002. Seismicity in the vicinity of Yucca Mountain, Nevada, for the period October 1, 2000, to September 30, 2001. Report to the Yucca Mountain Project, DOE–YMSCO, Las Vegas NV (DTN #MO0205UCC012DV.008).

Waldhauser, F., 2001. HYPODD – A Program to Compute Double-Difference Hypocenter Locations, Open-File Report 01-113, U. S. Geological Survey, Menlo Park, California.

Wong, I. G., and J. C. Stepp, 1998. Probabilistic seismic hazard analysis for fault motion displacements and vibratory ground motion at Yucca Mountain, Nevada: Final Report, Yucca Mountain Project, Las Vegas, Nevada (MOL #19980619.064)

List of Tables

- 4-1. Summary of Primary 2002 LSM Event Locations.
- 4-2. Peak Accelerations from the June 14, 2002, Earthquake.
- 6-1. Earthquakes Near Yucca Mountain in FY2002.
- 7-1 Earthquake Focal Mechanisms for FY2002

Table 4-1.

Summary of primary 2002 LSM event locations.
Q data - DID #012DV.014

	Origin	Time	Longitude	Latitude	Depth	ML	
5/25/2002	(145)	12:03:32.824	-116.2996	36.7261	9.4	2.79	#1
6/14/2002	(165)	12:40:44.589	-116.2994	36.7175	11.9	4.42	
6/18/2002	(169)	16:24:31.533	-116.3090	36.7150	11.2	2.80	#2

Table 4-2.
 Peak Accelerations from the June 14, 2002 Earthquake
 Q data - derived from source data in MOL #'s 20020920.0275 and 20020912.0548

Peak Accelerations Recorded from the
 14 June 2002 Little Skull Mountain Earthquake

Station	DIST km	UP cm/s ²	N-S cm/s ²	E-W cm/s ²
LSC	2.9	85.6	-	83.7
FOCS	7.5	16.4	32.0	27.8
SPRS	11.6	22.2	45.9	27.6
LWLS	11.7	24.0	44.9	41.0
S Y M	13.3	25.4	31.9	21.9
CAF	14.2	17.3	32.7	21.8
FRG	15.5	5.8	10.8	6.9
MDVS	18.3	11.3	13.5	14.8
WHBS	18.5	16.9	31.7	20.6
EXHS	18.5	11.5	12.5	15.2
TYMS	20.0	6.1	8.5	9.0
SYMS	20.2	13.9	8.0	13.7
RPY	20.6	9.1	9.4	6.6
AL5	21.1	3.1	3.7	2.9
SCF	22.2	4.5	6.1	6.2
S T O	22.4	18.5	20.6	13.6
CRF	23.4	3.5	3.7	4.0
WCTS	30.0	3.7	3.4	7.4

Notes:

DIST is the epicentral distance.

Peak Accelerations are estimated from one half the maximum
 peak to peak values on the accelerograms.

Table 6-1

Earthquakes Near Yucca Mountain in FY2002
(Q data from DID #012DV.014)

date			time			latitude		longitude		depth	mag.
year	mo	da	hr	mn	sec	deg	min	deg	min	(km)	ML
2002	03	11	02	33	12.54	36	51.83	116	20.74	11.75	-0.32
2002	05	15	16	39	48.54	36	51.04	116	22.75	7.65	-0.27
2002	07	03	08	16	00.00	36	50.80	116	23.34	3.54	-0.42
2002	08	02	01	24	07.44	36	49.54	116	34.32	4.54	-0.25
2002	08	04	15	50	22.59	36	44.49	116	27.99	6.07	-0.29
2002	09	11	04	42	11.36	36	51.35	116	20.94	4.27	-0.19
2002	09	16	17	21	34.17	36	49.81	116	22.76	5.18	-0.50

Table 7-1
Focal Mechanisms for FY2002
(Q data—DID #012DV.015)

date	origin time	latitude	longitude	depth	mag	# gap	del	TT	hor	ver	dip	dip	rake
Fj	nobs	avwt	stdr	delta^		(km)	ML	rms	err	err	dir	ang	
	hhmm	sec	deg	min	deg	min							
strdiprak													
20011214	1917	35.01	36-57.10	116-39.26	9.94	1.01	40 77	9.0	0.13	0.3	0.7	150	80 50
0.02	21	0.12	0.66	0.00	20	20	45						
20011220	1309	15.34	37-00.57	116-12.70	8.68	1.27	37 93	12.0	0.13	0.3	1.1	95	70-160
0.06	16	0.12	0.64	0.00	8	10	10						
20011223	1307	17.10	37-18.01	116-22.50	12.63	1.33	39 212	5.0	0.13	0.4	0.7	185	75 30
0.00	19	0.06	0.62	0.00	3	8	20						
20011225	0228	09.52	37-12.65	116-20.91	6.80	1.38	34 130	2.0	0.12	0.3	0.5	120	65 160
0.02	18	0.09	0.61	0.00	8	10	30						
20020119	1506	38.60	36-48.82	116-04.47	7.69	2.83	30 154	14.0	0.11	0.4	1.6	120	45 -90
0.06	34	0.21	0.74	0.00	35	33	30						
20020124	1949	35.13	36-48.73	116-04.47	8.37	2.71	46 79	14.0	0.13	0.2	1.0	110	45-100
0.05	31	0.20	0.73	0.00	38	28	50						
20020127	0853	58.61	36-59.34	116-03.63	11.25	1.41	42 78	10.0	0.11	0.3	0.8	80	45-130
0.00	15	0.15	0.63	0.00	30	13	20						
20020128	0410	00.31	36-48.80	116-04.35	7.15	1.17	38 156	14.0	0.11	0.3	1.2	145	60 -50
0.08	18	0.17	0.81	0.00	30	38	55						
20020202	2307	25.17	36-30.56	116-35.17	8.66	2.94	40 90	21.0	0.13	0.3	1.2	245	60 150
0.00	41	0.14	0.80	0.00	23	40	60						
20020203	0231	59.61	36-30.91	116-35.07	5.87	1.13	31 92	20.0	0.11	0.3	1.3	175	90 0
0.06	24	0.21	0.79	0.00	20	33	45						
20020207	1358	02.05	36-23.67	116-53.54	11.80	2.71	36 93	19.0	0.11	0.3	1.3	170	85 0
0.02	37	0.15	0.81	0.00	23	53	50						
20020218	2328	12.12	37-12.63	116-34.91	7.61	1.11	32 162	14.0	0.11	0.4	1.0	210	85 0
0.00	20	0.14	0.92	0.00	25	63	70						
20020304	1212	11.58	36-39.72	116-20.38	8.92	1.10	34 94	2.0	0.10	0.3	0.5	150	60 -80
0.02	24	0.13	0.79	0.00	30	23	40						
20020311	1010	29.36	37-17.38	116-11.58	13.98	1.14	26 228	11.0	0.13	0.7	0.7	295	70-170
0.09	19	0.22	0.59	0.00	20	25	70						
20020323	1549	35.48	37-07.48	116-15.51	9.08	1.15	41 86	11.0	0.11	0.2	0.9	205	85 0
0.00	17	0.07	0.75	0.00	8	45	25						
20020328	1407	51.02	37-07.62	116-15.35	12.02	2.17	53 88	11.0	0.11	0.2	0.6	295	75-160
0.00	26	0.13	0.66	0.00	15	33	60						
20020329	1150	20.90	37-07.63	116-15.33	11.53	1.90	52 88	11.0	0.12	0.2	0.6	285	85-170
0.12	28	0.24	0.74	0.00	25	35	70						
20020329	1203	21.87	37-07.30	116-15.56	9.63	1.10	43 84	12.0	0.13	0.2	0.9	290	80 180
0.04	19	0.12	0.77	0.00	15	40	50						
20020329	1803	16.44	37-07.57	116-15.41	10.91	1.68	43 87	11.0	0.12	0.3	0.6	200	85 10
0.04	18	0.19	0.74	0.00	25	45	40						
20020330	2136	47.62	37-07.67	116-15.73	8.59	1.25	45 87	11.0	0.12	0.3	1.0	200	60 -30
0.04	18	0.14	0.58	0.00	8	13	40						
20020403	1452	46.50	36-51.60	115-56.39	6.16	1.74	31 222	10.0	0.12	0.5	1.1	75	45-180
0.08	21	0.24	0.62	0.00	23	30	20						
20020407	0917	57.94	37-07.26	116-15.32	10.31	2.14	42 84	12.0	0.12	0.2	1.0	195	75 0
0.02	28	0.08	0.75	0.00	8	45	30						
20020408	2036	59.72	37-07.69	116-15.58	10.35	1.12	41 88	11.0	0.12	0.2	0.8	175	50 -60
0.08	19	0.16	0.52	0.00	5	10	10						
20020413	1602	32.36	36-49.11	116-04.16	6.64	1.25	45 156	14.0	0.12	0.2	0.7	130	60 -70
0.02	21	0.11	0.72	0.00	10	20	15						
20020414	1801	47.10	37-07.58	116-15.52	10.53	1.17	37 87	11.0	0.11	0.2	1.0	165	60 -70
0.00	19	0.07	0.45	0.00	3	5	5						
20020418	2159	47.12	37-07.34	116-15.22	10.26	1.97	42 85	12.0	0.13	0.3	1.0	200	60 -10
0.00	24	0.11	0.65	0.00	13	43	40						
20020419	0105	39.75	37-07.58	116-15.53	11.48	1.78	48 87	11.0	0.12	0.2	0.7	285	55-150
0.05	27	0.18	0.67	0.00	13	43	40						
20020422	0603	55.18	37-12.89	116-30.35	13.72	1.23	39 153	11.0	0.12	0.3	0.8	175	70 -20
0.06	20	0.14	0.54	0.00	5	15	10						
20020428	0513	48.69	37-01.15	116-22.64	12.60	2.07	30 128	3.0	0.12	0.4	0.6	195	80 20
0.04	30	0.15	0.60	0.00	8	18	10						
20020505	1011	41.32	37-08.10	116-14.01	8.93	1.16	41 96	12.0	0.13	0.3	1.1	200	65 -20
0.09	25	0.18	0.62	0.00	8	20	20						
20020509	1127	59.43	37-07.46	116-15.62	8.73	1.01	48 85	11.0	0.13	0.2	1.0	100	70-160
0.07	21	0.15	0.67	0.00	10	30	35						
20020512	0719	44.70	37-07.67	116-15.36	10.52	1.14	47 89	11.0	0.12	0.2	0.8	165	60 -70
0.03	23	0.11	0.46	0.00	10	5	5						
20020525	1203	33.09	36-42.88	116-18.25	10.97	3.09	51 59	3.0	0.11	0.2	0.4	260	85 160
0.00	50	0.10	0.69	0.00	8	35	35						
20020528	0517	53.18	37-17.95	116-21.74	11.80	1.02	31 211	7.0	0.12	0.5	0.7	235	75 0
0.00	18	0.06	0.86	0.00	20	40	50						

20020614	1240	44.79	36-43.03	116-17.93	12.81	4.42	46	58	3.0	0.10	0.2	0.4	140	50	-60
0.04	51	0.12	0.60	0.00	13	15	20								
20020618	1624	31.83	36-42.58	116-18.51	11.67	3.13	50	47	3.0	0.10	0.2	0.4	120	50	-110
0.04	48	0.12	0.63	0.00	18	13	30								
20020702	2344	04.81	36-48.97	116-13.87	0.23	1.03	31	126	10.0	0.13	0.3	11.3	100	85	-170
0.00	15	0.13	0.77	0.00	8	40	30								
20020706	2320	13.37	36-32.59	116-13.98	0.51	1.00	15	167	11.0	0.10	0.6	9.2	160	85	10
0.12	18	0.30	0.71	0.00	18	53	40								
20020708	0625	50.46	36-40.34	116-16.00	8.54	1.18	24	96	6.0	0.07	0.3	0.6	135	45	-50
0.08	24	0.16	0.66	0.00	20	10	20								
20020727	0001	28.29	37-08.89	116-36.89	6.40	1.15	32	136	9.0	0.15	0.3	0.9	225	80	-150
0.06	18	0.15	0.67	0.00	3	28	60								
20020727	0214	55.33	37-08.85	116-36.79	6.31	1.47	32	136	10.0	0.14	0.4	1.2	140	65	-10
0.00	23	0.10	0.65	0.00	10	10	40								
20020727	0216	12.93	37-08.76	116-36.90	6.90	1.20	39	135	9.0	0.14	0.3	0.5	325	75	-40
0.05	16	0.15	0.62	0.00	5	10	10								
20020727	0241	50.54	37-09.10	116-37.05	6.32	1.14	41	140	9.0	0.12	0.3	0.5	145	90	0
0.00	17	0.10	0.70	0.00	10	45	35								
20020727	0300	57.49	37-09.04	116-36.51	6.12	1.26	40	137	10.0	0.13	0.4	0.8	135	80	-10
0.04	21	0.13	0.74	0.00	10	33	30								
20020902	0509	05.28	36-50.05	115-55.56	7.74	1.17	37	231	13.0	0.13	0.5	1.8	265	80	-170
0.03	22	0.19	0.69	0.00	10	45	40								
20020903	0320	36.47	36-50.71	115-58.83	6.39	1.09	36	204	12.0	0.13	0.3	0.7	175	75	10
0.03	16	0.15	0.69	0.00	25	25	25								

Table 7-1 (cont'd)
Focal Mechanisms for FY2002

Column definitions:

columns 1-50 are usual HYP071 hypocenter parameters and magnitude
= number of P and S phases with weights > 0.1
gap = maximum azimuthal gap in degrees
del = distance (km) to nearest station
TT rms = rms travel-time residual (s)
hor err = horizontal standard error (km)
ver err = vertical standard error (km)
dip dir = direction of the fault plane dip (90° from the strike angle of fault plane)
dip ang = dip of the fault plane from horizontal
rake = angle at which the hanging wall moves relative to foot wall, counterclockwise from horizontal
Fj = misfit function (0 to 1, with 1 best)
nobs = number of first-motion observations
awwt = mean data weight (0 to 30, with 30 best)
stdr = station distribution indicator (0 to 1, with 1 best)
delta strdiprak = 95% confidence region for strike angle (str), dip angle (dip), and rake (rak)

List of Figures

- 2-1. Stations of the Southern Great Basin Digital Seismic Network.
- 2-2. Stations of the Southern Great Basin Seismic Network (analog).
- 2-3. Seismic telemetry nodes for the SGBDSN.
- 2-4. Displacement response of the SGBDSN S-13 and CMG-40 weak-motion instruments and of a strong-motion instrument. (For corroborative use only.)
- 2-5. Downtime of the SGBDSN network for FY2002.
- 2-6. Data Flow for the SGBDSN seismic recording and processing.
- 2-7. Distribution of location errors for FY2002 catalog earthquakes.
- 3-1. Historical seismicity (1868 to 1978) of the Yucca Mountain area. (For corroborative use only.)
- 3-2. Seismicity (1978-1995) of the Yucca Mountain area from the analog SGBSN. (For corroborative use only.)
- 3-3. Seismicity (FY1996-FY2001) of the Yucca Mountain area from the digital SGBDSN.
- 3-4. Seismicity of the Yucca Mountain area from the digital SGBDSN in FY2002.
- 3-5. FY2002 seismicity plotted on shaded elevation background, with events not scaled by magnitude.
- 3-6. Cumulative moment for earthquakes from August 1978 to September 2002 within the 65-km ring around station RPY and having $M \geq 3.0$. (For corroborative use only.)
- 3-7. Density of reported depths in the FY2002 SGBDSN catalog. The density has been computed separately for "LSM" = Little Skull Mountain and "non-LSM" = all other earthquakes.
- 3-8. Recurrence curve for the FY2002 SGBDSN catalog. The line is a maximum-likelihood fit according to Aki (1965).
- 4-1. Base map showing the preliminary locations of the 2002 LSM sequence. (For corroborative use only.)
- 4-2a. Close-in view of 2002 sequence. (For corroborative use only.)
- 4-2b. Locations of all events in the Little Skull Mountain area from June through September 2002.

- 4.3 Perspective view showing the geometry of the 2002 activity. (For corroborative use only).
- 4.4 Stations-distance distribution used to calculate the magnitude of the June 14th mainshock.
- 4-5a. UC Berkeley broadband regional moment tensor solution for the June 14th mainshock. (For corroborative use only.)
- 4-5b. Short-period focal mechanism of the June 14, M 4.4, mainshock.
- 4-5c. Focal mechanism of the May 25, 2002, earthquake within the Little Skull Mountain aftershock zone.
- 4-5d. Focal mechanism of the June 18, 2002, earthquake within the Little Skull Mountain aftershock zone.
- 4.6. Waveforms of the primary events of the 2002 sequence.
- 4.7. Filtered composite and mainshock records showing that the composite time series captures the mainshock record in the 1-8 Hz band.
- 4.8. Geographic distribution of the peak ground motions from acceleration records in the Yucca Mountain area.
- 4.9. Relationship between PGA and distance from strong-motion recordings of the June 14, 2002, earthquake.
- 4.10. Time-series records of the June 14, 2002, earthquake from Lathrop Wells and Little Skull Cliff strong-motion stations.
- 4.11. Acceleration spectra from three components at Lathrop Wells and two components at Little Skull Cliff.
- 4.12. Velocity time-series records from SGBDSN stations AL5 (Alcove 5 at a depth of 300 meters) and RPY (almost above the repository and Alcove 5).
- 4.13. Acceleration spectra at AL5 and RPY for the June 14, 2002, earthquake.
- 4.14. Raw and smoothed spectral ratios between RPY and AL5 (RPY/AL5).
- 4.15. Comparison of acceleration time-series records at WHBS and MDVS.
- 4.16. Acceleration spectra of WHBS and MDVS strong-motion records.
- 4.17. Comparison of acceleration time-series records at strong-motion stations at SYMS and TYMS.

- 4.18. Acceleration spectra from the SYMS and TYMS strong-motion stations.
- 4.19. Acceleration time-series records at Lathrop Wells from the June 14, 2002, and the September 13, 1992, earthquakes. (For corroborative use only.)
- 4-20. Acceleration spectra at Lathrop Wells for the June 14, 2002, and the September 13, 1992, earthquakes. (For corroborative use only.)
- 5-1. Seismicity in the Death Valley National Park region during FY2002. (For corroborative use only.)
- 6-1. Earthquakes in FY2002 near Yucca Mountain.
- 7-1. Focal mechanisms for FY2002 earthquakes in the SGBDSN catalog. Up (crosses) and down (circles) first motions are plotted on the lower focal hemisphere.
- 7-2. Pressure and tension axes of the focal mechanisms for FY2002. These are plotted on the lower focal hemisphere.
- 8-1. Location of blasts in the SGBDSN monitoring region in FY2002. (For corroborative use only.)

SGBDSN -- FY2002

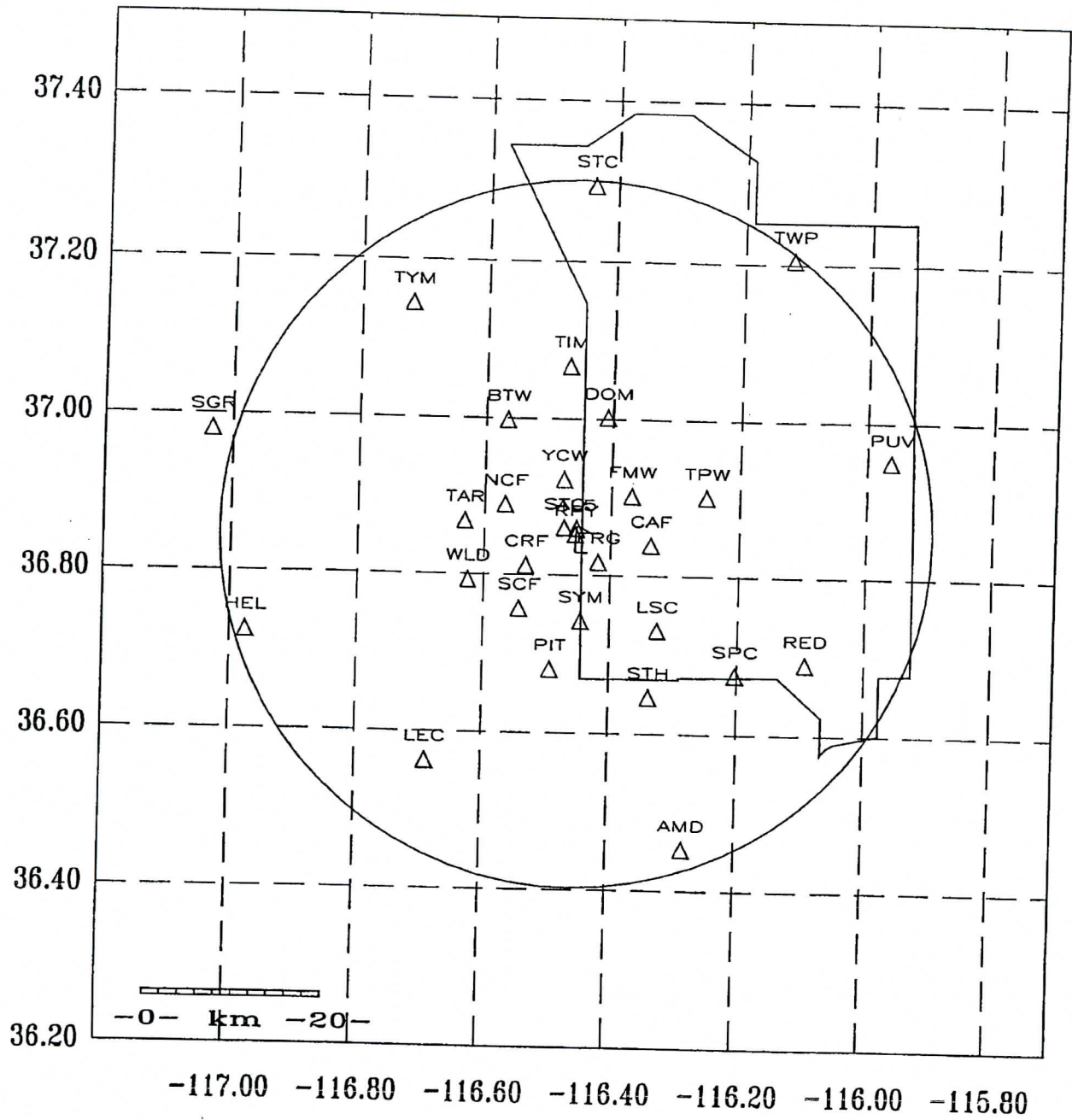


Figure 2-1. Stations of the Southern Great Basin Digital Seismic Network.

Analog Stations in Southern Great Basin

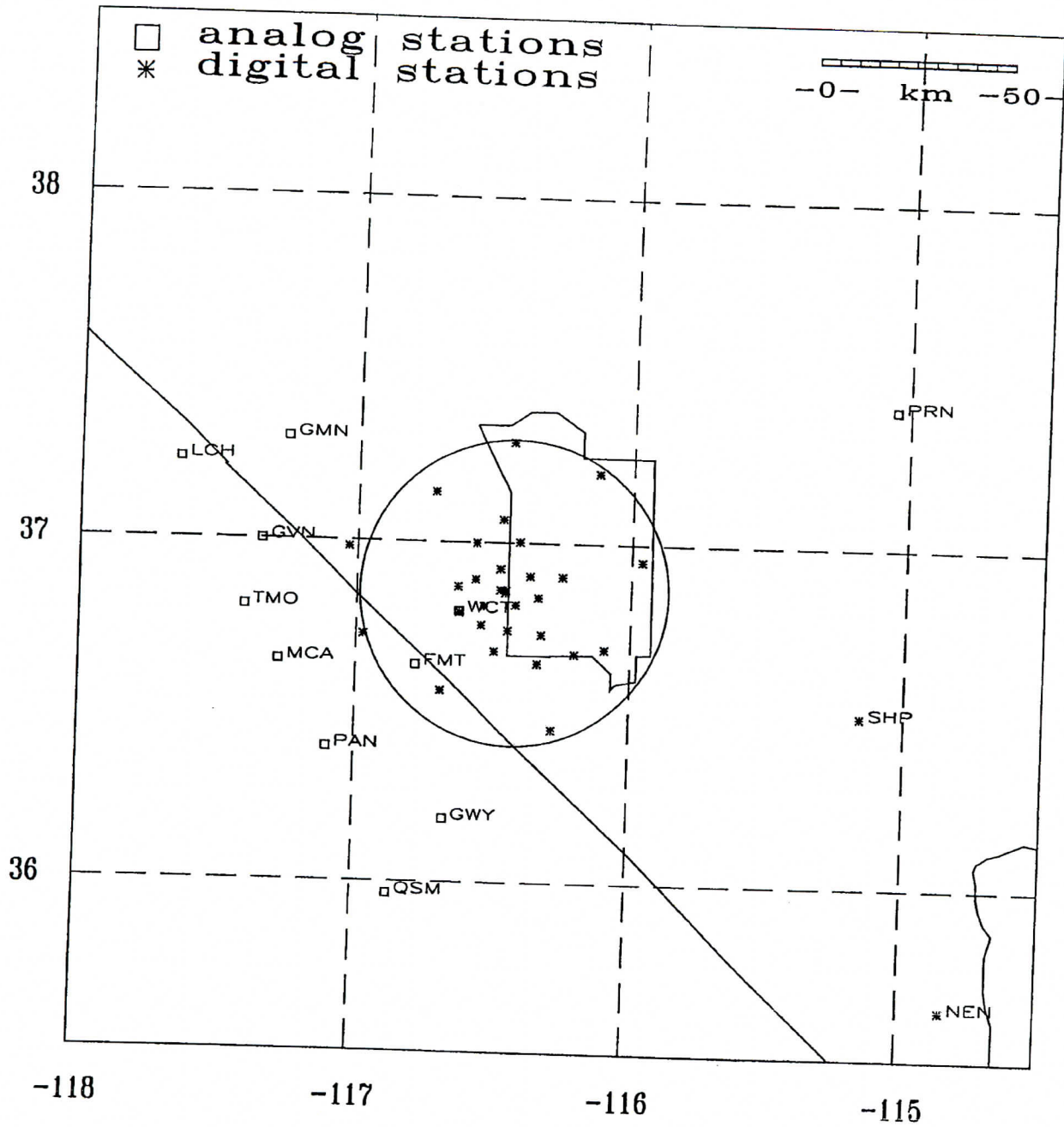


Figure 2-2. Stations of the Southern Great Basin Seismic Network (analog).

Seismic Telemetry Nodes for the SGBDSN

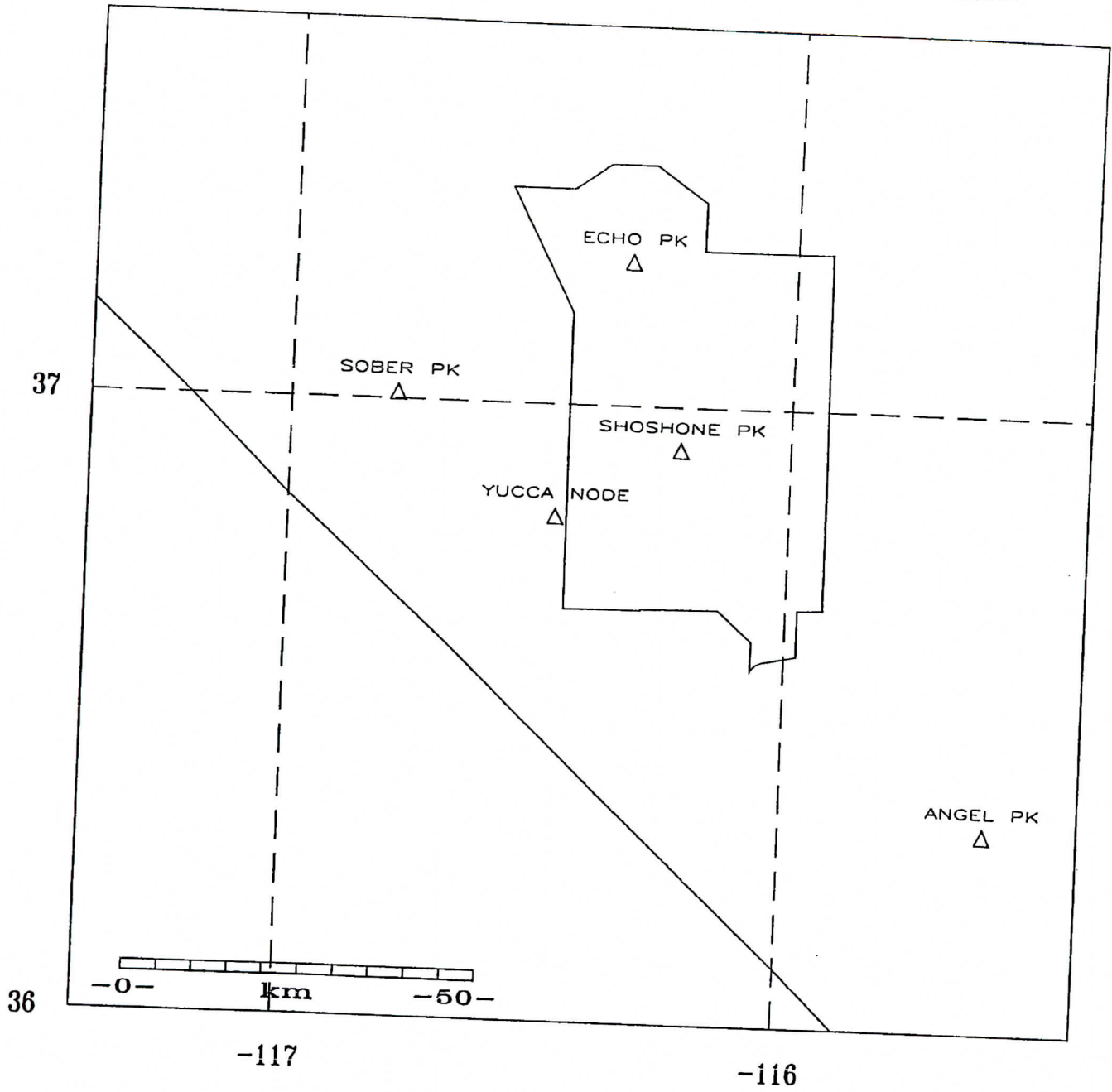


Figure 2-3. Seismic telemetry nodes for the SGBDSN.

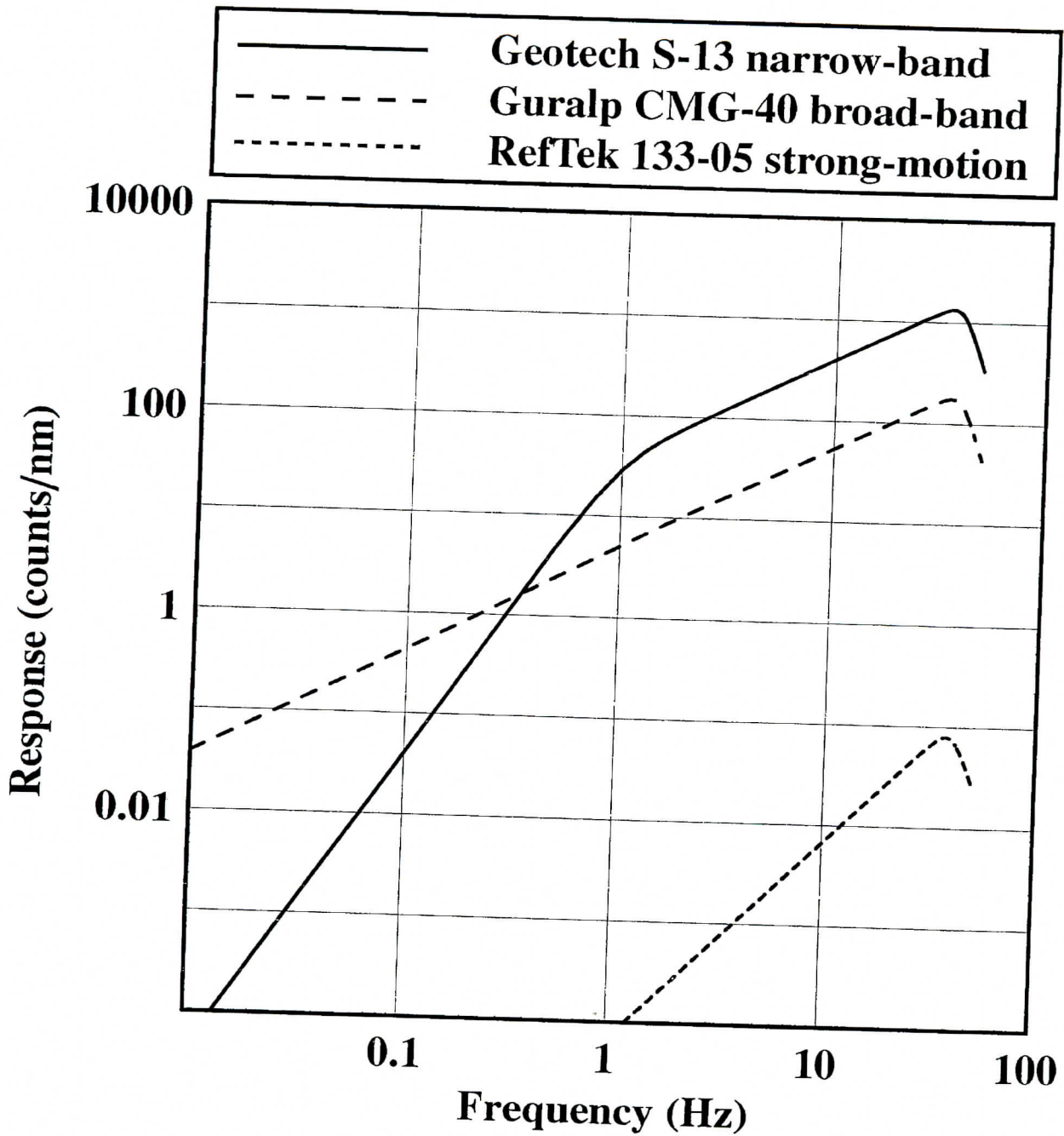


Figure 2-4. Displacement response of the SGBDSN S-13 and CMG-40 weak-motion instruments and of a strong-motion instrument. (For corroborative use only.)

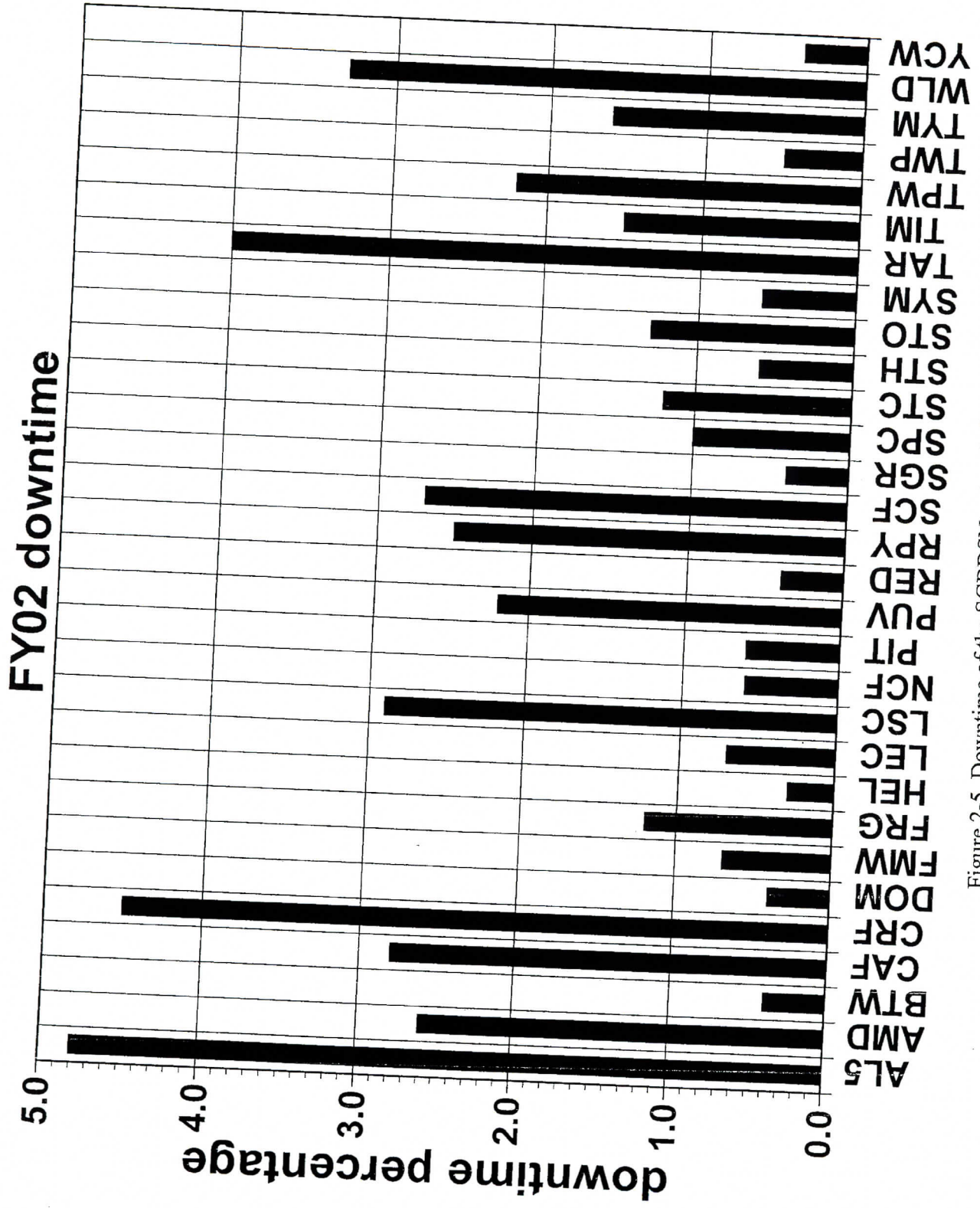


Figure 2-5. Downtime of the SGBDSN network for FY2002.

SGBDSN Data Flow

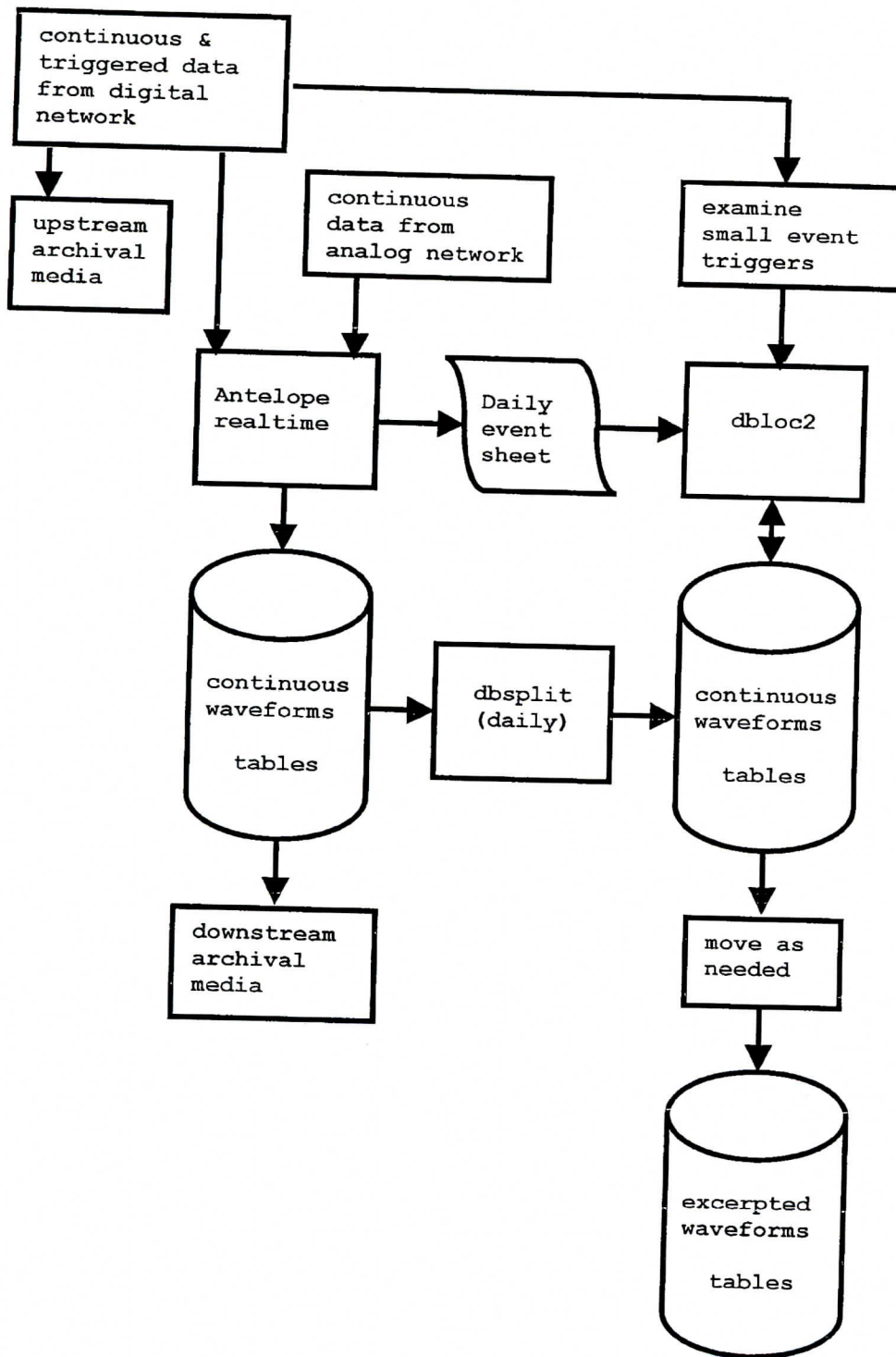


Figure 2-6. Data Flow for the SGBDSN seismic recording and processing.

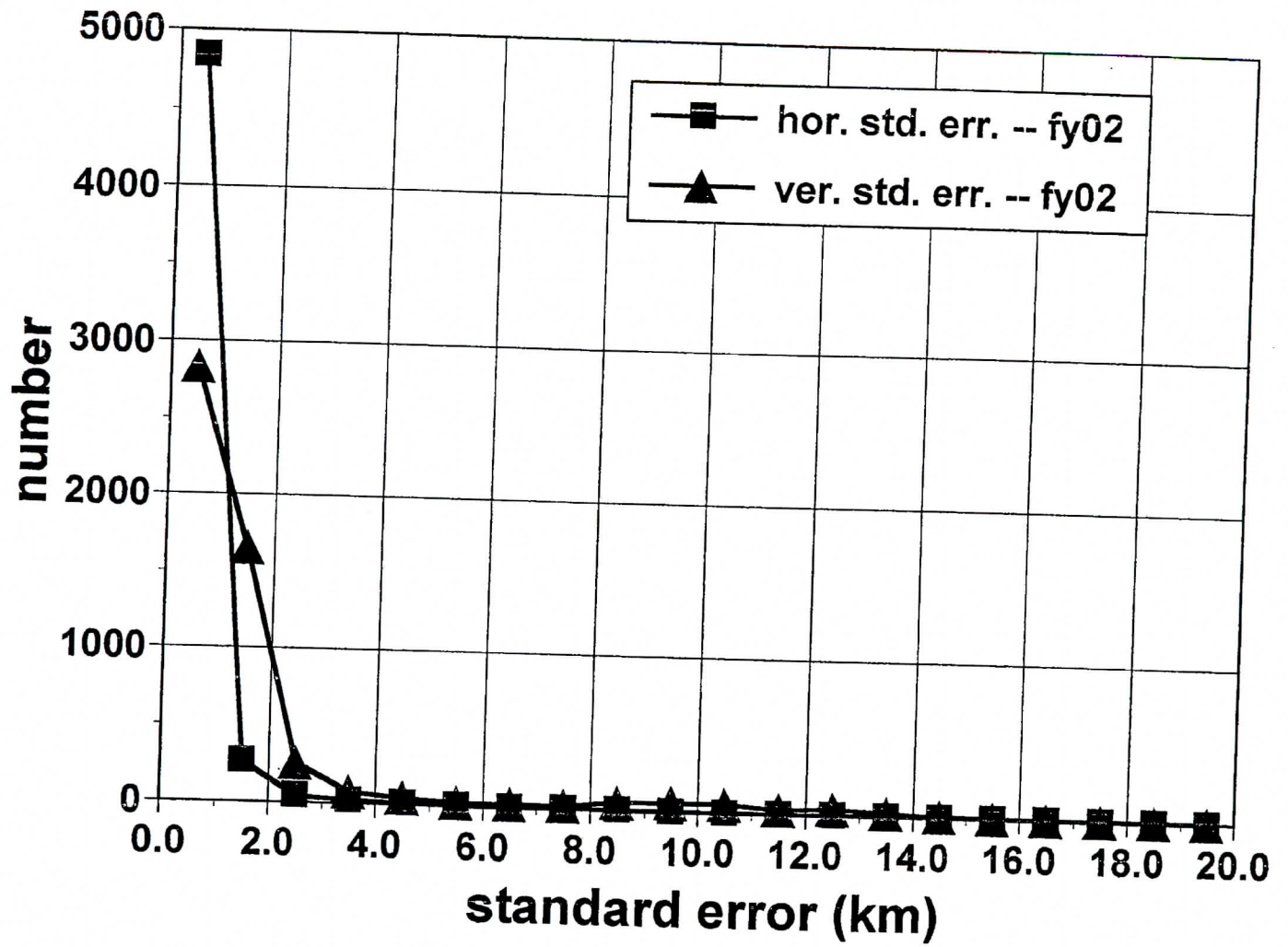


Figure 2-7. Distribution of location errors for FY2002 catalog earthquakes.

1868-1978 EARTHQUAKES IN THE YUCCA MOUNTAIN REGION

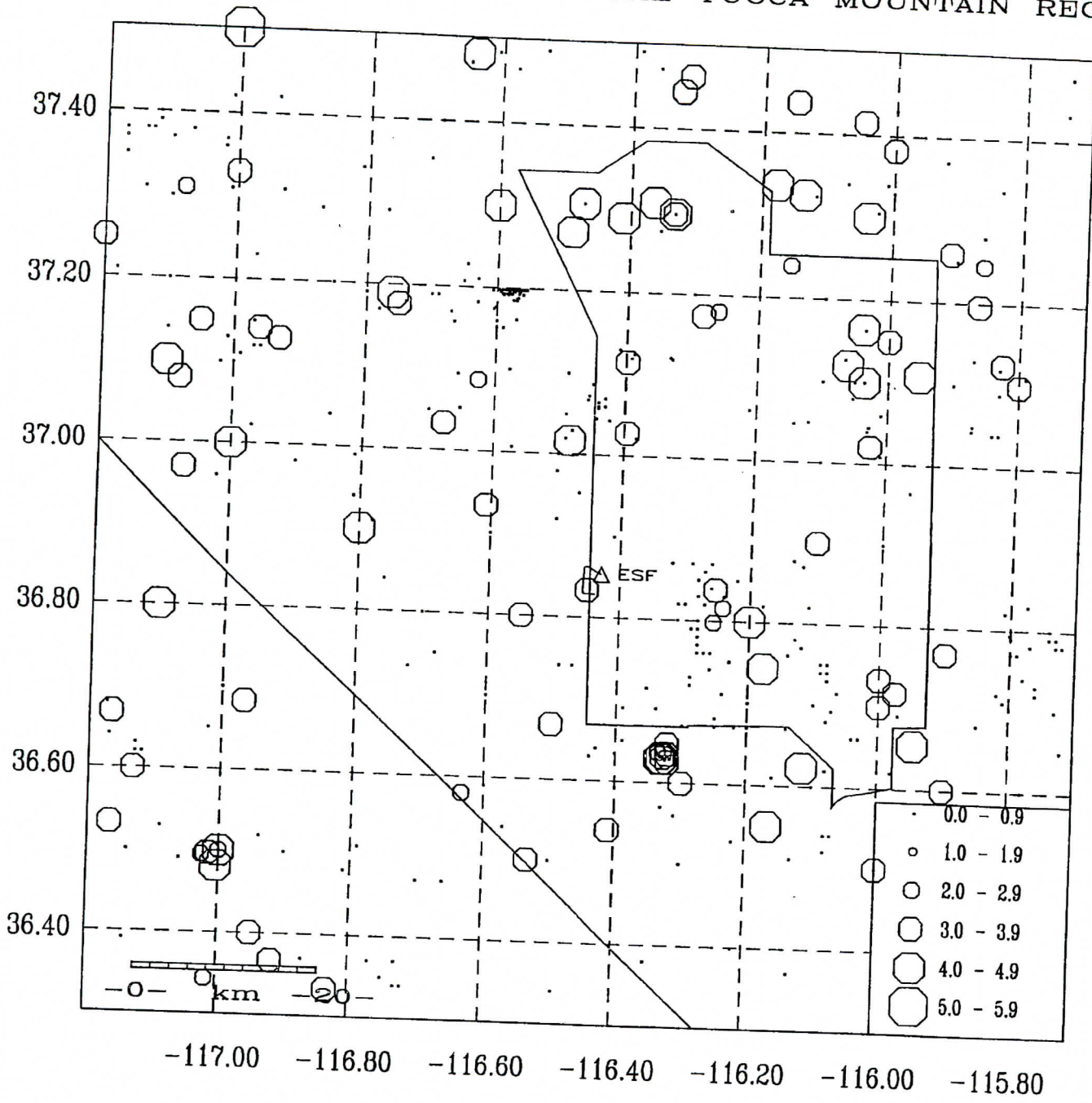


Figure 3-1. Historical seismicity (1868 to 1978) of the Yucca Mountain area.
(For corroborative use only.)

SGBSN Located Earthquakes -- 1978 to 1995

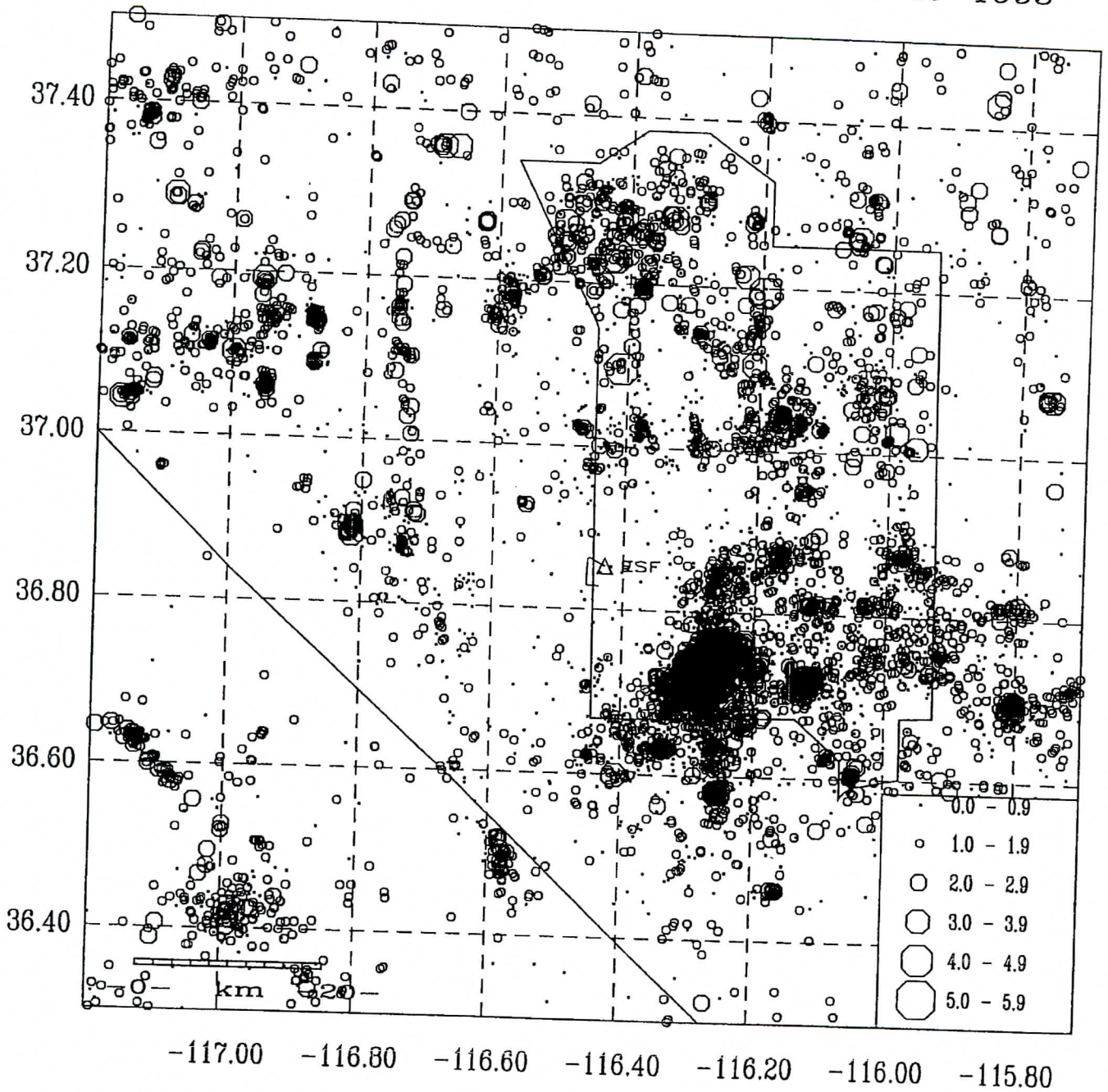


Figure 3-2. Seismicity (1978-1995) of the Yucca Mountain area from the analog SGBSN.

(For corroborative use only.)

SGBDSN Located Earthquakes -- FY1996 to FY2001

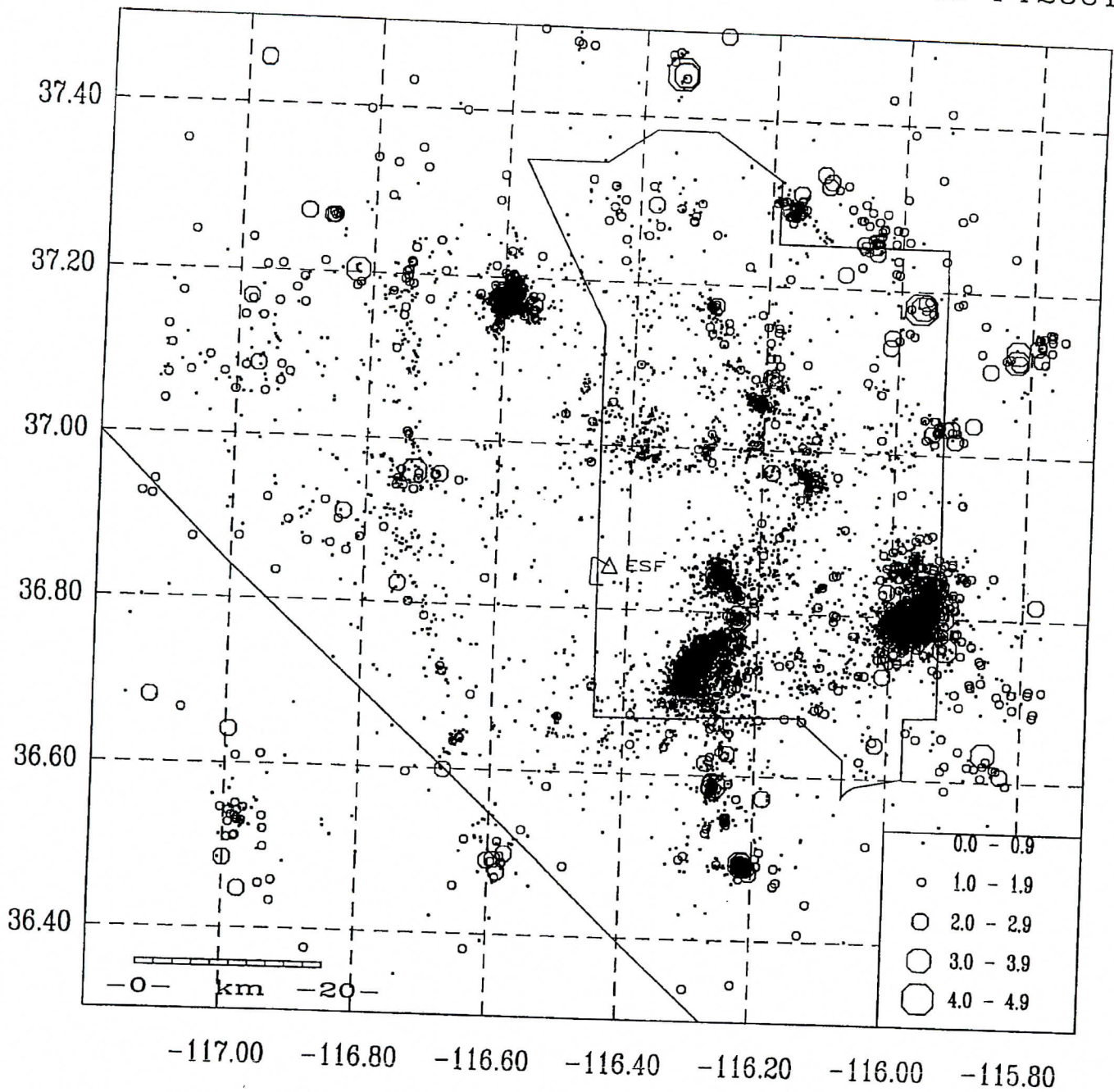


Figure 3-3. Seismicity (FY1996-FY2001) of the Yucca Mountain area from the digital SGBDSN.

SGBDSN Located Earthquakes -- FY2002

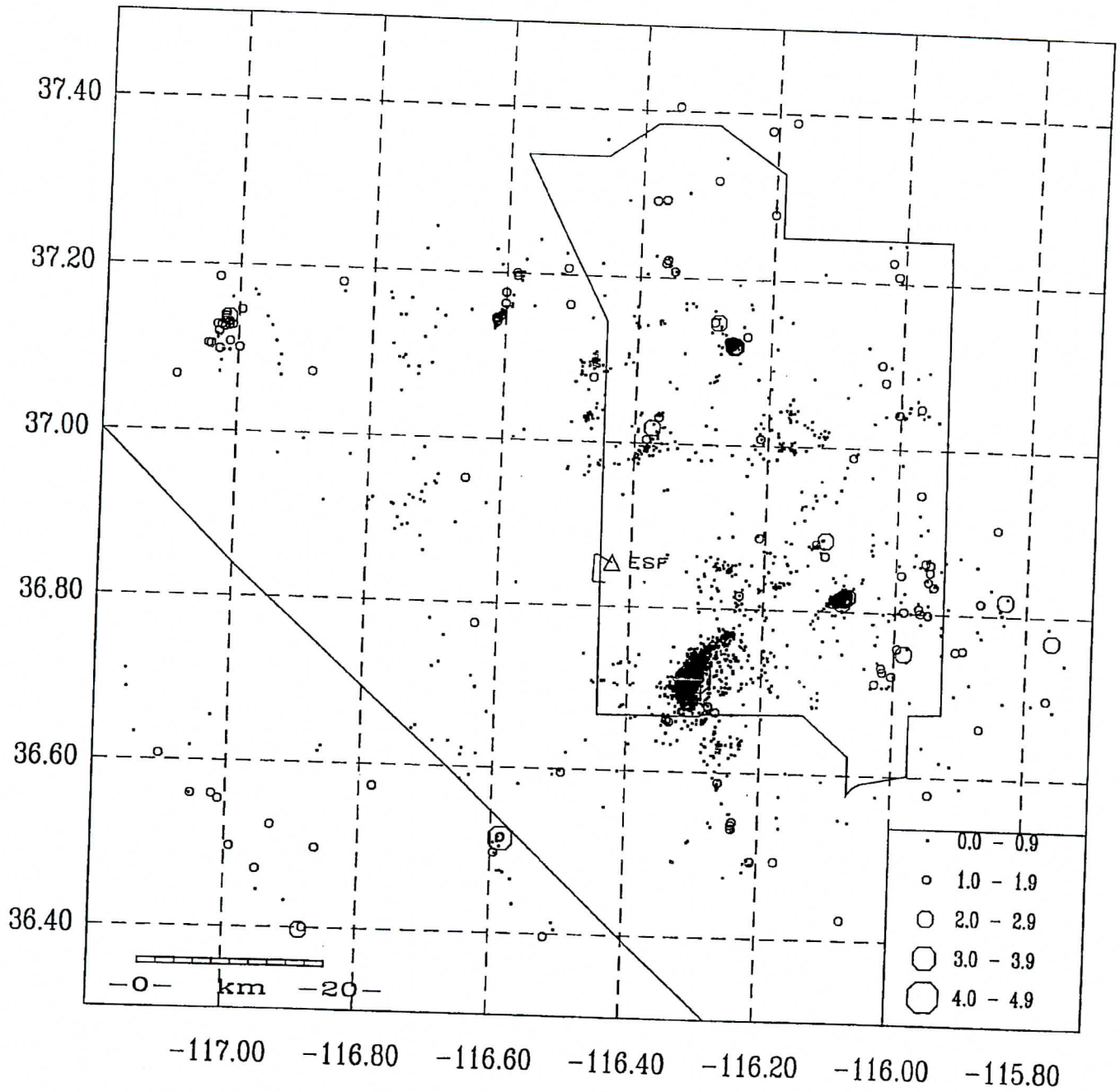
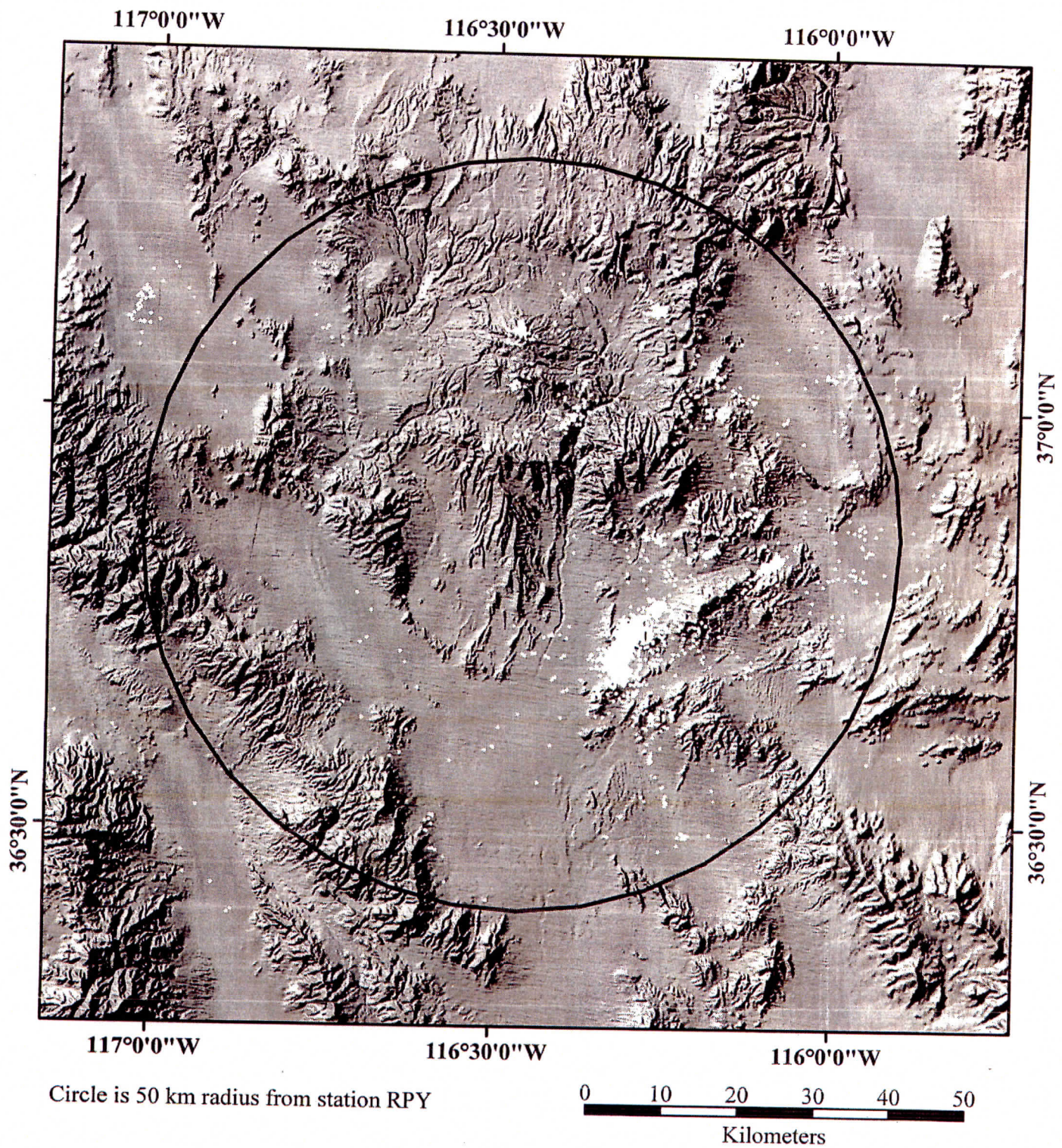


Figure 3-4. Seismicity of the Yucca Mountain area from the digital SGBDSN in FY2002.

Location of earthquakes near Yucca Mountain for the FY2002



Circle is 50 km radius from station RPY

Figure 3-5. FY2002 seismicity plotted on shaded elevation background, with events not scaled by magnitude.

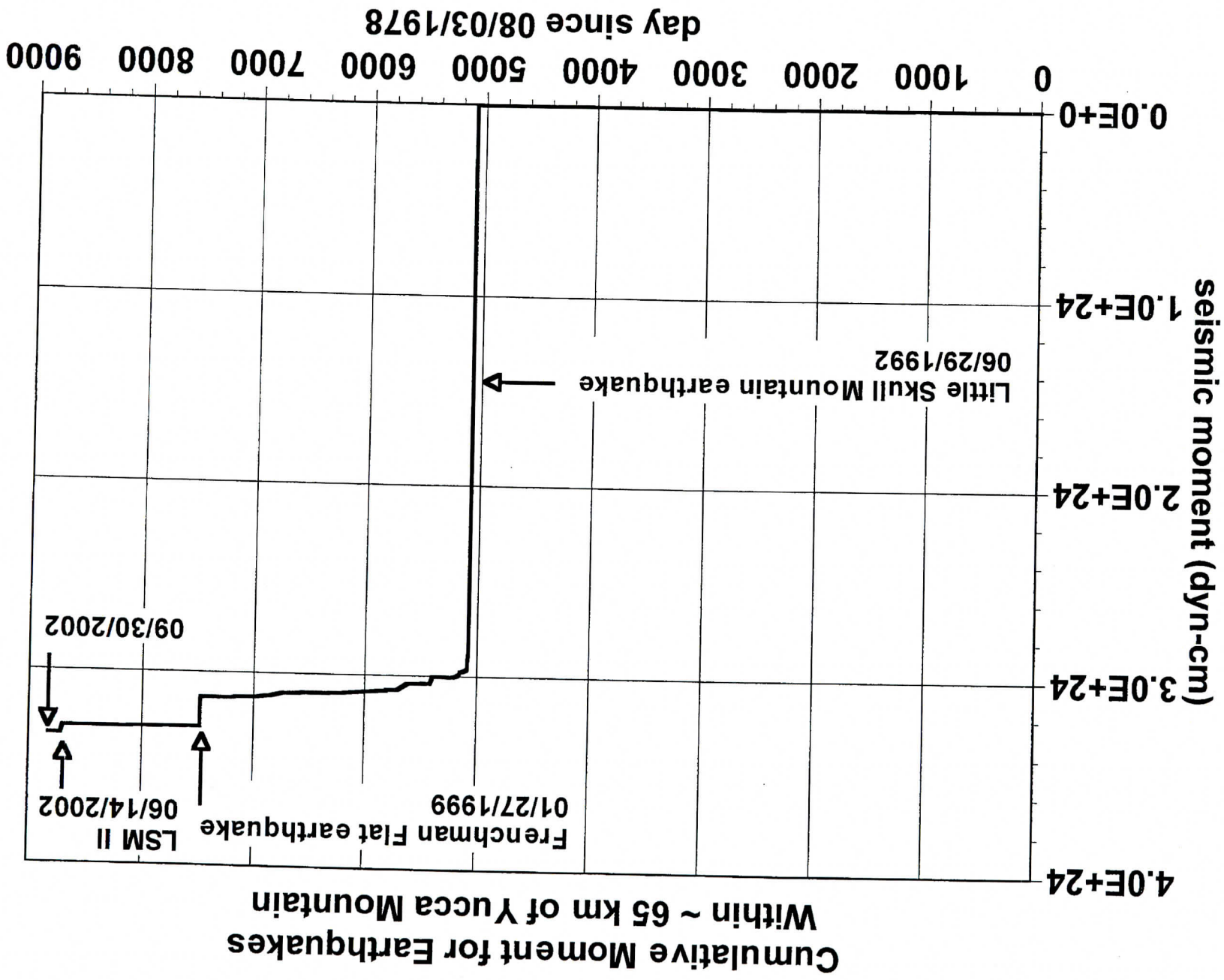
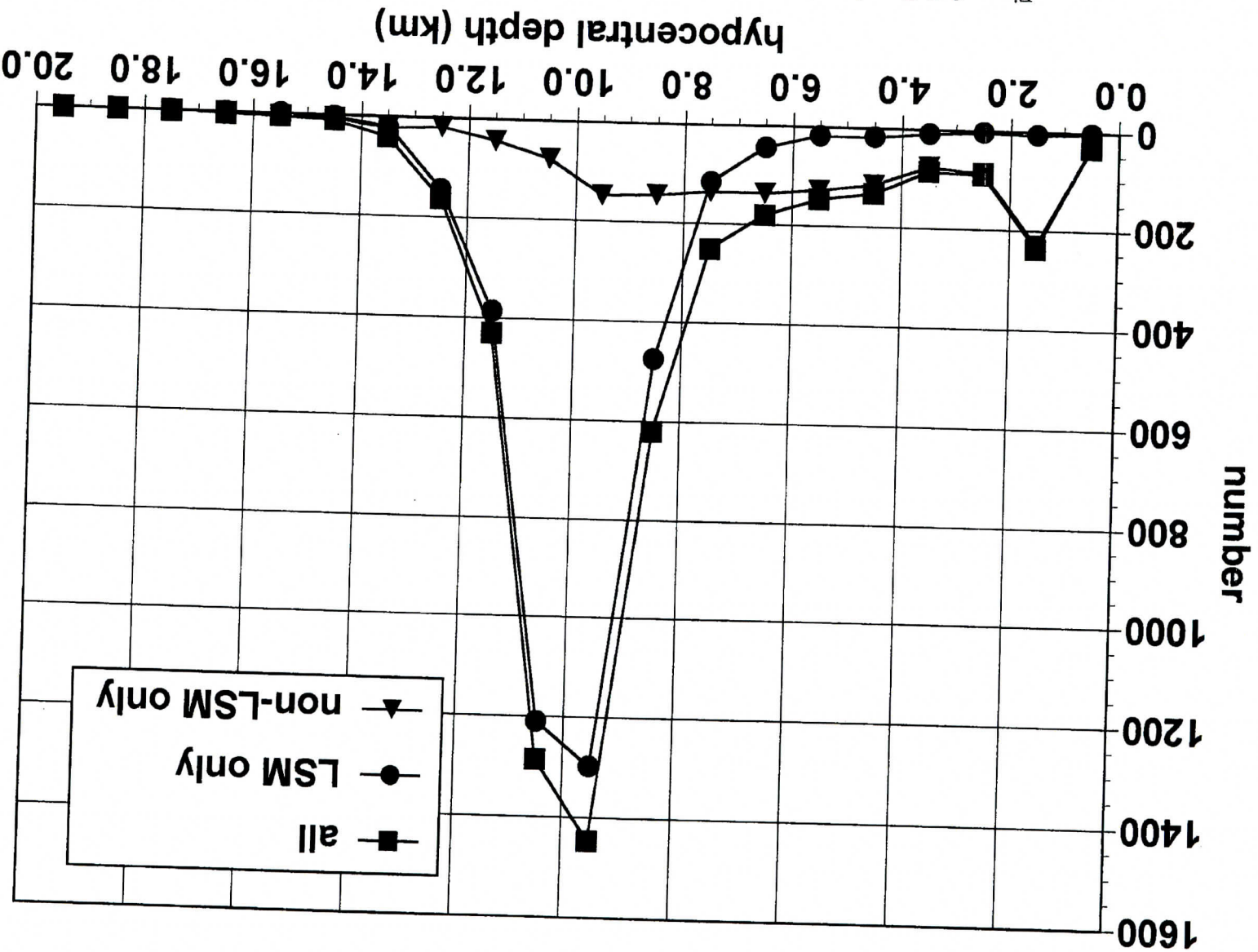


Figure 3-6. Cumulative moment for earthquakes from August 1978 to September 2002 within the 65-km ring around station RPV and having $M \geq 3.0$. (For corroborative use only.)

Figure 3-7. Density of reported depths in the FY2002 SGBDSN catalog. The density has been computed separately for "LSM" = Little Skull Mountain and "non-LSM" = all other earthquakes.



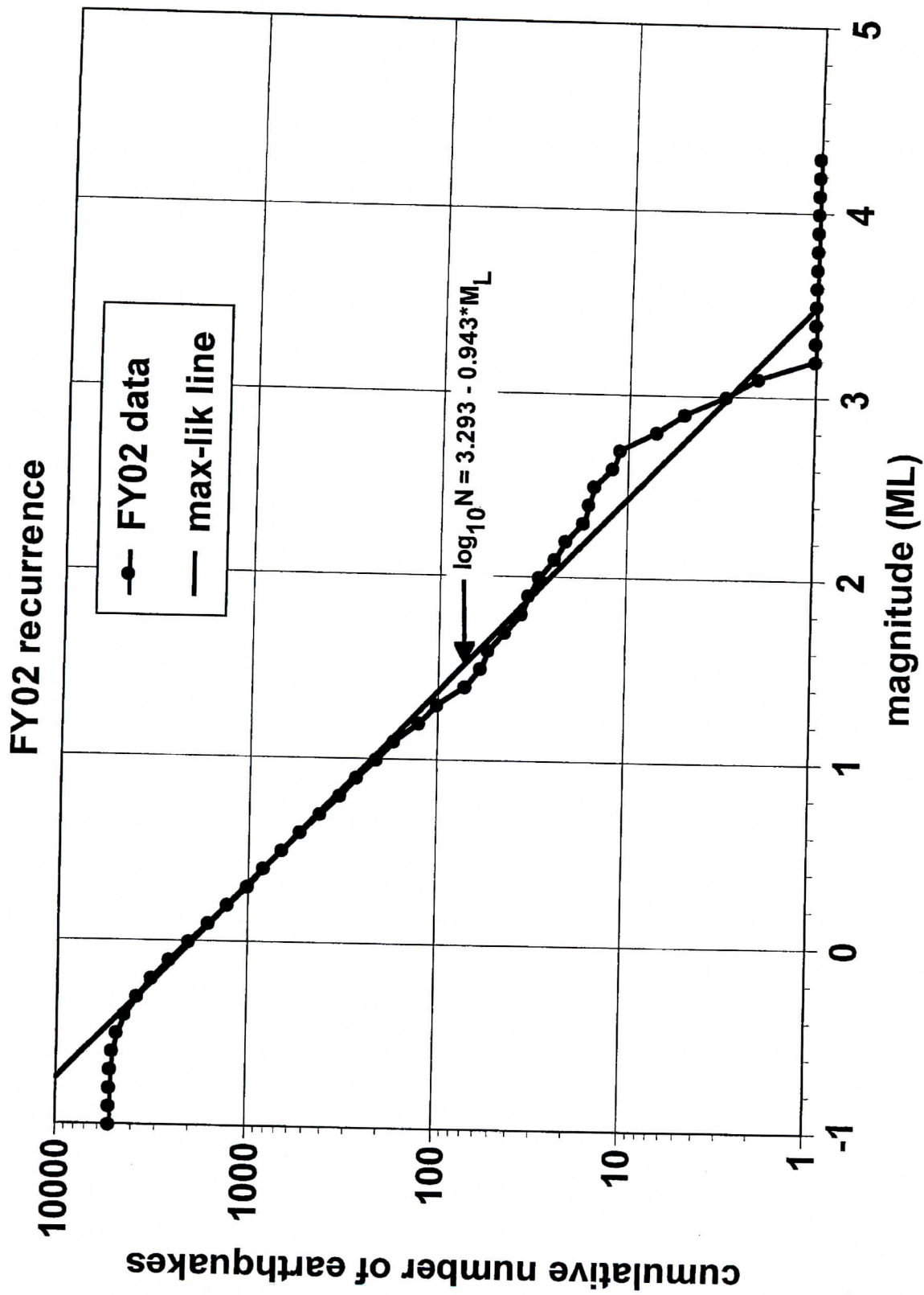


Figure 3-8. Recurrence curve for the FY2002 SGBDSN catalog. The line is a maximum-likelihood fit according to Aki (1965).

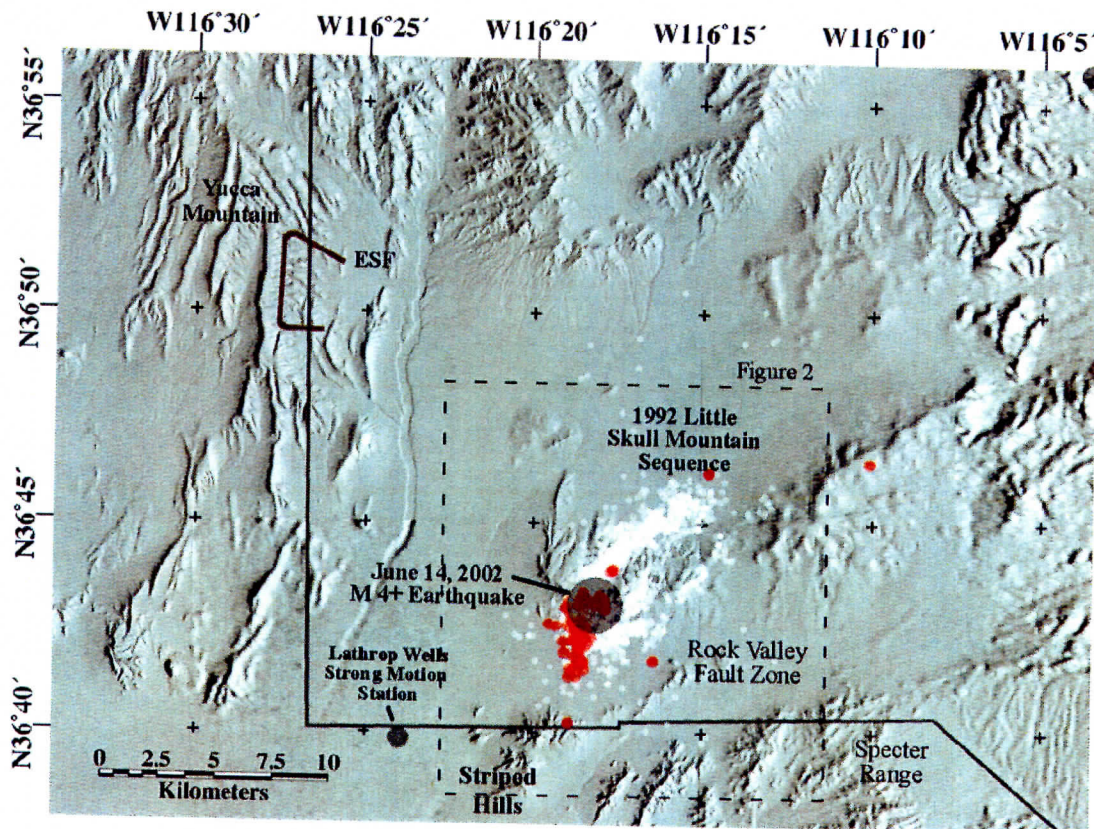
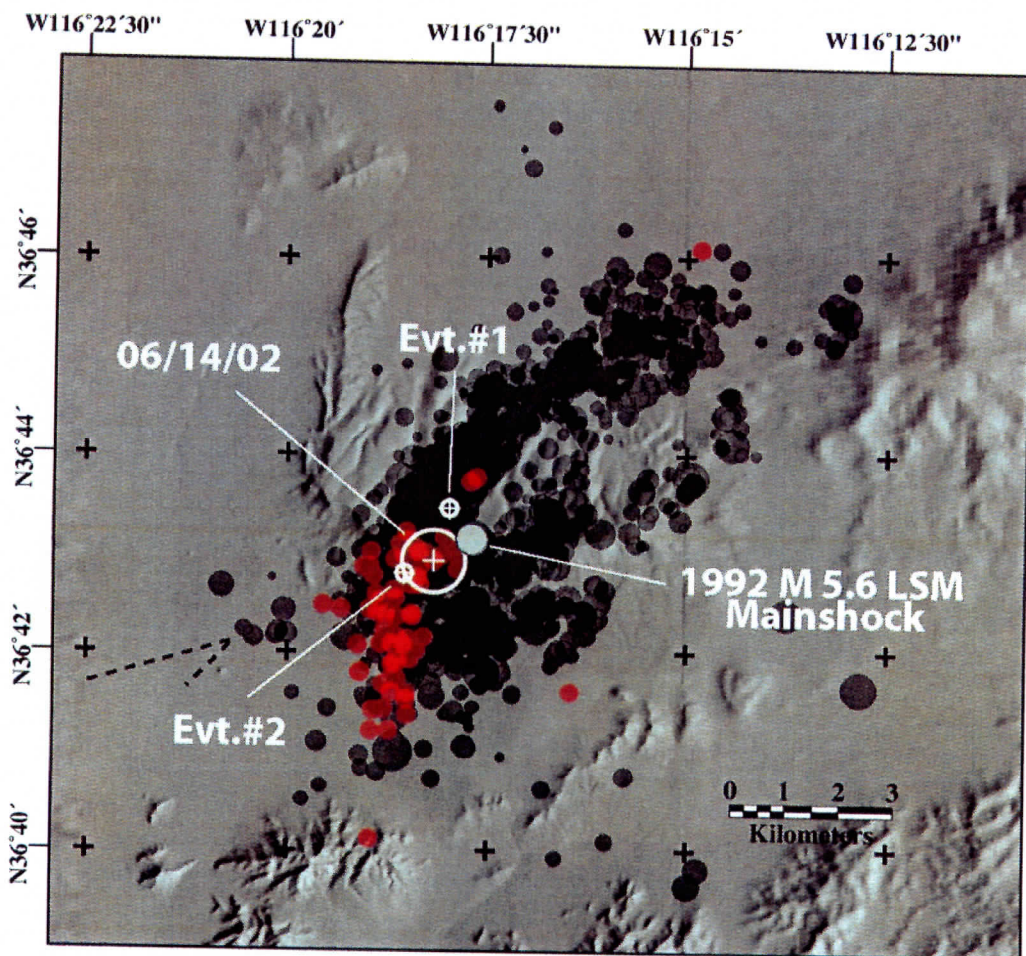


Figure 1

Figure 4-1. Base Map showing locations of the 2002 sequence (red) and the 1992 Little Skull Mountain sequence relocations from Smith et al., 2001, (white) and Yucca Mountain. The location of the June 14th mainshock is shown as the large dark symbol. Reference for Figure 4-2a is shown as a dashed box. (For corroborative use only.)



Black: 1992 LSM Aftershocks

Red: Reviewed Aftershock Locations of June 14, 2002 Event
Locations as of June 24.

----- Perspective Fig. 4-3

Figure 4-2a. Close in view of sequence showing the details of the 2002 activity with respect to the geometry of the 1992 sequence. Waveforms for Evt. #'s 1 and 2 are used to construct a composite of the mainshock. (For corroborative use only.)

Earthquake Location from June through September 2002

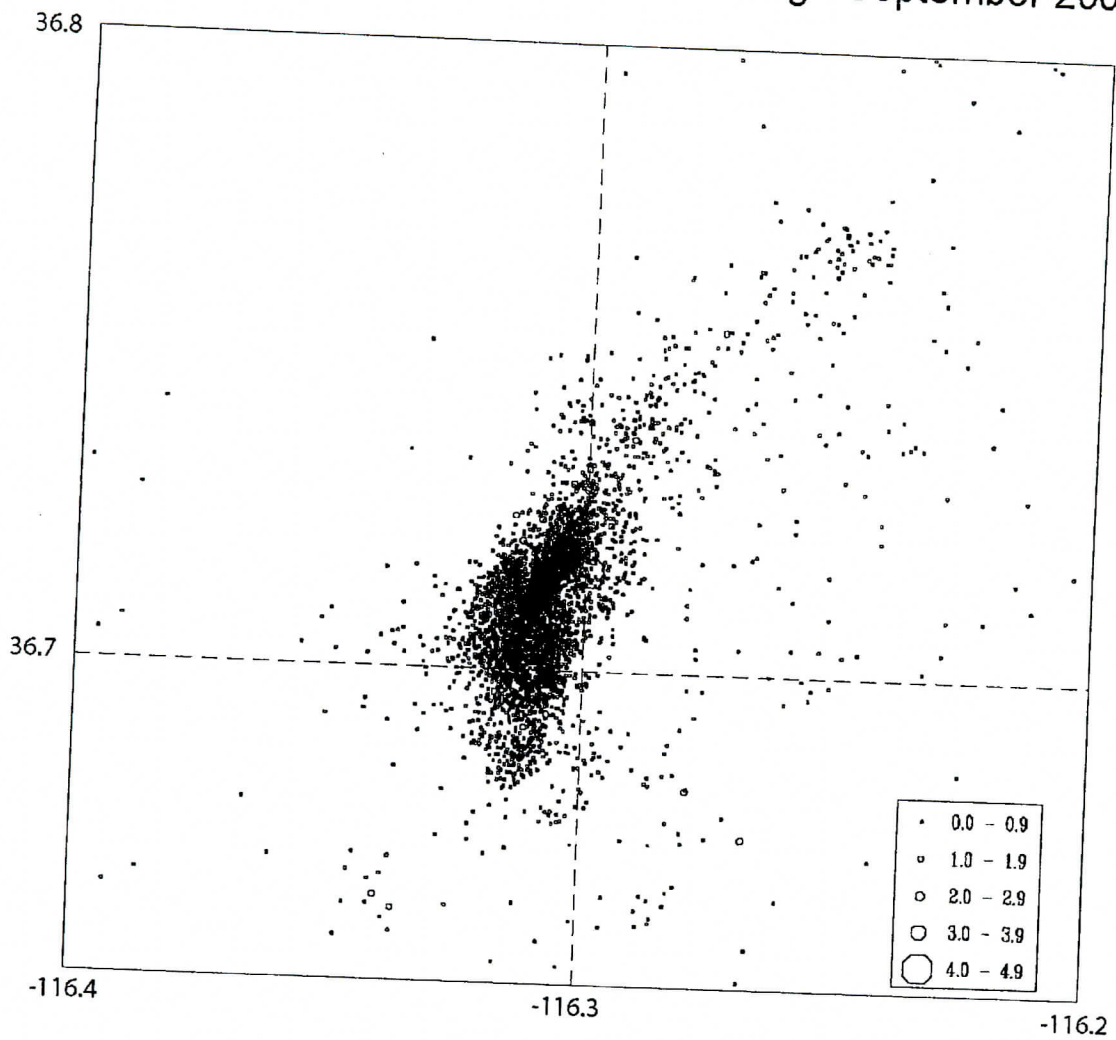
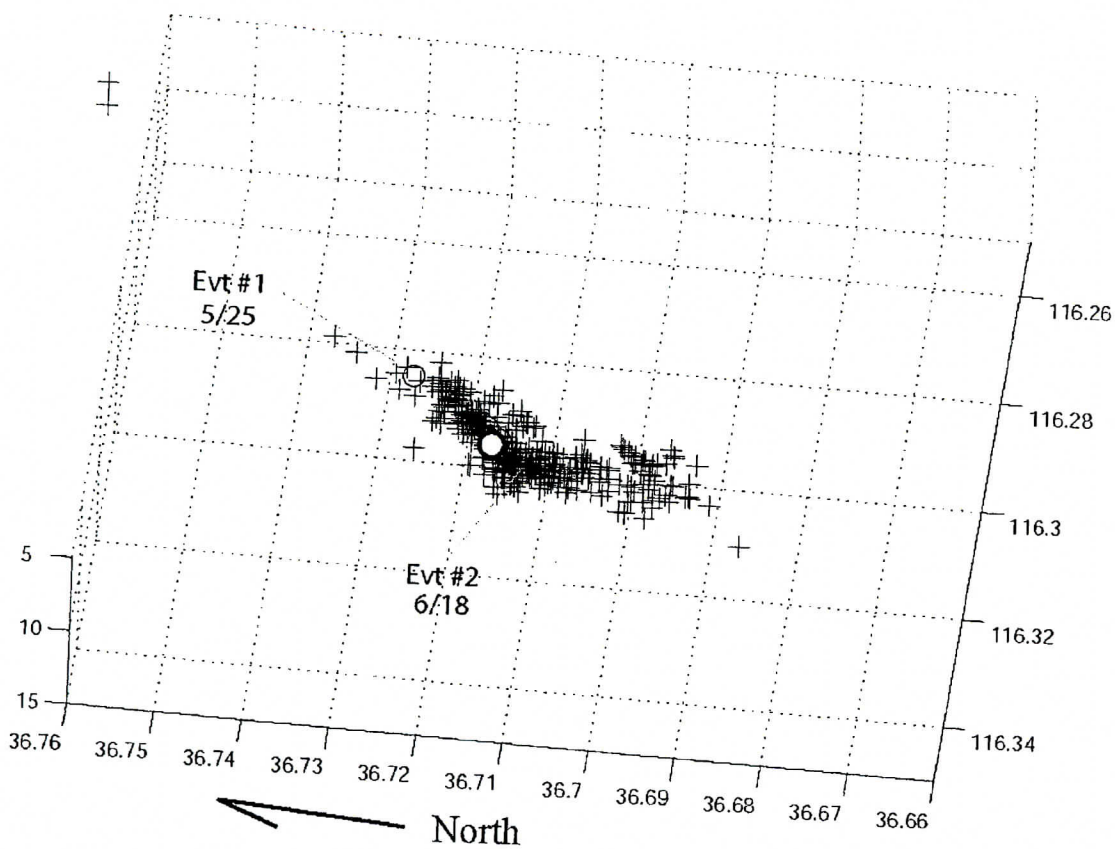


Figure 4-2b. Locations of all events in the Little Skull Mountain area from June through September 2002.

June 14 Event and Reviewed Aftershocks Double Difference Locations



○ Location of June 14 Mainshock
View From N95W ~75 Degrees Down Dip - Eastward

Figure 4-3. Perspective view showing the geometry of the 2002 activity and the relative locations of the mainshock (dark o) and Evt. #'s 1 and 2. Perspective is used to capture the geometry of dipping fault planes. (For corroborative use only.)

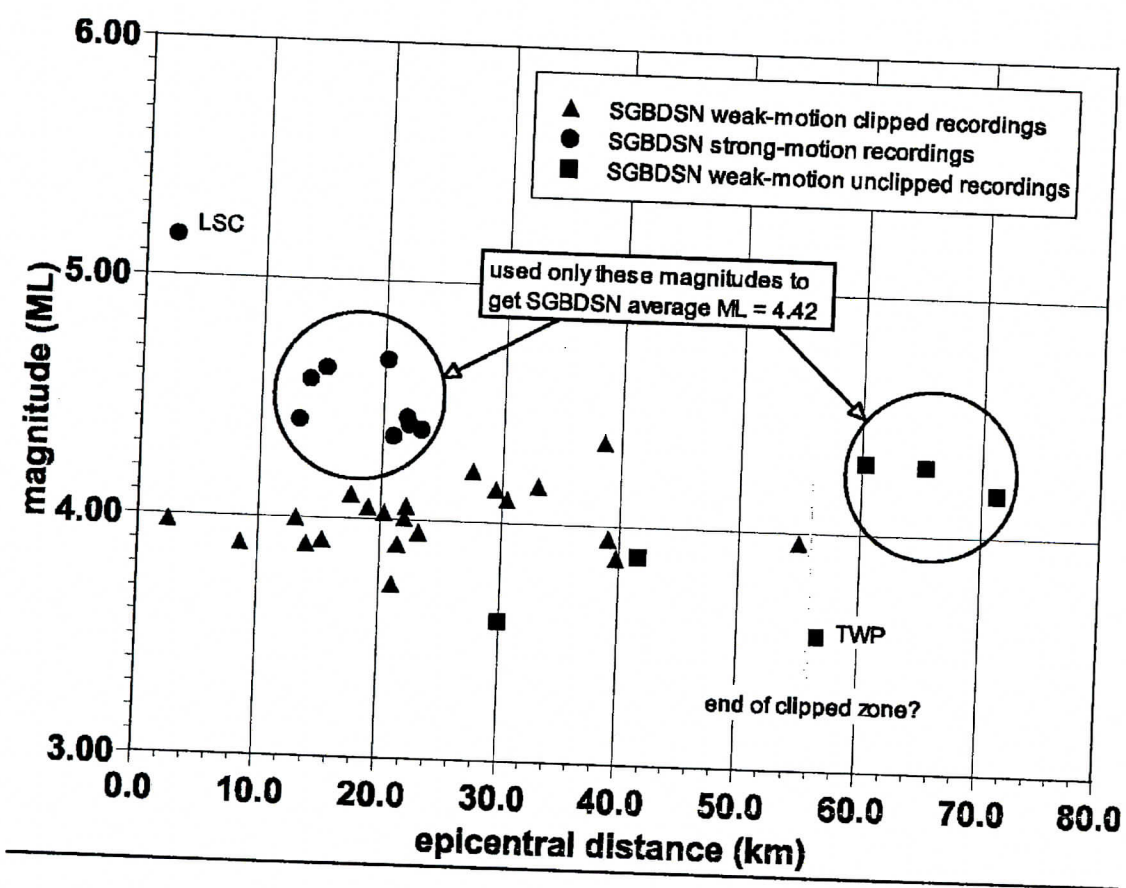


Figure 4-4. Stations distance distribution used to calculate the magnitude of the June 14th mainshock.

Summary of Source Mechanisms:

UC Berkeley Moment Tensor Solution Summary:

Plane	Strike	Rake	Dip
NP1	2	-121	75
NP2	248	-28	34

Principal Axes:

Axis	Plunge	Azimuth
T	24	115
P	50	237

Source Composition:

Type	Percent
DC	65.7
CLVD	34.3
Iso	0.0

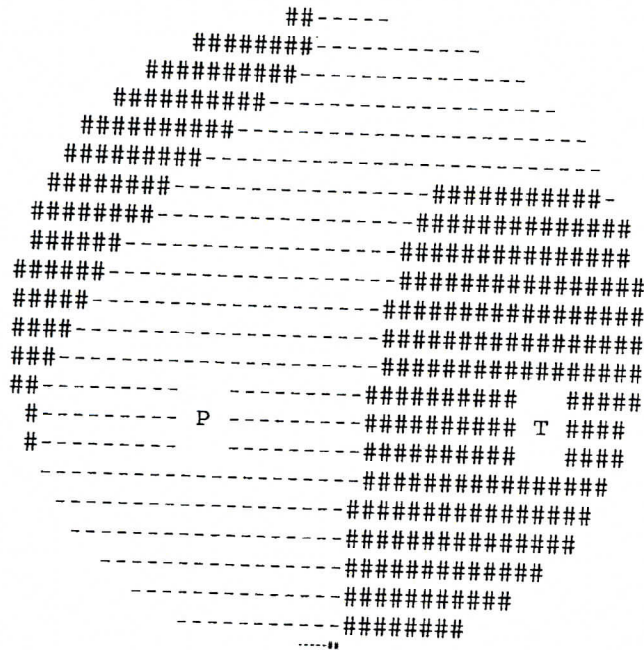


Figure 4-5a. UC Berkeley broadband regional moment tensor solution for the June 14th mainshock. (For corroborative use only.)

20614 12:40 44.81
 36-43.05 116-17.95
 DEPTH = 12.69 KM
 MAG = 4.42

RMS = 0.09 S
 DMIN = 3 KM
 AZM GAP = 58
 # FM = 51

ERH = 0.2 KM
 ERZ = 0.4 KM
 MISFIT = 0.04 (+.08)
 STDR = 0.60

STRIKE UNCERTAINTY = 13
 DIP UNCERTAINTY = 15
 RAKE UNCERTAINTY = 20

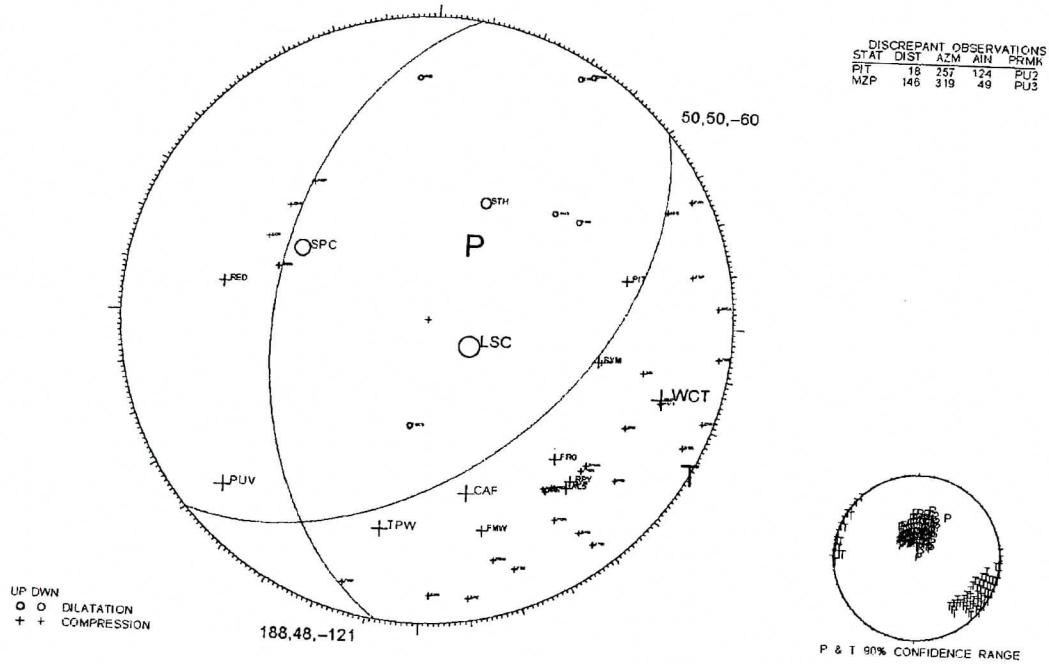


Figure 4-5b. Short period focal mechanism of the June 14, M 4.4, mainshock.
Parameters of mechanism fit (applies to all short period first motion solutions)

- RMS: RMS error from the location.
- DMIN: nearest station; minimum distance
- AZM GAP: station geometry gap in location determination.
- # FM: number of first motions used in location.
- ERH: horizontal error in location
- ERZ: vertical (depth) error in location
- MSFIT: degree of fit; uncertainty in unique solution
- STDR: degree of station coverage relative to the solution (0-1).

20525 12:03 33.13
 36-42.94 116-18.21
 DEPTH = 10.67 KM
 MAG = 3.09

RMS = 0.10 S
 DMIN = 3 KM
 AZM GAP = 60
 # FM = 50

ERH = 0.3 KM
 ERZ = 0.5 KM
 MISFIT = 0.00 (+ 10)
 STDR = 0.70

STRIKE UNCERTAINTY = 8
 DIP UNCERTAINTY = 35
 RAKE UNCERTAINTY = 35

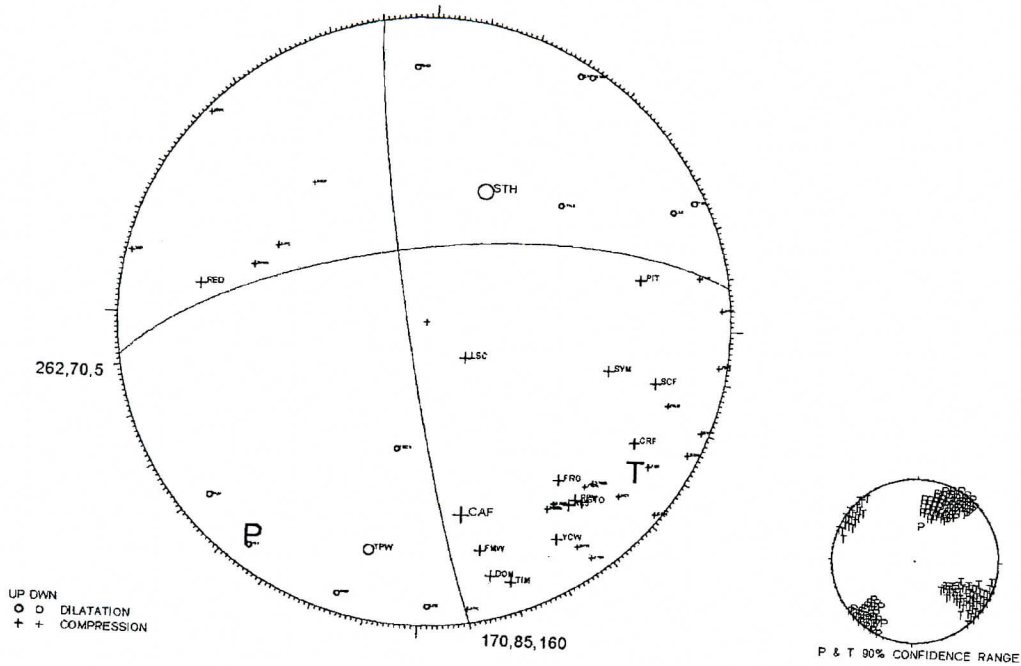


Figure 4-5c. Focal mechanism of the May 25, 2002 earthquake within the Little Skull Mountain aftershock zone.

20618 16:24 31.83
 36-42.58 116-18.51
 DEPTH = 11.67 KM
 MAG = 3.13

RMS = 0.10 S
 DMIN = 3 KM
 AZM GAP = 47
 # FM = 40
 ERH = 0.2 KM
 ERZ = 0.4 KM
 MISFIT = 0.04 (+.07)
 STDR = 0.62

STRIKE UNCERTAINTY = 18
 DIP UNCERTAINTY = 13
 RAKE UNCERTAINTY = 20

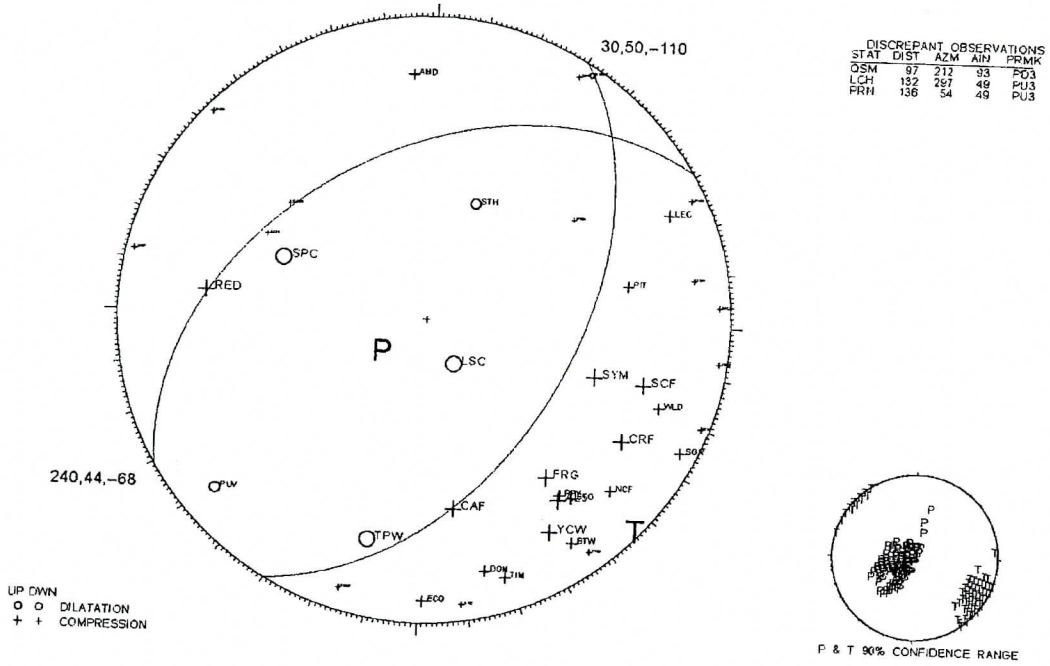


Figure 4-5d. Focal mechanism of the June 18, 2002 earthquake within the Little Skull Mountain aftershock zone; an aftershock of the June 14 mainshock.

Comparison of Mainshock and Composite and Two M 2.8 Events used to Construct Composite

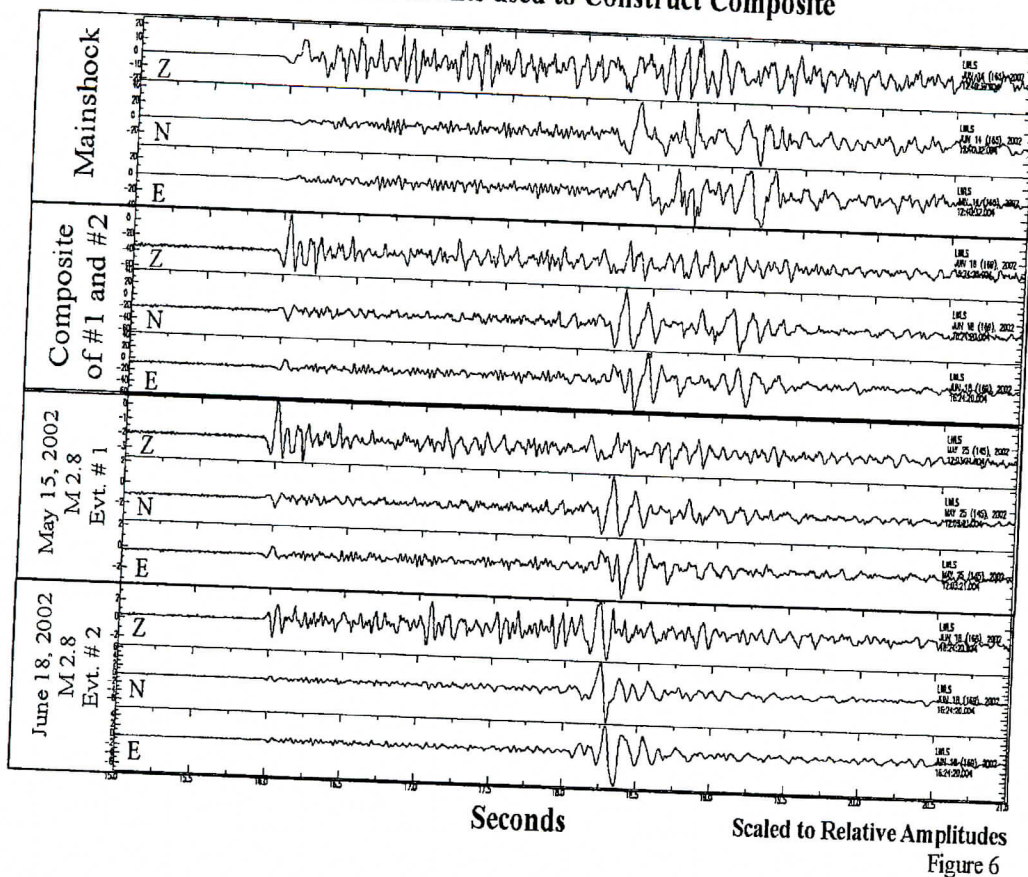


Figure 6

Figure 4-6. Waveforms of the primary events of the mid-2002 sequence. All records are from the YMP Strong Motion station at Lathrop Wells. The composite time-series record is constructed by summing and time shifting Evt. #'s 1 and 2 records to best approximate the observed mainshock record at Lathrop Wells.

Mainshock and Composite Bandpass Filtered at 1-8 Hz

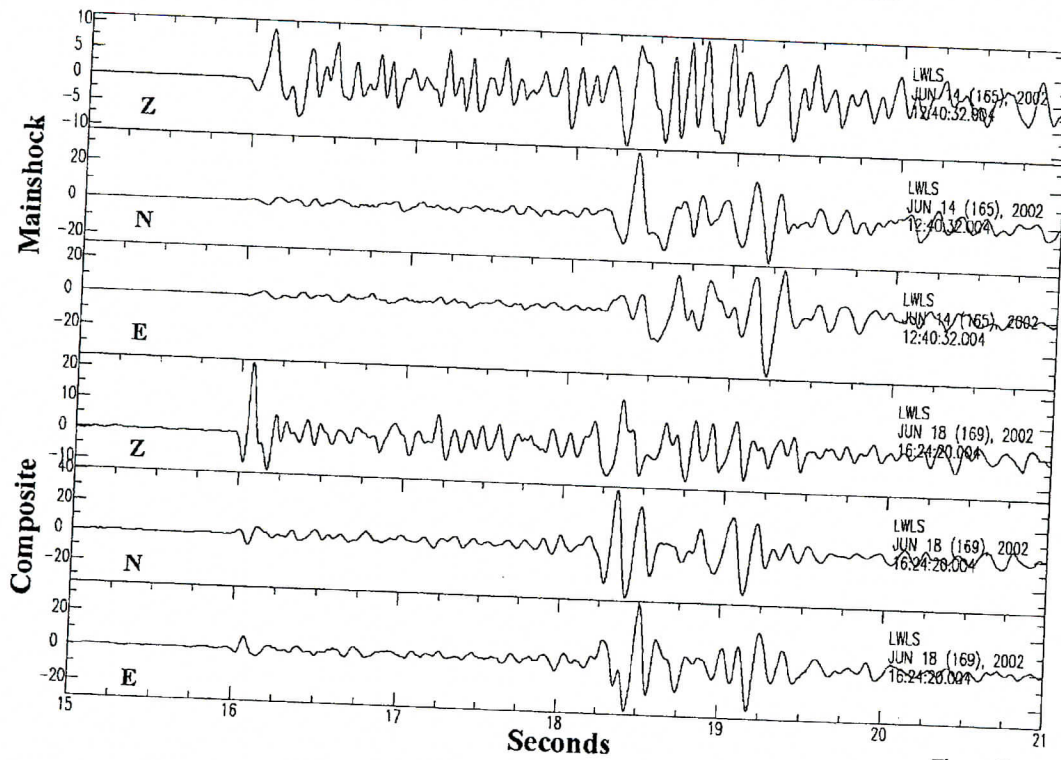


Figure 7

Figure 4-7. Filtered composite and mainshock record showing that the composite time-series captures the mainshock record in the 1-8 Hz band.

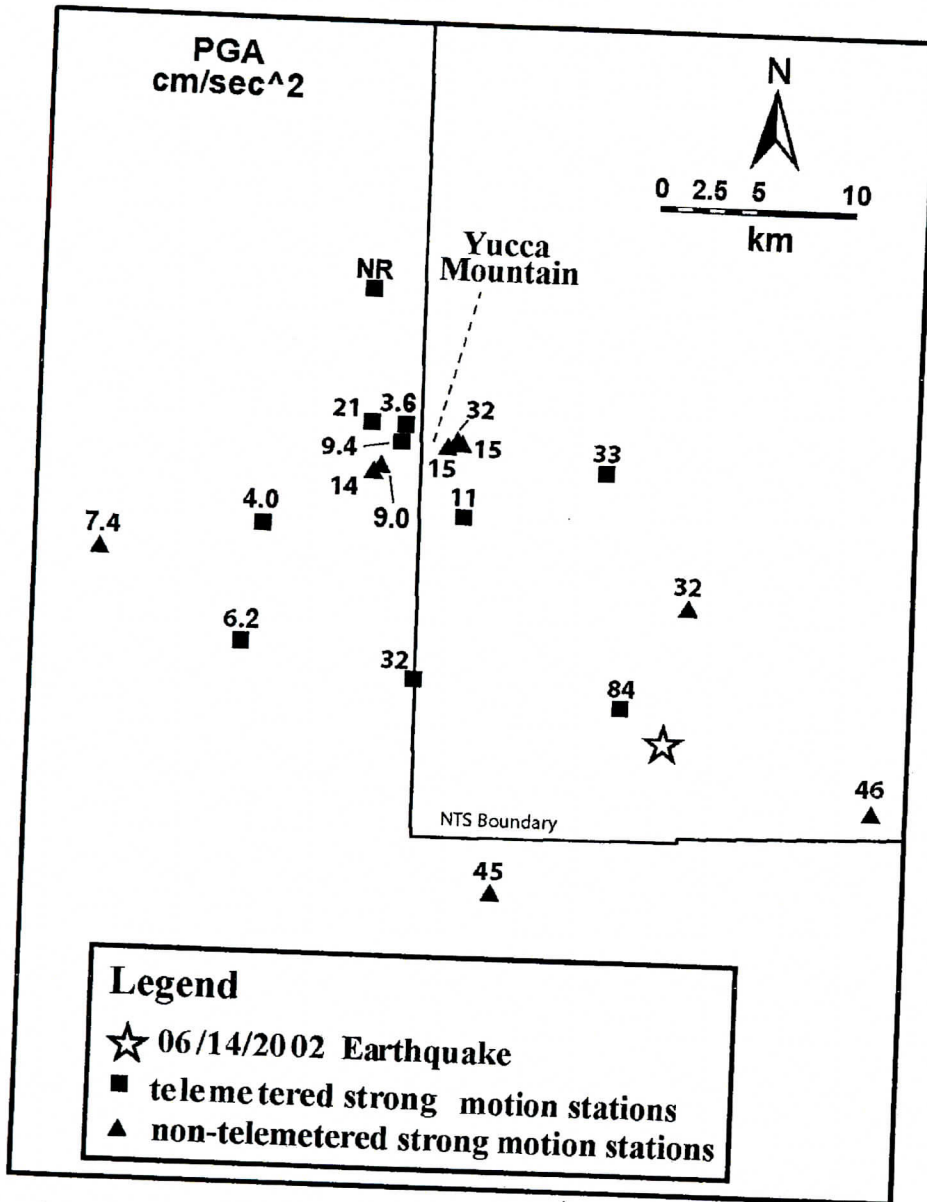


Figure 4-8. Geographic distribution of Peak Ground Motions from acceleration records in the Yucca Mountain area. The compilation is from both the telemetered and non-telemetered strong motion stations.

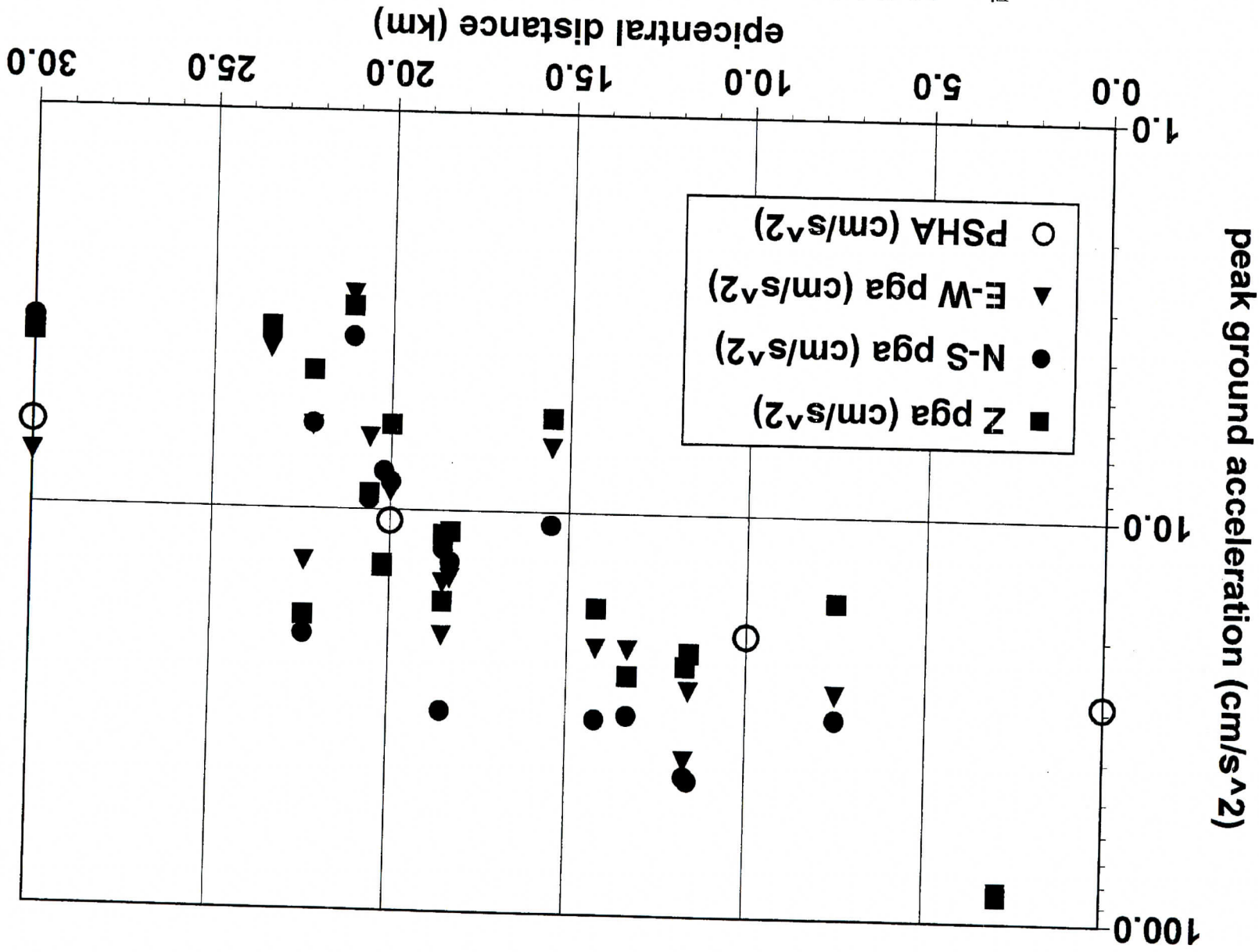


Figure 4-9. Relationship between Peak-Ground-Acceleration and distance from strong motion recordings of the June 14, 2002, earthquake.

Strong Motion Records and Acceleration Spectra:

Three-component records with the station name shown in the plots that are not referenced to a channel orientation are in Vertical-North-East orientation.

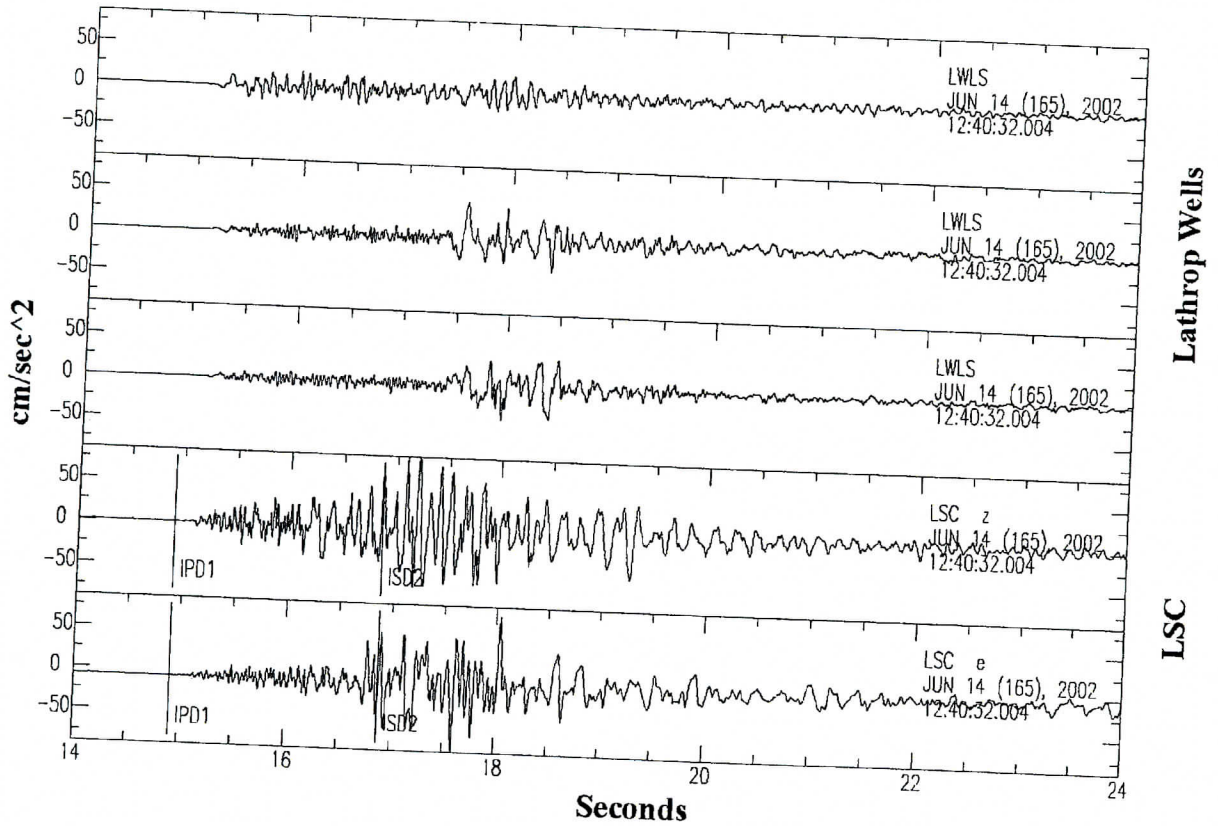


Figure 4-10. Time-series records of the June 14th earthquake from Lathrop Wells and Little Skull Mountain strong motion stations. The North component at the Little Skull Mountain crest station, LSC, was not operating properly.

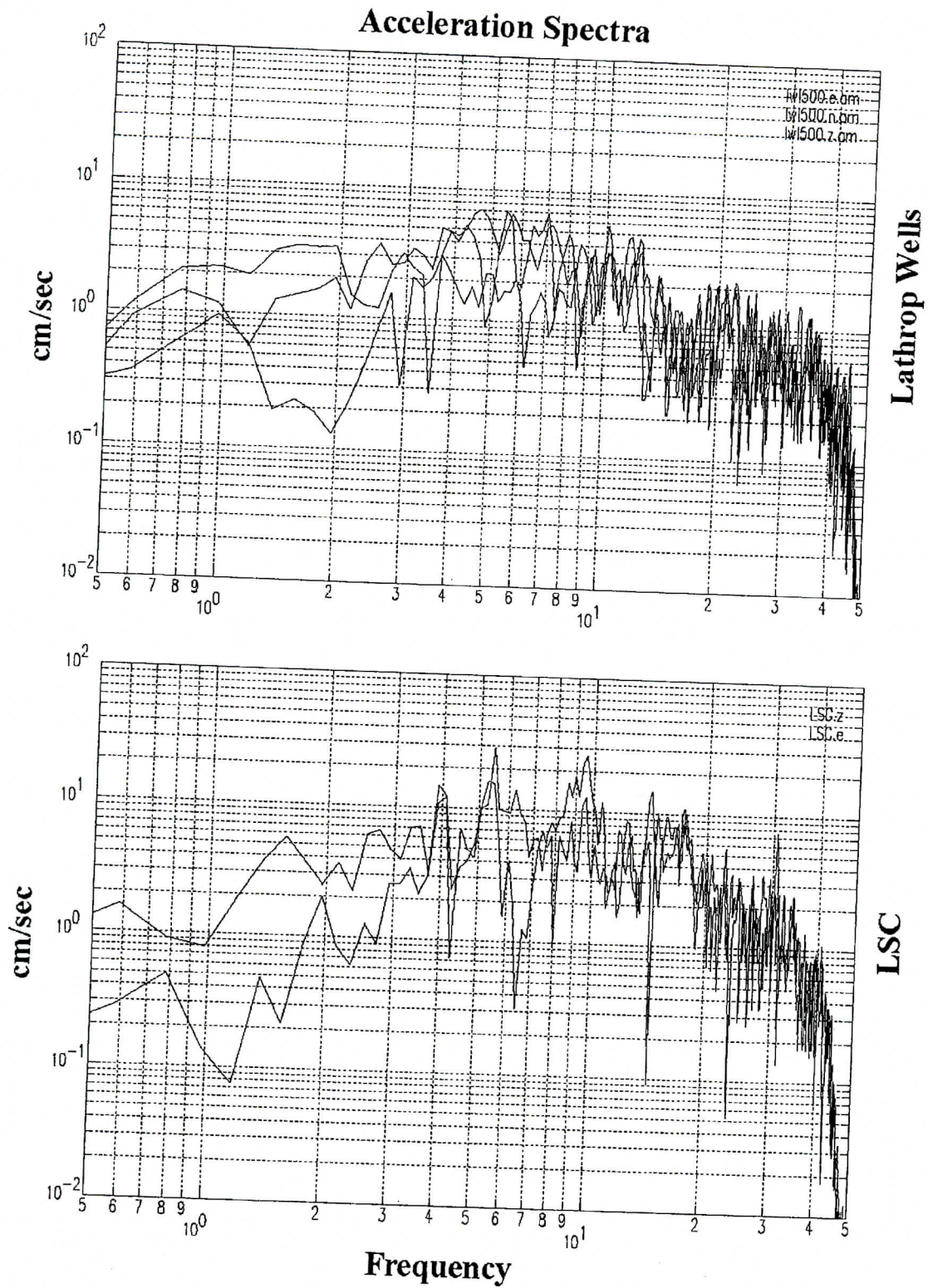


Figure 4-11. Acceleration spectra from 3 components at Lathrop Wells and two components at LSC strong motion stations.

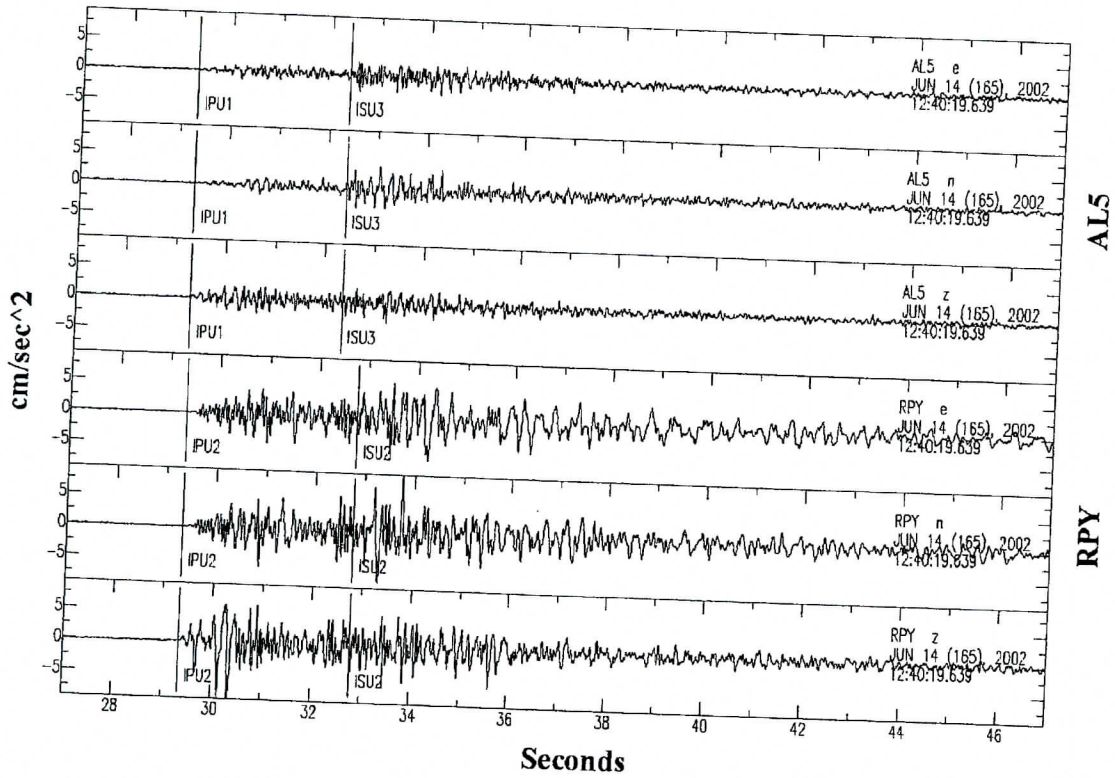


Figure 4-12. Velocity time-series records from SGDSN stations AL5 (Alcove 5 at a depth of 300 meters) and RPY (almost above the repository and Alcove 5). Shows the relative amplitude differences between the free surface and ESF records.

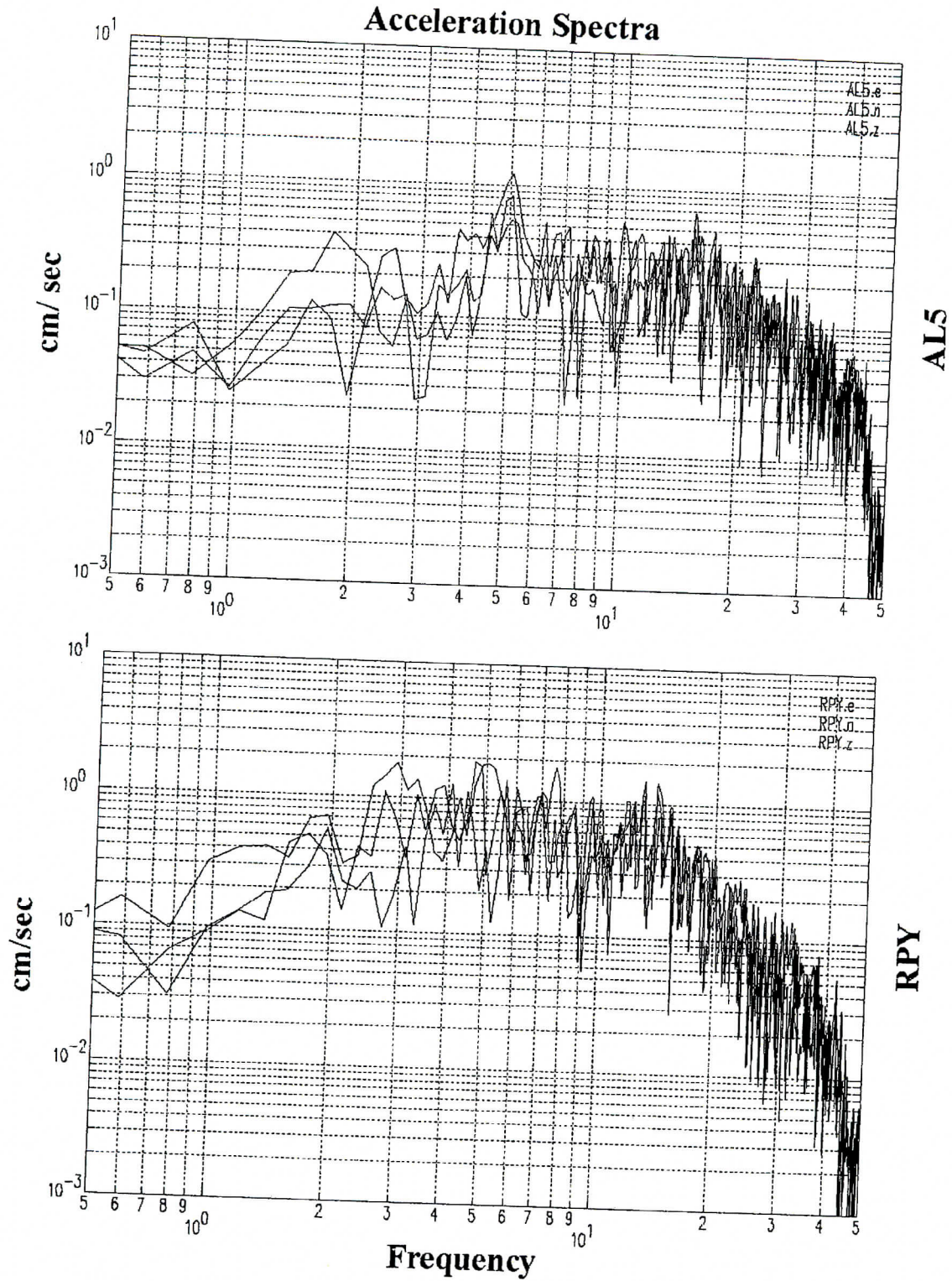


Figure 4-13. Acceleration spectra at AL5 and RPY for the June 14 earthquake.

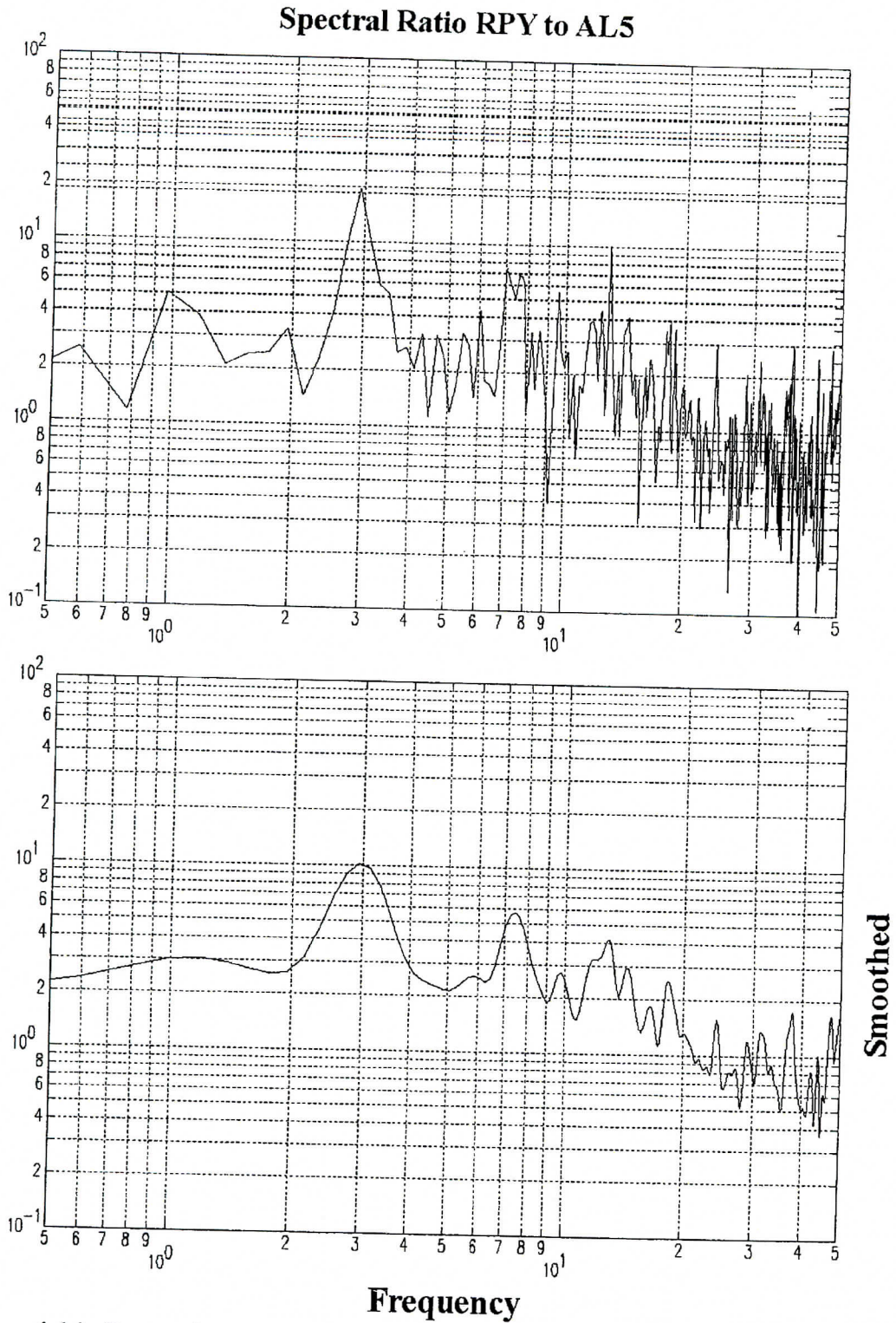


Figure 4-14. Raw and smoothed spectra ratios between RPY and AL5. RPY/AL5 spectral ratio.

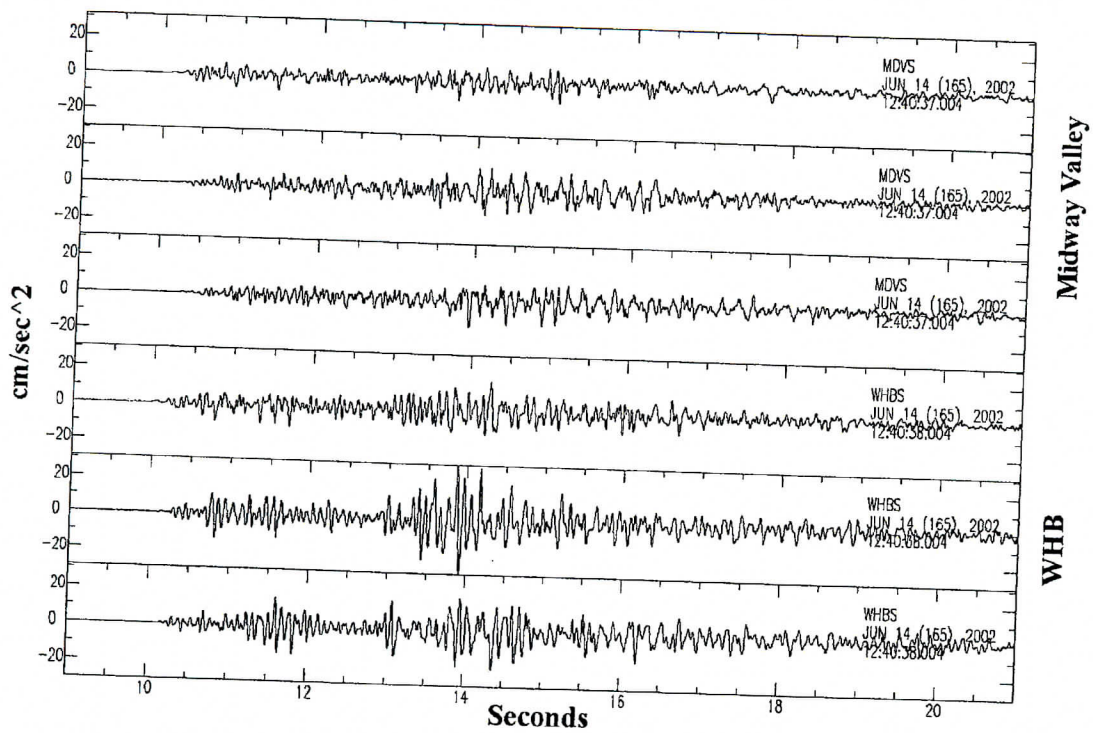


Figure 4-15. Comparison of acceleration time-series records; WHB (near location of proposed waste handling buildings on ESF Pad on thick concrete pad) and free-field station on sediments in Midway Valley about 300 meters east of the ESF Pad and station WHB.

Acceleration Spectra

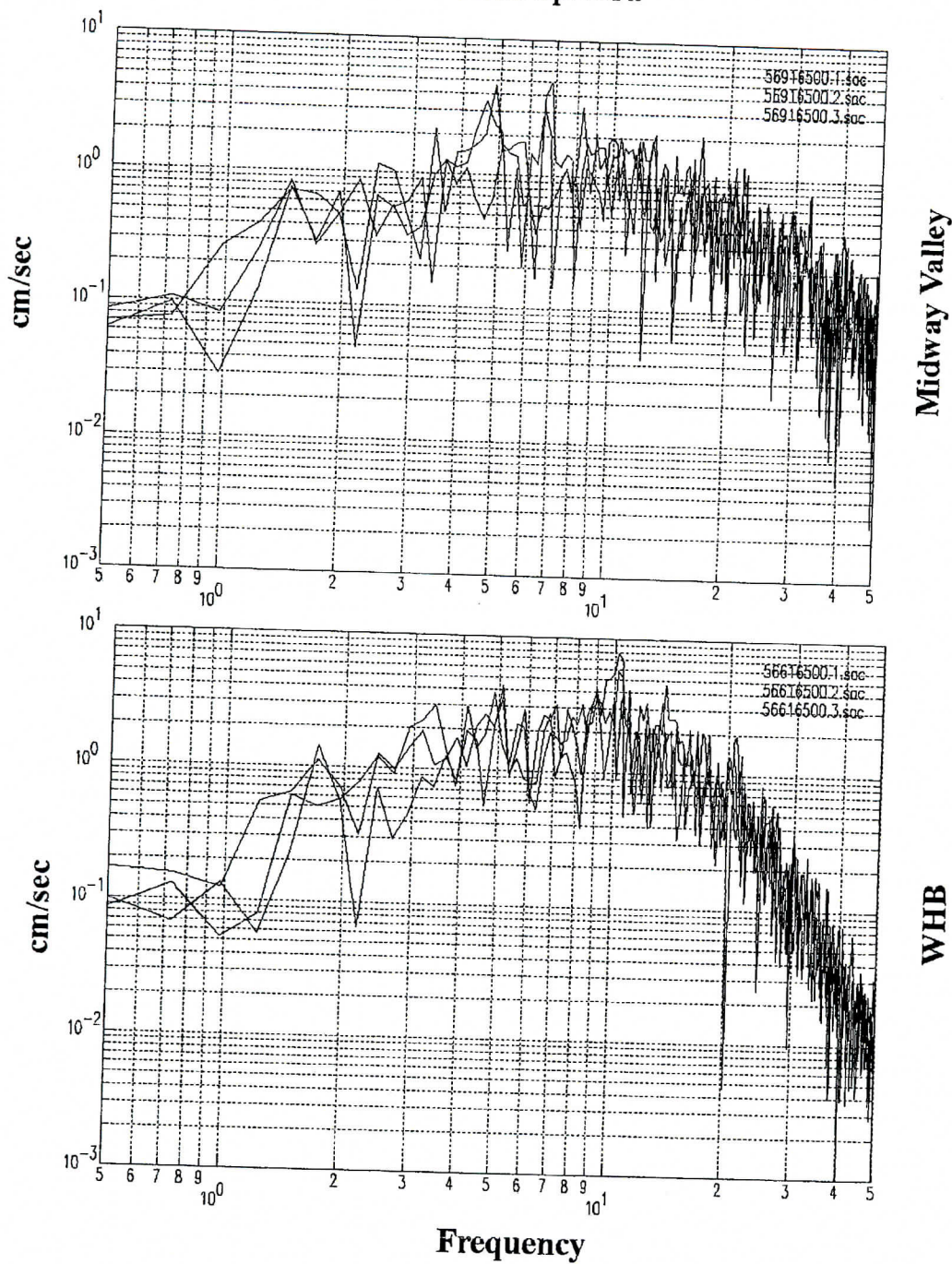


Figure 4-16. Acceleration spectra of WHB and Midway Valley strong motion records.

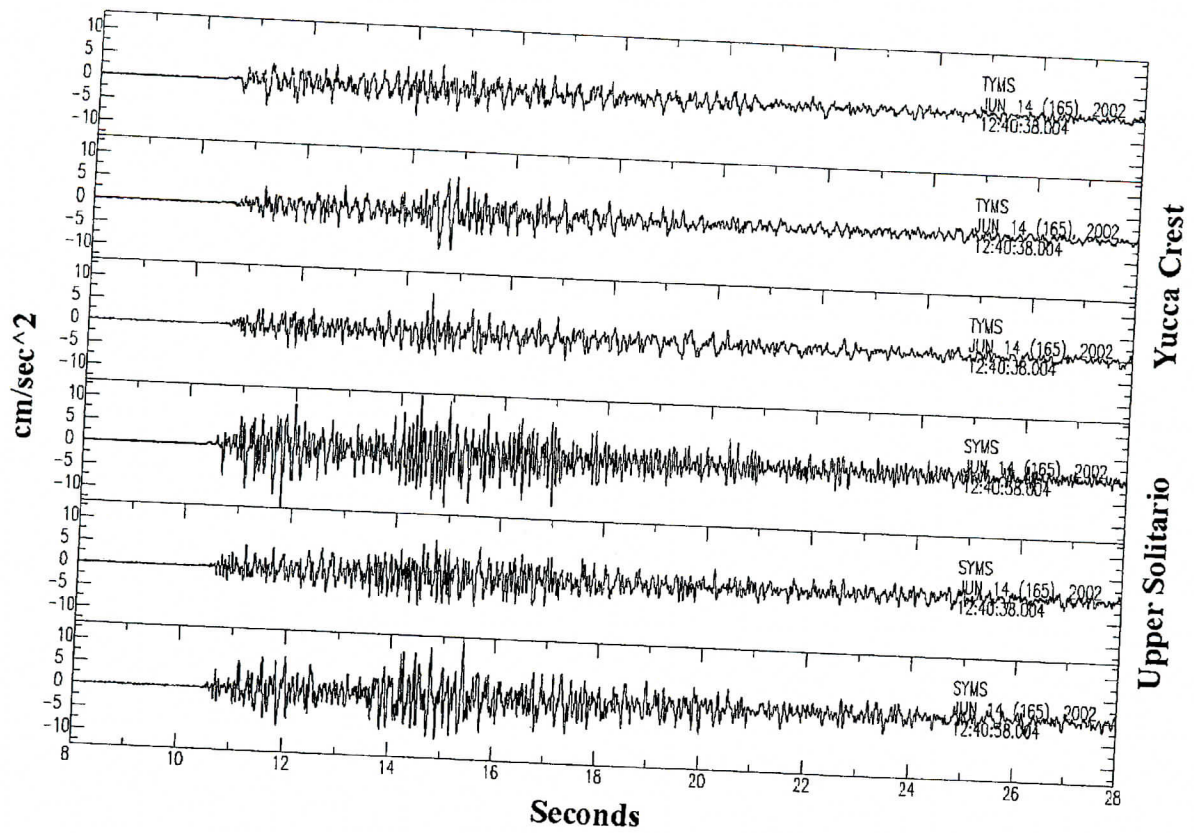


Figure 4-17. Comparison of acceleration time-series records at strong motion stations at the crest of Yucca Mountain and the Upper Solitario Canyon station that is midway between the Yucca Mountain crest and the base of Solitario Canyon on tuff on the west facing slope above trenches exposing the Solitario Canyon fault steep slope. The Upper Solitario Canyon station is midway between the Yucca Mountain crest and the base of Solitario Canyon.

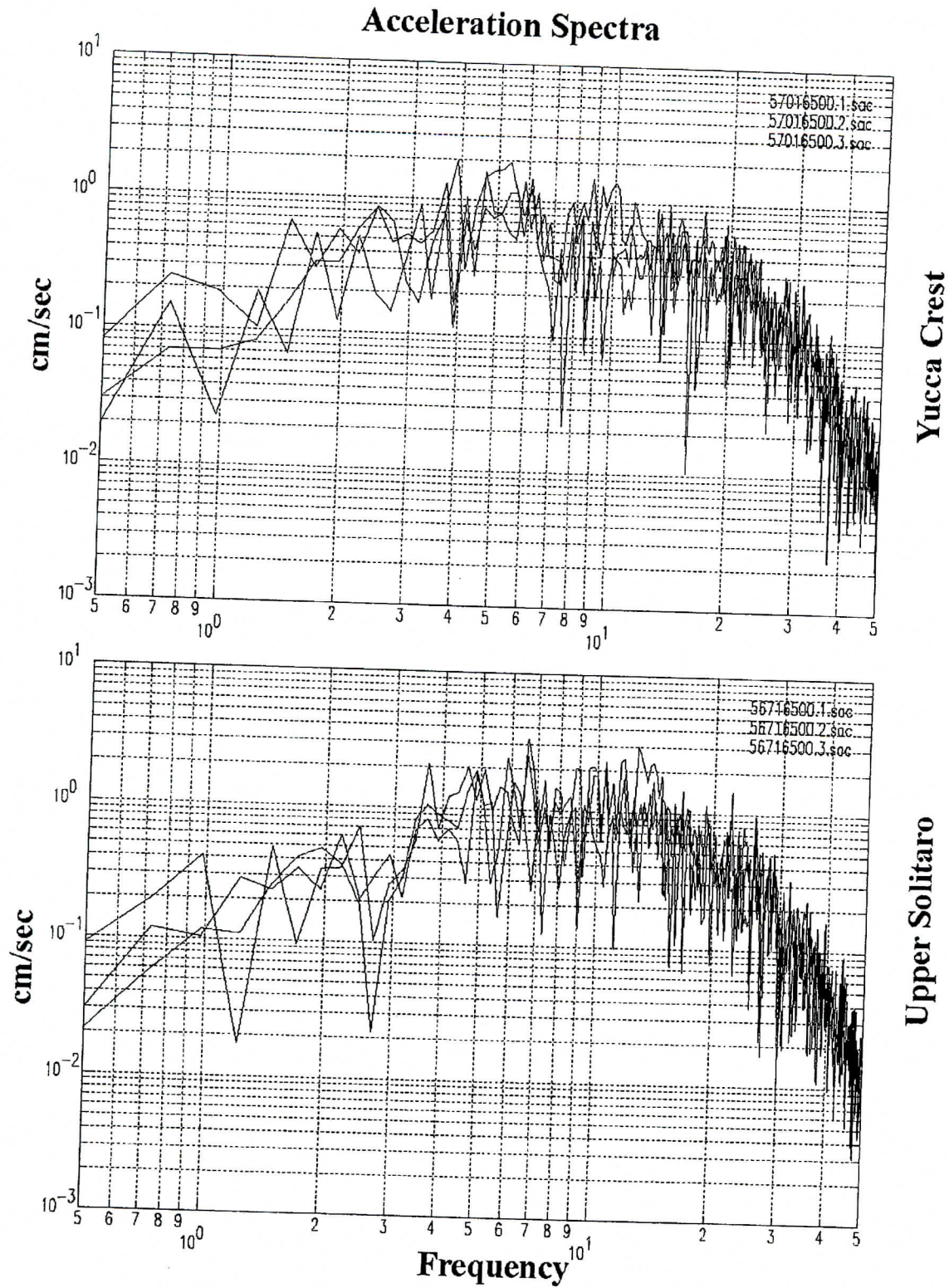


Figure 4-18. Acceleration spectra from the Yucca Crest and Upper Solitario Canyon stations.

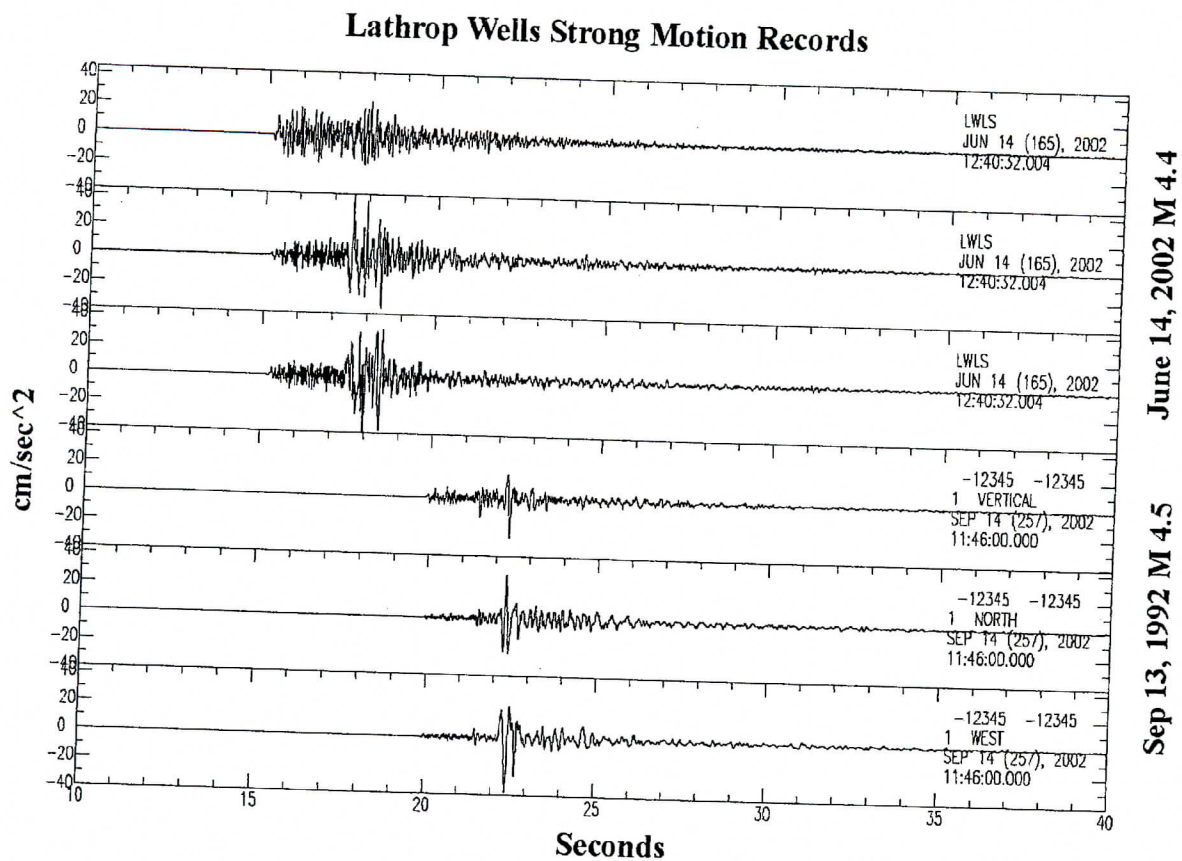
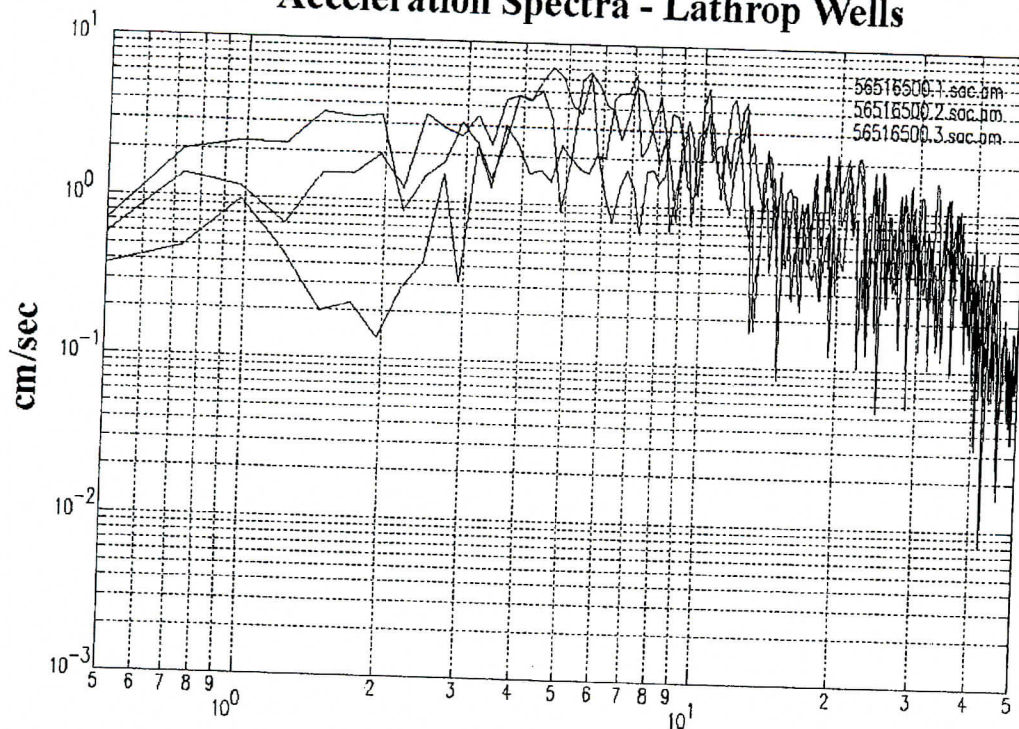
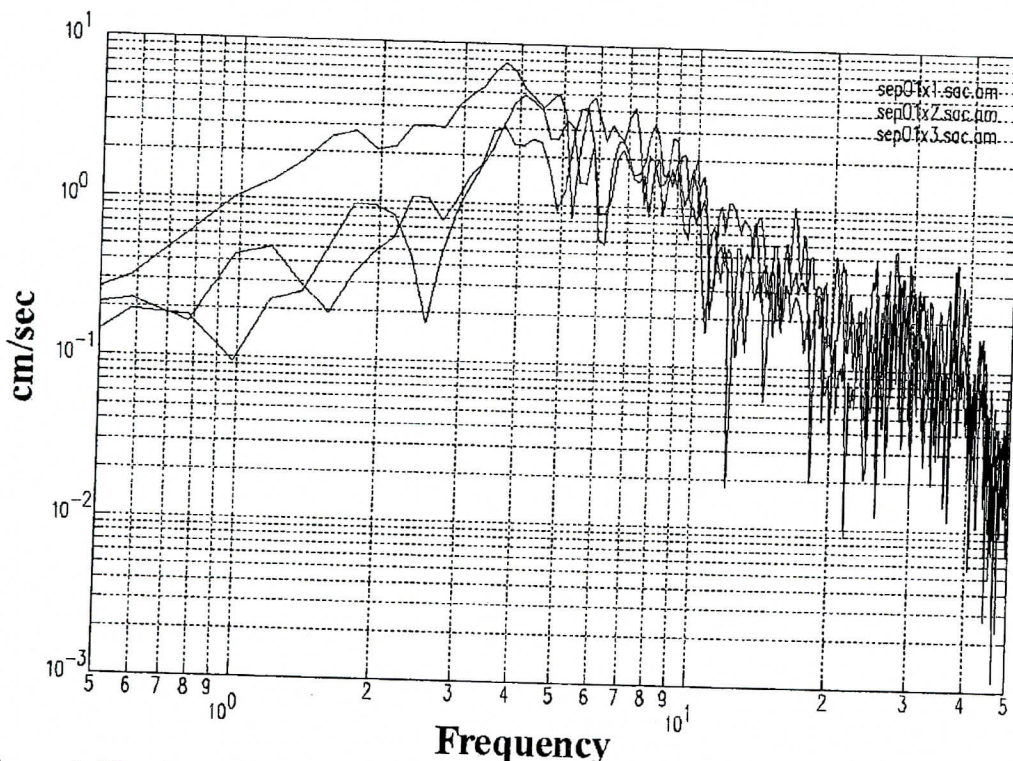


Figure 4-19. Acceleration time-series records at Lathrop Wells from the June 14, 2002, and September 13, 1992 M 4.4 and M 4.5, respectively, Little Skull Mountain aftershocks. The 1992 event was recorded on the Blume strong motion network and the 2002 event was recorded on the Yucca Mountain network station that was co-located at the Blume location. Note the clear differences in the complexities of the records for these two events with similar focal mechanisms (Smith et al., 2001) and hypocentral parameters. (For corroborative use only.)

Acceleration Spectra - Lathrop Wells



June 14, 2002



Sep 13, 1992

Figure 4-20. Acceleration spectra Lathrop Wells from the June 14, 2002, and September 13, 1992 M 4.4 and M 4.5, respectively, Little Skull Mountain aftershocks. (For corroborative use only.)

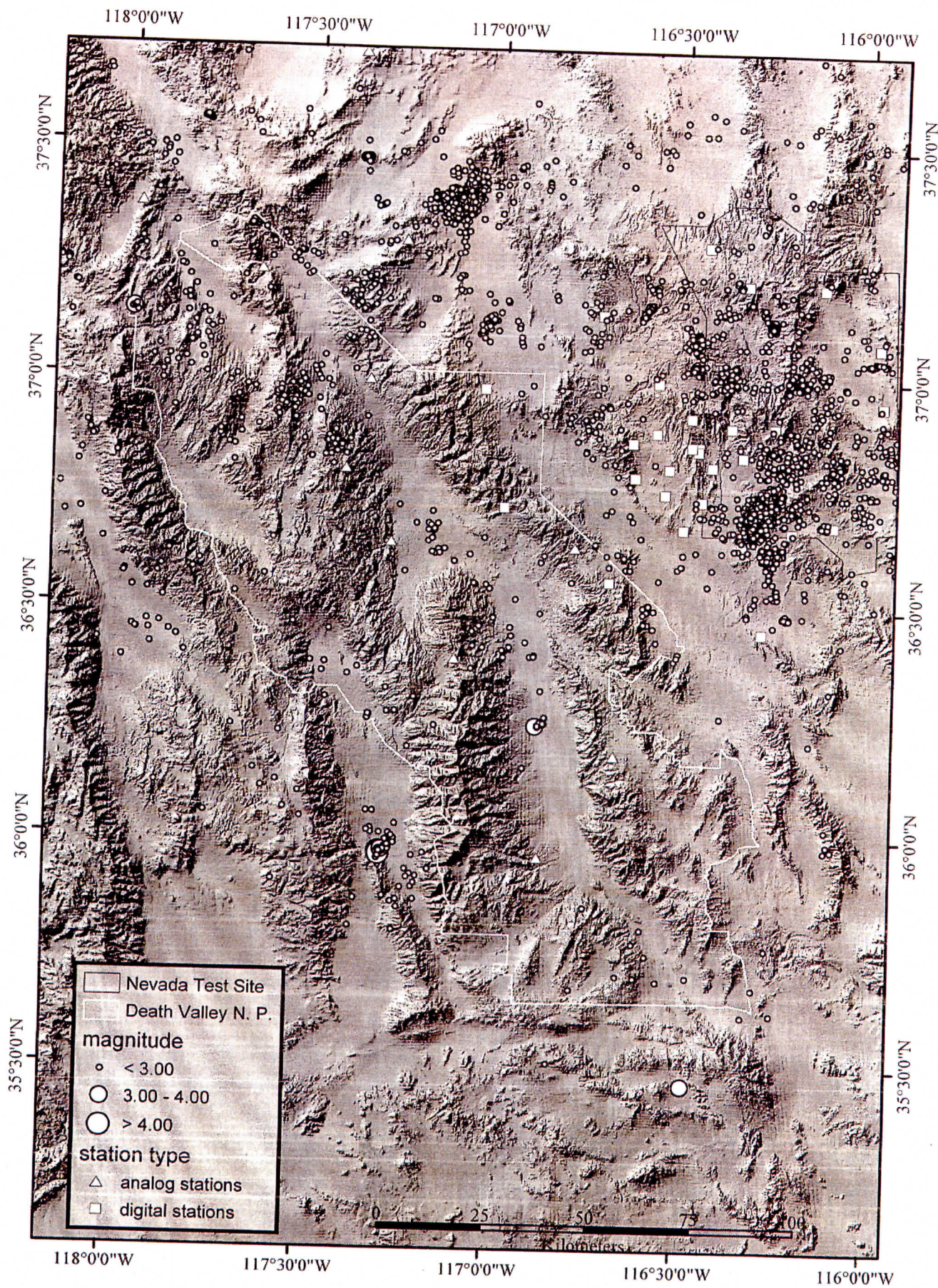
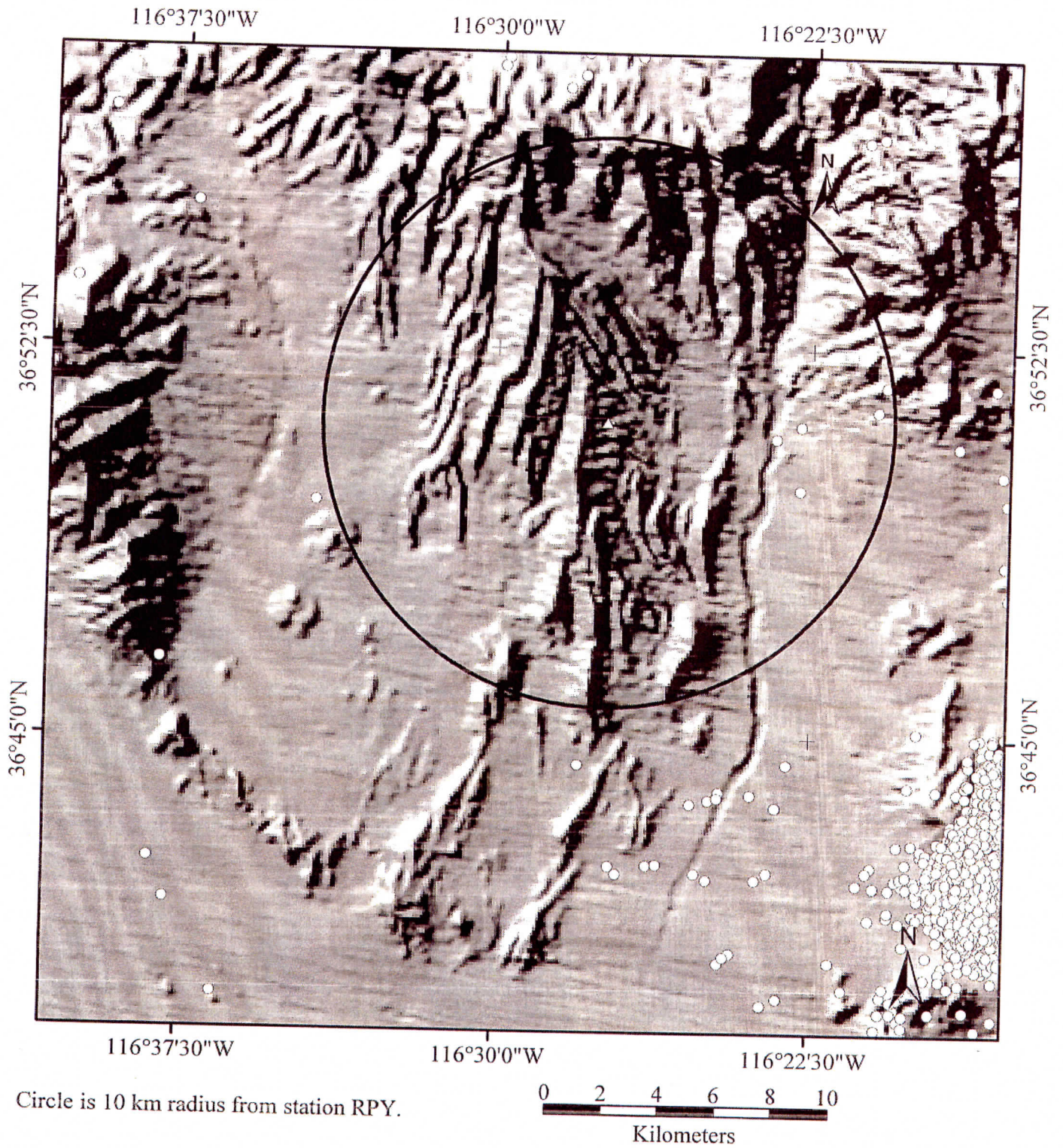


Figure 5-1. Seismicity in the Death Valley National Park region during FY2002.
 (For corroborative use only.)

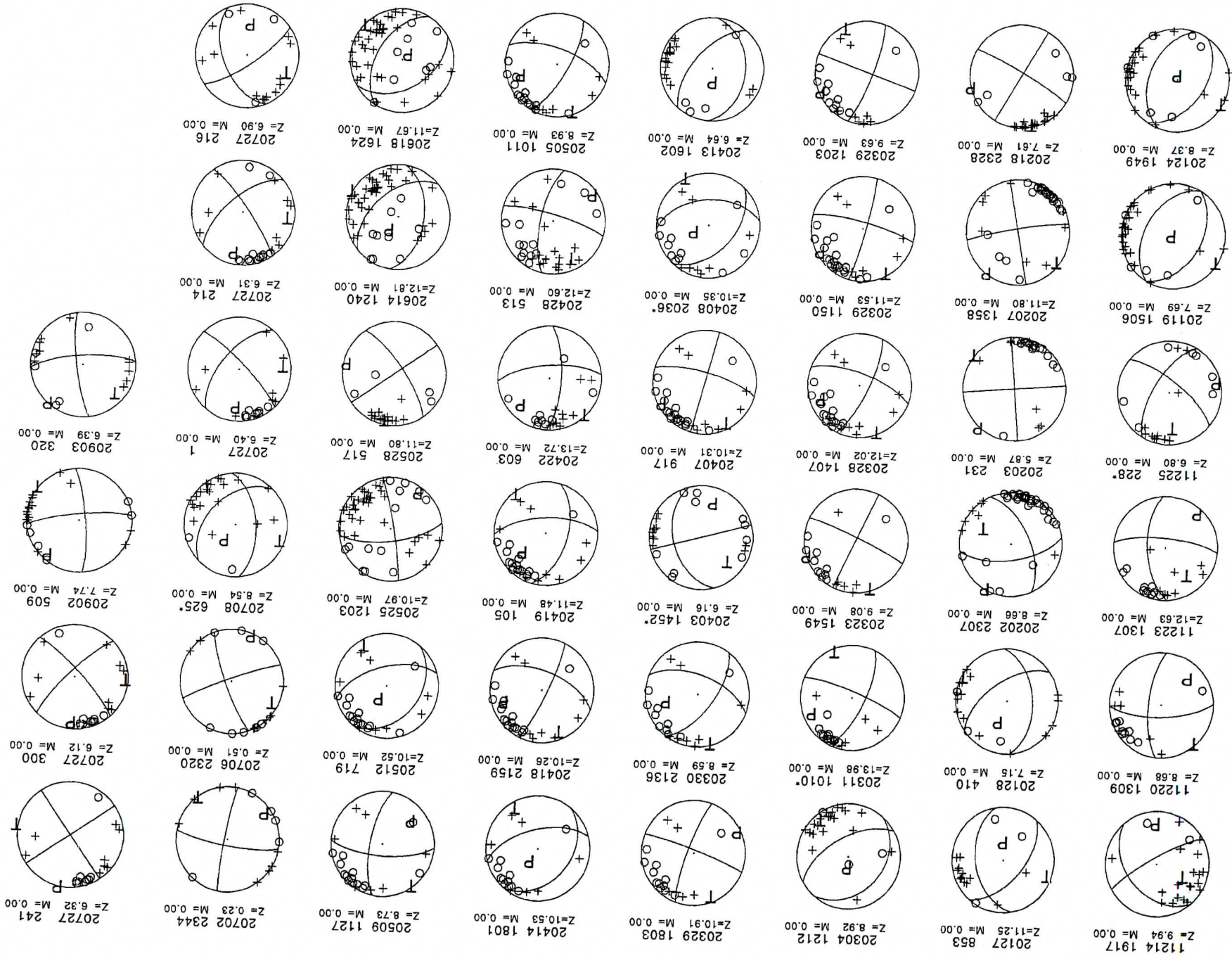
FY2002 Activity Near Yucca Mountain



Circle is 10 km radius from station RPY.

Figure 6-1. Earthquakes in FY2002 near Yucca Mountain.

Figure 7-1. Focal mechanisms for FY2002 earthquakes in the SGBDSN catalog. Up (crosses) and down (circles) first motions are plotted on the lower focal hemisphere.



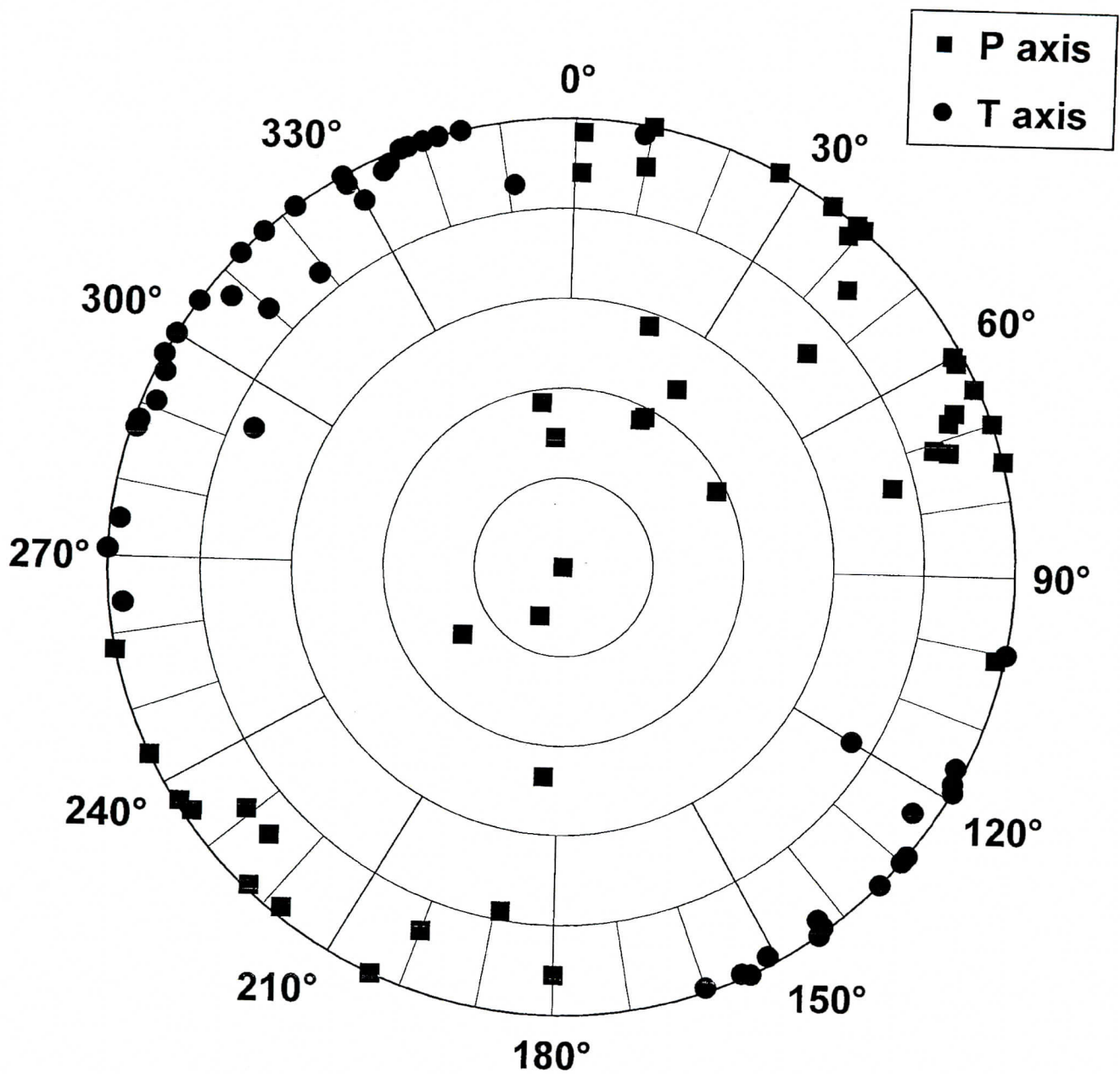


Figure 7-2. Pressure and tension axes of the focal mechanisms for FY2002. These are plotted on the lower focal hemisphere.

FY2002 Blasts in the SGBDSN Region

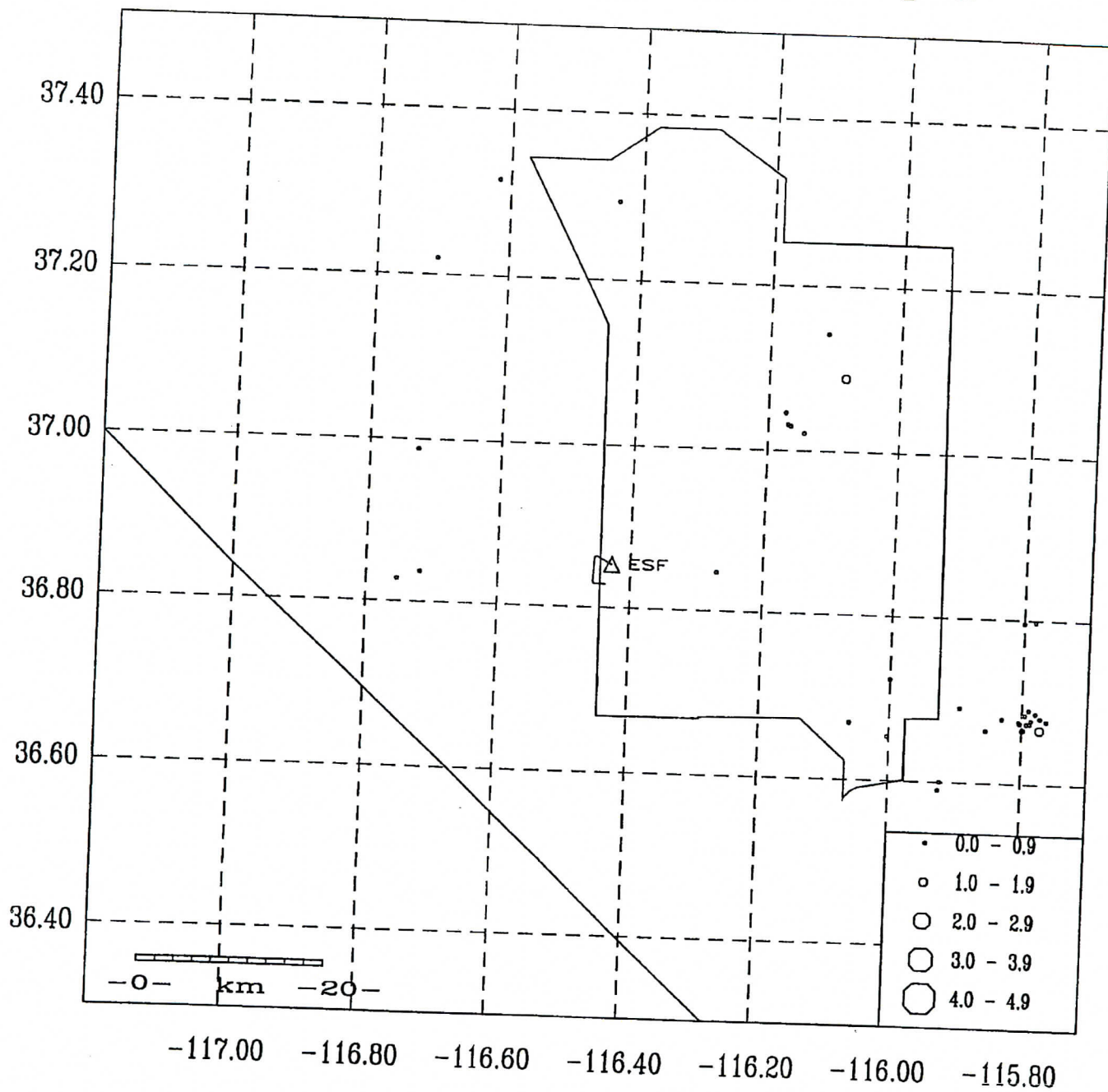


Figure 8-1. Location of blasts in the SGBDSN monitoring region in FY2002.
(For corroborative use only.)

Appendix 1

Status of the Data

In order to produce a final product, seismic data collected for earthquake studies pass through a number of formats and are moved from file to file, even between computing systems at the NSL (Nevada Seismological Laboratory). The control and management of this data is described in the following implementing procedures

IPR-001, Operation of the Yucca Mountain Digital Seismic Network

IPR-002, Determining the Location of Earthquakes Recorded by the Yucca Mountain Seismic Network

IPR-003, Determining the Magnitude of Earthquakes Recorded by the Yucca Mountain Seismic Network

IPR-004, Operation of the Yucca Mountain Strong Motion Network

Added details are often contained in the scientific notebook UCCSN-UNR-012 (*Development and Operation of the Hardware and Software for the UNRSL Seismic Monitoring Network*). Together, these IP's and the scientific notebook cover the electronic control of data recorded and developed in conjunction with this study, according to UCCSN QAP-3.1 (*Control of Electronic Data*). Integrity of the data throughout this process has been documented in that notebook. Methodology described in this report for seismic monitoring activities meets the requirements of the QARD. Data collection, reduction, and analysis are governed by applicable UCCSN Implementing Procedures (IP) listed above and by an approved UCCSN Scientific Investigation Plan (SIP-UNR-004). There are no "models" treated in this report.

The earthquake location and magnitude data (Appendix 3) and focal mechanism data (Table 7-1) are the main data in FY02 developed for this report. The location/magnitude data were generated under appropriate quality-assurance controls; namely, IPR-002 and IPR-003. A preliminary set of this data has been submitted to the TDMS (Technical Data Management System) under UCCSN # 012DV.014 as “non-Q” data, pending final review and approval of this report. The FY02 focal mechanism data were submitted to the TDMS under UCCSN # 012DV.015; again, this was submitted as “non-Q” pending report approval.

This report makes use of prior location/magnitude datasets that have been submitted to the TDMS by the NSL (or, in the last instance, the TDA); their DTN’s and status are as follows:

Period of Data	DTN (DID) #	Status
FY01	MO0205UCC012DV.008	Q
FY00	UN0106SPA012JB.001	Q
FY98-99	UN0007SPA012DV.002	Q
FY97	MO9906SEISYMN.000	Q
FY96	MO970483117412.002	Q
1995 (01/01-09/30)	MO0208UCC012DV.012	Q
1994 (01/01-12/31)	GS950383117412.003	Q
1993 (01/01-12/31)	GS950183117412.001	Q
1992 (10/01-12/31)	MO0208UCC012DV.011	Q
1978 (08/08) – 1992 (09/30)	012DV.019	non-Q

Other FY02 data shown in graphs and tables herein were generated from the raw source data which have been submitted to the Records Processing Center under the titles “Raw seismic data collected by the Southern Great Basin Digital Seismic Network -- 10/01/01 to 09/30/02”, and “YMP Strong Motion Network: Data: Period ... to ...” where “...” covers several specific dates within FY02. These data were collected under appropriate quality-assurance procedures; namely, IPR-001 and

IPR-004. Details of data collection, data flow, and data processing and locations of data files, both raw and developed, are given in scientific notebook UCCSN-UNR-012. This notebook was last reviewed in May 2002.

Reference is made to data of the “analog” and “digital” networks within this report. Prior to October 1995, this analog network was the primary monitoring network and all data were collected under controls of the USGS QA program. After this date the digital network became the primary monitoring network, and the raw data from the analog network were not used in developing hypocenters or focal mechanisms. However, in January of 2000 raw data from a greatly reduced analog network were again used in developing this final data. The analog data collection since that time is treated in IPR-001 to assure its quality. Only timing and polarity are addressed, and the raw data of the analog stations are not used in any ground-motion amplitude calculations.

Appendix 2
Station Data and Description for the SGBDSN and Strong-Motion Sites
Q data – DTN #UN0006SPA012DV.001

Permanent Network Monitoring Sites

code	station name and area	latitude north	longitude west	elevation km	on date	seismometer	strong motion ⁺
AL5	Alcove 5, ESF	36.8596	116.4547	1.0660	1998252	Mark Products L4	y
AMD	Amargosa Desert, BLM	36.4526	116.2809	0.7560	1997115	Geotech S-13&	n
BTW	Beatty Wash, NAFB	36.9978	116.5665	1.3910	1995230	Geotech S-13	n
CAF	Calico Fan, NTS	36.8391	116.3377	1.1100	1995034	Geotech S-13	y
CRF	Crater Flat, BLM	36.8118	116.5340	1.0320	1995165	Geotech S-13	y
DOM	Dome Mountain, NTS	37.0021	116.4086	1.7110	1995333	Geotech S-13	n
ECO	Echo Peak, NTS	37.2108	116.3296	2.2320	1999197	Geotech GS-13	n
FMW	Forty Mile Wash, NTS	36.9021	116.3688	1.1460	1995165	Geotech S-13	n
FRG	Fran Ridge, NTS	36.8169	116.4195	1.1550	1995165	Geotech S-13	y
HEL	Hell'sGate, Death Valley NP	36.7246	116.9750	0.7470	2002175	Geotech S-13	n
LEC	Lee's Camp, Death Valley NP	36.5627	116.6896	1.1130	2002057	Geotech S-13	n
LSC	Little Skull Cliff, NTS	36.7307	116.3255	1.2380	1995034	Geotech S-13	y
NCF	North Crater Flat	36.8899	116.5682	1.1510	1995034	Geotech S-13	n
PUV	Plutonium Valley, NTS	36.9494	115.9633	1.2530	1995258	Geotech S-13	n
PIT	Cinder Pit, BLM	36.6798	115.4937	0.0850	2000334	Geotech S-13	n
RED	Red Mountain, NTS	36.6895	116.0930	1.1430	1996037	Geotech S-13	n
RPY	Repository, NTS	36.8515	116.4563	1.3010	1996038	Geotech S-13*	y
SCF	South Crater Flat, BLM	36.7568	116.5440	0.9090	1995034	Geotech S-13	y
SGR	South Grapevine, DVNP	36.9805	117.0327	1.5600	1998127	Geotech S-13	n
SPC	Specter Range, NTS	36.6746	116.2030	1.0640	1996075	Geotech S-13\$	n
STC	Silent Canyon, NTS	37.2939	116.4358	1.9600	1995209	Geotech S-13	n
STH	Stripped Hills, NTS	37.6457	116.3375	1.0500	2000179	Geotech S-13	n
STO	Solitario Canyon, BLM	36.8603	116.4742	1.3590	1995165	Geotech S-13	y
SYM	South Yucca Mountain, NTS	36.7416	116.4460	0.9950	1995034	Geotech S-13	y
TAR	Tarantula Canyon, BLM	36.8680	116.6322	1.2310	1996023	Geotech S-13	n
TIM	Timber Mountain, NAFB	37.0667	116.4694	1.8710	1996143	Geotech S-13#	n
TPW	Topopah Wash, NTS	36.9016	116.2519	1.5730	1995258	Geotech S-13	n
TWP	Twin Peaks, NTS	37.2047	116.1234	1.5760	1995205	Geotech S-13	n
TYM	Thirsty Mountain, NAFB	37.1441	116.7208	1.4570	1996275	Geotech S-13*	n
WLD	Wildcat Mountain, BLM	36.7927	116.6257	0.9300	1995193	Geotech S-13	n
YCW	Yucca Wash, NTS	36.9224	116.4756	1.4980	1996032	Geotech S-13	y
YFT	Yucca Flat, NTS	37.0762	115.9735	1.3540	1999197	Geotech GS-13	n

+ "y" indicates that a RefTek 133-05 strong-motion instrument has been added at the site
&station AMD used a Guralp CMG-40 until 03/06/2002
\$station SPC used a Guralp CMG-40 until 02/27/2002
#station TIM used a Guralp CMG-40 until 05/01/2002
*station TYM used a Guralp CMG-40 until 04/10/2002

Management Units:

BLM Bureau of Land Management
DVNP Death Valley National Park
NTS Nevada Test Site, DOE
NAFB Nellis Air Force Base

Independent Strong-Motion Sites

code	station name and area	latitude north	longitude west	elevation km
SPRS	Specter Range Strong Motion	36.6847	116.1800	1.2741
LWLS	Lathrop Wells Strong Motion	36.6433	116.3983	0.5639
BYMS	Bottom Yucca Mountain Strong Motion	36.8394	116.4778	1.2009*
SYMS	Side Yucca Mountain Strong Motion	36.8378	116.4725	1.3625
WCTS	Wildcat Canyon Strong Motion	36.7986	116.6269	0.7010
MDVS	Midway Valley Strong Motion	36.8514	116.4222	1.0607
TYMS	Top Yucca Mountain Strong Motion	36.8406	116.4683	1.6612
FOCS	FOC Strong Motion	36.7778	116.2878	1.0973
EXHS	Exile Hill Strong Motion	36.8497	116.4303	0.9845
WHBS	Waste Handling Building Strong Motion	36.8529	116.4249	1.2730

*BYMS station was removed in January 2002 and relocated at WHBS

Appendix 3

Earthquake Catalog for FY2002

submitted as an electronic dataset (DID # 012DV.014)

Appendix 4

Events Identified and Located As Blasts In FY2002 Non-Q data (DID # 012DV.017)

Date	hh:mm:ss.ttt	latitude	longitude	magnitude
10/20/2001	18:39:19.906	36.6542	-116.0027	0.02
11/16/2001	17:18:49.145	37.0464	-116.1737	0.42
11/18/2001	16:48:51.012	37.0303	-116.1655	0.22
11/18/2001	17:07:14.412	37.0325	-116.1700	0.17
12/13/2001	08:57:23.077	37.1422	-116.1122	-0.02
1/26/2002	22:35:36.992	36.9882	-116.7271	0.47
2/27/2002	21:35:38.749	36.6698	-116.0612	0.62
3/03/2002	21:32:42.067	36.8473	-116.2707	0.29
3/09/2002	07:21:34.243	37.2944	-116.4356	0.62
4/02/2002	03:48:38.299	36.7961	-115.8005	0.15
4/02/2002	03:50:36.541	36.7974	-115.7828	0.70
4/09/2002	02:55:14.760	36.6658	-115.7998	0.50
4/09/2002	03:46:11.819	36.6641	-115.8546	0.40
4/09/2002	04:33:09.637	37.3161	-116.6172	0.64
4/10/2002	03:16:19.789	36.6770	-115.7628	0.85
4/10/2002	18:42:32.285	36.7228	-116.0007	0.39
4/10/2002	20:19:45.514	36.8369	-116.7192	0.34
4/10/2002	21:22:30.367	36.8276	-116.7534	0.44
4/11/2002	19:26:18.965	36.6862	-115.7792	0.51
4/12/2002	02:47:17.094	36.6845	-115.7955	0.42
4/12/2002	03:35:01.977	36.6664	-115.7977	0.46
4/23/2002	00:56:08.722	36.5901	-115.9247	0.46
7/05/2002	01:09:02.340	36.6003	-115.9225	0.67
7/26/2002	15:40:01.964	37.0217	-116.1447	0.78
8/26/2002	23:38:49.950	36.6905	-115.7896	0.86
8/26/2002	23:58:23.075	36.6805	-115.7721	0.77
8/27/2002	23:59:13.995	36.6753	-115.8048	0.86
8/28/2002	23:58:52.601	36.6740	-115.8031	0.75
8/29/2002	03:46:06.194	36.6740	-115.7876	0.59
8/29/2002	03:49:32.322	36.6912	-115.8948	0.79
8/29/2002	09:25:46.994	36.6787	-115.8305	0.59
8/29/2002	09:27:45.270	36.6775	-115.7858	0.90
8/29/2002	09:32:22.547	36.6665	-115.7724	1.75
8/29/2002	09:35:22.661	36.6735	-115.7929	0.56
8/30/2002	06:03:15.712	37.2198	-116.7093	0.18
9/28/2002	21:25:18.724	37.0891	-116.0837	1.59